Increasing Staphylococcus Aureus Antibiotic Susceptibility Through Membrane Charge Manipulation Using Peptides and Small Molecules:

Author: Chelsea Weidman

INCREASING *STAPHYLOCOCCUS AUREUS* ANTIBIOTIC SUSCEPTIBILITY THROUGH MEMBRANE CHARGE MANIPULATION USING PEPTIDES AND SMALL MOLECULES

A thesis by

CHELSEA WEIDMAN

Submitted in partial fulfillment

of the requirements for the degree of

Master of Science

Boston College

Graduate School of Arts and Sciences

Department of Chemistry

December 2017

Increasing *Staphylococcus aureus* Antibiotic Susceptibility through Membrane Charge Manipulation using Peptides and Small Molecules

Chelsea Weidman

Advisor: Professor Jianmin Gao

With the rapid evolution of antibiotic resistance, the need for more effective antibiotics is imminent. Bacterial membranes are an appealing target due to their accessibility and relatively conserved structures. Membrane targeting antibiotics, especially cationic antimicrobial peptides (CAMPs) such as host defense peptides, have been increasingly explored as novel antibiotics and tunable innate antimicrobials. The latter could be achieved by treatment with an antibiotic adjuvant: a compound that would increase the potency of host CAMPs without killing the bacteria on its own. Boosting the host's own immune system with an adjuvant is beneficial over using antibiotics and would theoretically avoid triggering bacterial resistance.

One mechanism of bacterial resistance is increasing the cationic charge of the membrane. As CAMPs are electrostatically attracted to anionic bacterial membranes, making the membrane more cationic decreases that attraction, rendering CAMPs less effective. To target this resistance mechanism chemically, two antibiotic adjuvant strategies were explored as co-treatments with various CAMPs: membrane targeting peptides used to bind and block surface amines, and small molecules used to either acetylate surface amines or convert a cationic membrane phospholipid to an anionic phospholipid.

Co-treatment of the *Staphylococcus aureus* (*S. aureus*) membrane targeting peptide KAM-CT and various CAMPs increased *S. aureus* susceptibility to those CAMPs. Bacterial surface

acetylation using sulfo-NHS-acetate followed by CAMP treatment caused up to 10 times increased CAMP potency. Hydrazine and hydroxylamine were shown to cleave the lysine moiety from the lysyl-phosphatidylglycerol (Lys-PG) phospholipid to generate phosphatidylglycerol (PG) in liposome models. *S. aureus* was treated with a hydroxylamine-CAMP conjugate, but it showed decreased antibiotic activity compared to the CAMP alone. To better understand what was happening in the bacteria, a novel Lys-PG quantification protocol was created by fluorophore labeling Lys-PG and quantifying the labeled Lys-PG via normal phase high-performance liquid chromatography (NP-HPLC).

Cyclic peptides, such as KAM-CT, represent complex yet synthetically attainable moieties that could be used as novel antibiotics adjuvants. Expanding the repertoire of reversible covalent chemistries, especially those applied to peptide cyclization, is desirable due to the high potency and selectivity of such interactions. Herein, we also describe a novel reversible covalent chemistry between 2-formylphenylboronic acid (FPBA) and 2,3-diaminopropionic acid (Dap): the imidazolidino boronate (IzB) conjugate. It was found to be potent (K_d = 100 μM) and quickly reversible (t_1 = ~6 sec) under physiological conditions. IzB formation was successfully employed as a peptide cyclization strategy as there was little interference from biologically relevant small molecules, except cysteine. Cysteine interference was utilized to create “smart” peptides that can linearize upon increasing cysteine concentrations via thiazolidino boronate (TzB) formation with the FPBA moiety in the peptide. Such “smart” peptides could be used as pH-responsive peptides or cysteine sensors able to report on the cysteine concentration in complex media.

To my mom, Kyle, and my friends:

Thank you for your unconditional love and support,

I am so grateful.

ACKNOWLEDGMENTS

I would like to thank my advisor, Professor Jianmin Gao, for his support, knowledge and encouragement. He has helped me grow tremendously as a scientist and insightful thinker.

I would also like to thank the other members of my committee, Professor Eranthie Weerapana and Professor Jia Niu, for taking the time to read my thesis and providing helpful feedback.

Thank you to my co-workers for their advice and help with experiments and feedback on this thesis. Your friendship made being in lab more enjoyable.

I would especially like to thank the two most important people in my life: my mom and Kyle. I love you both to the moon and back!

TABLE OF CONTENTS

List of Figures ix

List of Schemes xi

List of Tables xii

Abbreviations and Acronyms i

CHAPTER 1: Introduction 1

1.1 General Antibiotic Resistance 2

1.2 The Bacterial Membrane 3

1.3 *Staphylococcus aureus* Phospholipids 5

1.4 Cationic Antimicrobial Peptides and Host Immunity 6

1.5 Studies on Lys-PG Synthesis and CAMP Resistance 7

1.6 Other Membrane Charge Altering Modifications Leading to CAMP Resistance 9

1.7 Peptide-based Antibiotics and Antibiotic Adjuvants 10

1.8 Reversible Covalent Chemistries for Peptide Cyclization 12

1.9 Experimental Goals 13

1.10 References 14

CHAPTER 2: Targeting Amines on the Staphylococcus aureus Membrane to Modulate Charge and Increase Antibiotic susceptibility 17

2.1 Lys-PG Binding Using Peptides 18

2.1.1 Protegrin-1 Synthesis 19

2.1.2 Lys-PG Binding Peptide and CAMP Co-Treatments 20

2.2 Lys-PG Modification Using Small Molecules 22

2.2.1 Lys-PG Acetylation 22

2.2.2 Lys-PG Cleavage with Pig Liver Esterase 24

2.2.3 Lys-PG Cleavage with Hydrazine- and Hydroxylamine-based Nucleophiles 24

2.2.4 Hydrazine or Hydroxylamine-Induced Cleavage of Lys-OMe 25

2.3 Activity of a Hydroxylamine-Functionalized CAMP: AOA-Hlys 27

2.4 Hlys and AOA-Hlys Liposome Binding 29

2.5 Lys-PG Quantification 29

2.5.1 Phospholipid 1D TLC 30

2.5.2 Phospholipid Normal-Phase Analytical HPLC 31

2.6 Conclusions 34

2.7 Experimental Procedures 36

2.7.1 General Methods 36

2.7.2 Peptide Synthesis and Characterization 37

2.7.3 Minimal Inhibitory Concentration (MIC) Assay 38
2.7.4 Cell Killing Assay 39
2.7.5 Small Molecule and Peptide Liposome Treatment 40
2.7.6 Lipid ESI-Mass Spectrometry Analysis 42
2.7.7 Hydrazine or Hydroxylamine-Induced Lys-OMe Cleavage NMR Kinetic Study 43
2.7.8 Tryptophan Fluorescence 43
2.7.9 *S. aureus* Lipid Extraction 44
2.7.10 Lipid TLC Analysis 44
2.7.11 Lipid Fluorescein Labeling 45
2.7.12 Lipid Analytical HPLC Analysis 45

2.8 References 46

CHAPTER 3: 2-Formylphenylboronic Acid-Based Reversible Covalent Chemistries as A Novel Peptide Cyclization Strategy 47

3.1 Reversible Bioorthogonal Chemistries 48

3.2 Previous Work: Thiazolidino Boronate (TzB) Formation 48

3.3 Imidazolidino Boronate (IzB) Formation 49
3.3.1 IzB Formation Between Dap and FPBA 49
3.3.2 The Bioorthogonality of IzB Conjugation 53

3.4 Attempts at TzB-Mediated Peptide Cyclization 54
3.4.1 Initial Peptide Synthetic Scheme 54
3.4.2 CW1 Peptide Synthesis 55
3.4.3 Serine Analog CW2 Peptide Synthesis 56
3.4.4 CW3 and CW4 Peptide Synthesis 57
3.4.5 Modified Peptide Synthetic Scheme 58
3.4.6 CW5 Peptide Synthesis 59
3.4.7 CW6 Peptide Synthesis 59

3.5 IzB-Mediated Peptide Cyclization with KL21 and KL22 60
3.5.1 KL21 and KL22 Peptide Synthesis 60
3.5.2 pH-Dependent Peptide Cyclization 61
3.5.3 Stability of IzB-Cyclized KL21 Peptide 63

3.6 Potential Application: Cysteine Sensing 63
3.6.1 Cysteine Reactivity of IzB-Cyclized Peptides 64
3.6.2 Cys-Dependent Linearization and Cys Oxidation of KL21 in FBS 65

3.7 Conclusions 67

3.8 Experimental Procedures 68
3.8.1 General Methods 68
3.8.2 NMR Studies of FPBA Conjugation with Dap 68
3.8.3 IzB Complex Crystallographic Information 68
3.8.4 Kinetic and Thermodynamic Studies of the IzB Complex Formation 69
3.8.5 Probing Small Molecule Interference of IzB Formation via NMR 71
3.8.6 Peptide Synthesis and Characterization 71
3.8.7 pH-Dependent Cyclization of KL21 and KL22 75
3.8.8 Probing Small Molecule Interference of Kl21 Cyclization via NMR 75

3.8.9 Cysteine-Induced KL21 Linearization ____ 75
3.8.10 Cysteine-Induced KL21 Linearization in Fetal Bovine Serum (FBS) ____ 76
3.8.11 KL21 Cysteine Oxidation in FBS ____ 76
3.8.12 Synthesis and Characterization of the Carboxylic Acid Derivative of FPBA (**4**) ____ 77

3.9 References ____ 83

CHAPTER 4: Conclusions and Future Directions ____ 85

4.1 Targeting *S. aureus* Membrane Amines ____ 86

4.2 FPBA-Based Reversible Covalent Chemistries ____ 88

4.3 Future Directions ____ 89

LIST OF FIGURES

Figure 1-1. Timeline of antibiotic clinical use and resistance

Figure 1-2. Gram-negative and Gram-positive bacterial membranes

Figure 1-3. Structures of mammalian and bacterial phospholipids

Figure 1-4. Membrane disrupting mechanism of action of CAMPs

Figure 1-5. CAMP-sensitive and CAMP-resistant membranes

Figure 1-6. Staphylococcal CAMP sensing and resistance mechanisms

Figure 1-7. Reversible covalent chemistries with APBA and FPBA

Figure 2-1. Structures of Lys-PG binding peptides and CAMPs used

Figure 2-2. Protegrin-1 characterization

Figure 2-3. Protegrin-1 circular dichroism

Figure 2-4. MIC assay results with KAM-CT and CAMP co-treatment

Figure 2-5. *S. aureus* acetylation followed by CAMP treatment

Figure 2-6. Lys-PG cleavage with small molecule nucleophiles

Figure 2-7. Lysine methyl ester cleavage with hydrazine or hydroxylamine

Figure 2-8. Hlys and AOA-Hlys activity with liposomes and *S. aureus* killing

Figure 2-9. Hlys and AOA-Hlys liposome binding via Trp fluorescence

Figure 2-10. *S. aureus* phospholipid TLC

Figure 2-11. Analytical NP-HPLC and MS of fluorophore-labeled *S. aureus* lipids

Figure 2-12. Analytical NP-HPLC of acetylated *S. aureus* lipids

Figure 3-1. Small molecule TzB and IzB NMR spectra

Figure 3-2. Kinetics of IzB formation between FPBA and Dap

Figure 3-3. Crystal structure of tetrameric IzB complex

Figure 3-4. Small molecule competition with FPBA-Dap IzB

Figure 3-5. LCMS of CW1 through CW4

Figure 3-6. Structure and LCMS of CW5 and CW6

Figure 3-7. UV and LCMS of KL21

Figure 3-8. Structure and NMRs showing pH-dependent KL21 and KL22 cyclization

Figure 3-9. Small molecule competition with cyclic KL21

Figure 3-10. Cys titration NMRs of KL21 and KL22

Figure 3-11. Cys responsiveness and oxidation of KL21 in FBS

LIST OF SCHEMES

Scheme 2-1. Lys-PG small molecule modifications

Scheme 3-1. Comparison of TzB and IzB conjugations

Scheme 3-2. Initial N-terminal Cys and FPBA-containing peptide synthesis (CW1 – CW4)

Scheme 3-3. Modified peptide synthesis (CW5 and CW6)

Scheme 3-4. KL21 and KL22 peptide synthesis

Scheme 3-5. Cartoon depicting Cys-mediated peptide linearization

LIST OF TABLES

Table 1-1. Structures and sequences of common mammalian CAMPs

Table 3-1. IzB crystal data and structure refinement

Table 3-2. Atomic coordinates of IzB crystal structure

Table 3-3. TzB- and IzB-cyclized peptide names and sequences

ABBREVIATIONS AND ACRONYMS

A, Ala	Alanine
Acm	Acetamidomethyl
APBA	2-Acetylphenylboronic acid
Boc	*tert*-Butyloxycarbonyl
C, Cys	Cysteine
CAMP	Cationic antimicrobial peptide
CD	Circular dichroism
CL	Cardiolipin
Dap	2,3-Diaminopropionic acid
DCM	Dichloromethane
DMF	*N,N*-Dimethylformamide
DMSO	Dimethyl sulfoxide
EDA	Ethylenediamine
EDT	1,2-Ethanedithiol
ESI	Electrospray ionization
EtOH	Ethanol
FAM	Fluorescein
Fm	9-Fluorenylmethyl
Fmoc	Fluorenylmethyloxycarbonyl
FPBA	2-Formylphenylboronic acid
G, Gly	Glycine
HBTU	*o*-(Benzotriazol-1-yl)-*N,N,N',N'*-tetramethyluronium hexafluorophosphate
IzB	Imidazolidino boronate
K, Lys	Lysine
LC	Liquid chromatography

Lys-PG	Lysyl-phosphatidylglycerol
Lysyl-DOPG	1,2-dioleoyl-*sn*-glycero-3-[phospho-*rac*-(3-lysyl(1-glycerol))]
MeOH	Methanol
MIC	Minimal inhibitory concentration
MprF	Multiple peptide resistance factor
MS	Mass spectrometry
NMM	*N*-methylmorpholine
NMR	Nuclear magnetic resonance
NP-HPLC	Normal phase high-performance liquid chromatography
PC	Phosphatidylcholine
PG	Phosphatidylglycerol
POPG	1-palmitoyl-2-oleoyl-*sn*-glycero-3-phospho-(1'-*rac*-glycerol)
RP-HPLC	Reverse phase high-performance liquid chromatography
S. aureus	*Staphylococcus aureus*
SM	Sphingomyelin
SPPS	Solid-phase peptide synthesis
tBu	*tert*-Butyl
TCEP	Tris(2-carboxyethyl)phosphine
TFA	Trifluoroacetic acid
Trt	Triphenylmethyl
TzB	Thiazolidino boronate
V, Val	Valine
W, Trp	Tryptophan

CHAPTER 1: INTRODUCTION

1.1 General Antibiotic Resistance

Bacterial resistance is an ever-growing problem for which discovery of novel antibiotics is not occurring at the pace needed to keep up with clinical demand. Resistance towards antibiotics has emerged in as little as one year after the onset of clinical application. Notably, antibiotic discovery has slowed significantly since the end of the "Golden Age of Antibiotics" in the 1960s where natural products were isolated from culturable soil-dwelling bacteria and screened for antimicrobial activity, leading to identification of the major types of antibiotics (**Figure 1-1**).[1] Once those resources were exhausted, novel antibiotics were innovated by synthetically altering the existing natural products to induce increased potency, generating second generation antibiotics. Altering natural products is synthetically challenging as most compounds are structurally complex, such as vancomycin. However, the lag in antibiotic discovery that has resulted allowed bacteria to gain widespread resistance.

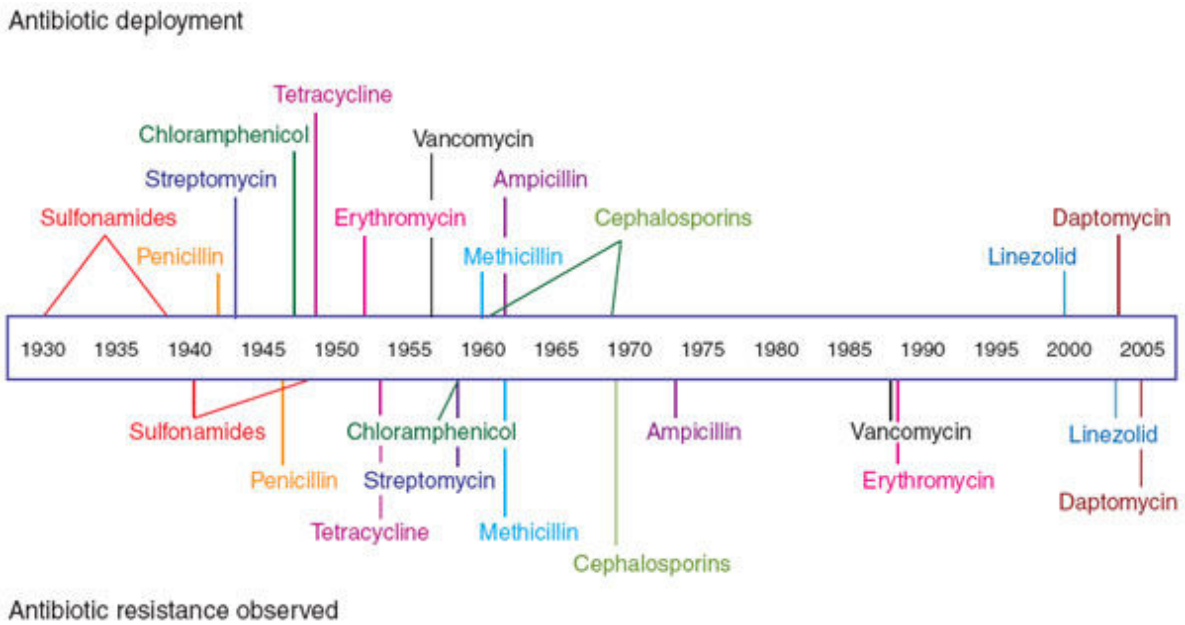

Figure 1-1: Year of antibiotic clinical use (top) and clinical antibiotic resistance observed (bottom). Adapted from Clatworthy, A. E.; Pierson, E.; Hung, D. T. *Nat Chem Biol* **2007**, *3* (9), 541–548.

Although antibiotic resistance was inevitable because bacteria evolve, it was exacerbated by a variety of factors: non-specific bacterial resistance mechanisms, including efflux pump upregulation to export antibiotics[2]; limited mechanisms of action, allowing for resistance to entire classes of antibiotics[1]; and horizontal gene transfer spreading resistance genes between species, creating multi-drug resistant bacteria.[3]

In efforts to decrease the appearance of resistance and maintain clinical efficacy, membrane targeting antibiotics have become increasingly popular. The bacterial membrane is an appealing target because it is easily accessible and comprised of relatively conserved structures. A conserved target coupled with the rapid antimicrobial activity of membrane targeting antibiotics[4] make resistance against membrane targeting antibiotics more difficult to select for.[5] This makes targeting bacterial membranes an effective approach to combat slow-growing or difficult to treat dormant bacteria.[6]

1.2 The Bacterial Membrane

Bacterial membranes act as a semi-permeable barrier which controls the transport of molecules and provides protection to the cellular contents.[7] All bacteria have an innermost cytoplasmic membrane, composed primarily of phospholipids. Gram-positive bacteria have a thick outer layer of peptidoglycan, while Gram-negative bacteria have a thin peptidoglycan layer with an outer membrane composed primarily of lipopolysaccharides (**Figure 1-2**).

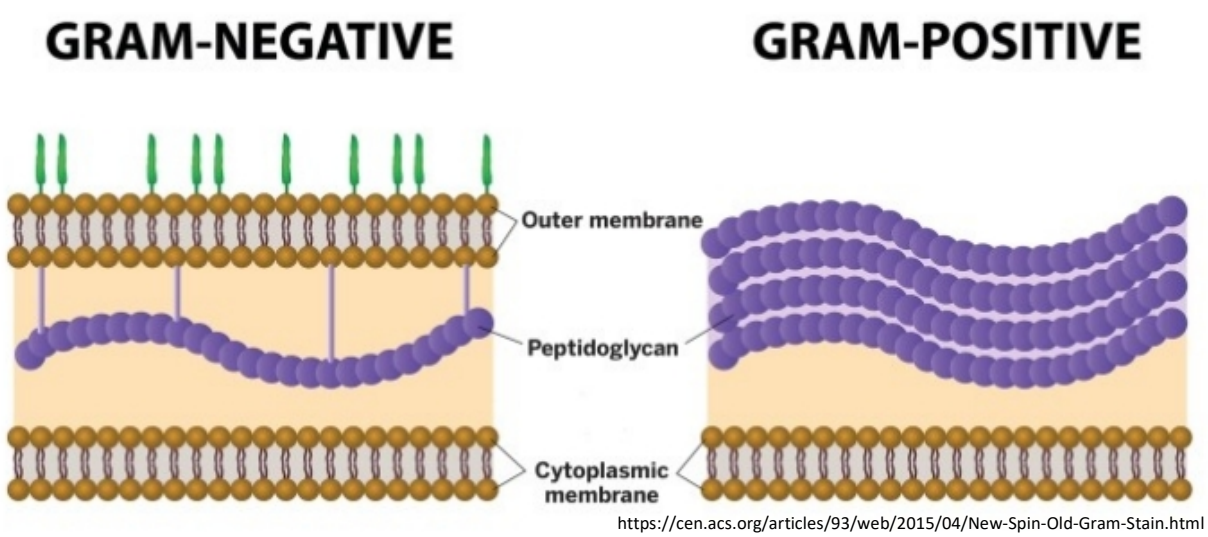

Figure 1-2: Depiction of the membrane structures of Gram-negative and Gram-positive bacteria.

The phospholipid composition of the cytoplasmic membrane of mammalian cells is distinct from bacteria, allowing for differentiation. The major mammalian phospholipids are zwitterionic sphingomyelin (SM) and phosphatidylcholine (PC), which afford neutral membranes (**Figure 1-3A**). In bacteria, especially Gram-positive species, the major phospholipids are anionic cardiolipin (CL) and phosphatidylglycerol (PG), generating anionic membranes. In some bacterial species, the cationic phospholipid lysyl-PG (Lys-PG) is also present, which can tune the membrane charge.[8] Exploiting this charge difference allows for identification of bacteria in mammalian hosts.

1.3 *Staphylococcus aureus* Phospholipids

Gram-positive *Staphylococcus aureus* (*S. aureus*) cytoplasmic membranes are composed of three main types of phospholipids: CL, PG, and Lys-PG, which is the lysine ester of PG (**Figure 1-3B**). The percentages of each relative to total phospholipids vary based on environmental conditions and stage of cell growth, but are typically around 38-76% PG, 5-30% CL, and 14-38% Lys-PG.[9,10]

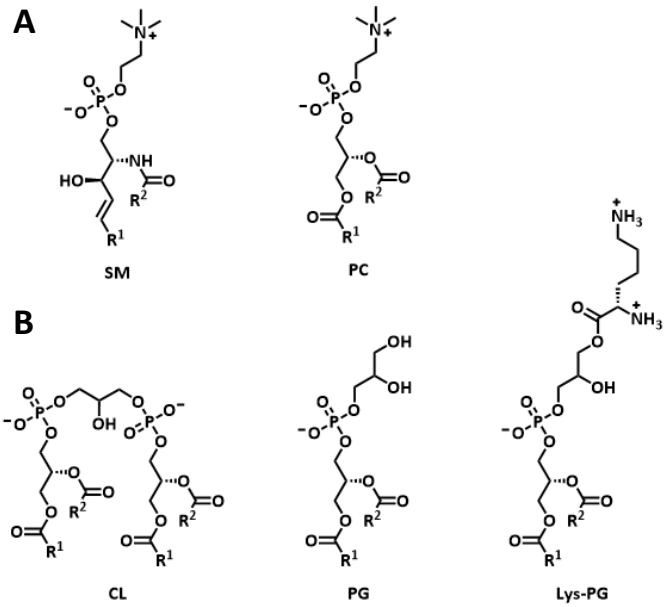

Figure 1-3: Structures of the major mammalian (A) and bacterial (B) phospholipids. Zwitterionic sphingomyelin (SM) and phosphatidylcholine (PC) primarily compose the mammalian cytosolic membrane, while anionic cardiolipin (CL) and phosphatidylglycerol (PG) are the main components of the bacterial cytosolic membrane. Cationic lysyl-PG (Lys-PG) is also present in some bacterial species.

Both PG and CL, also known as di-PG, have negatively charged headgroups, generating net negatively charged bacterial membranes. However, the lysine residue of Lys-PG carries two cationic charges at physiological pH, which makes the headgroup cationic. By controlling the amount of Lys-PG displayed, bacteria can adjust their membranes to become more cationic, causing less potency from antibiotics that typically exploit the net negative bacterial membrane charge, such as cationic antimicrobial peptides (CAMPs).

1.4 Cationic Antimicrobial Peptides and Host Immunity

CAMPs are short 12-50 residue peptides with a net cationic charge ranging from +2 to +7.[11] They are ubiquitous throughout all species of life and are a key part of the innate immune system, possessing broad spectrum antimicrobial activity as well as more recently discovered immunomodulatory effects.[12,13] While CAMPs have highly variable structures and sequences, they all possess two common features: 1) cationic charge due to the abundance of basic residues, such as arginine and lysine, and 2) amphiphilicity as they possess both hydrophilic cationic residues and hydrophobic residues (**Table 1-1**). While the cationic residues create an electrostatic attraction to the anionic bacterial membranes, the hydrophobic residues allow for partitioning of the peptides into the phospholipid membrane, inducing antimicrobial activity, typically through the formation of membrane pores or disruption of membrane structure (**Figure 1-4**).[14]

Peptide	Structural class	Sequence[a]
Rabbit α-defensin (NP-1)	β-sheet	VVC$_1$AC$_2$**RR**ALC$_3$LP**R**E**RR**AGFC$_3$**R**I**R**G**R**IHLC$_2$C$_1$**RR**
Human β-defensin 1	β-sheet	DHYNC$_1$VSSGQC$_2$LYSAC$_3$PIFT**K**IQGTC$_2$Y**R**G**K**A**K**C$_1$C$_3$**K**
Pig protegrin 1	β-sheet	**R**GG**R**LC$_1$YC$_2$**RRR**FC$_2$VC$_1$VG**R***
Human LL-37	α-helical	LLGDFF**RK**S**K**E**K**IG**K**EF**KR**IVQ**R**I**K**DFL**R**NLVP**R**TES*
Human histatin 5	α-helical	DSHA**KR**HHGY**KRK**FHE**K**HHSH**R**GY*
Cattle indolicidin	Extended	ILPW**K**WPWWPW**RR***
Pig PR39	Extended	**RRR**P**R**PPYLP**R**P**R**PPPFFPP**R**LPP**R**IPPGFPP**R**FPP**R**FP*
Cattle bactenecin	Loop	**R**LC$_1$**R**IVVI**R**VC$_1$**R**

[a]One letter amino acid code with the following additions: positively charged residues at neutral pH are in bold; the subscript numbers represent amino acids that are joined by cysteine disulfides; a star at the end of a peptide implies that the peptide is known to be amidated at its carboxy terminus.

Table 1-1: Structures and sequences of common mammalian cationic antimicrobial peptides. Adapted from Hancock, R. E. W.; Diamond, G. *Trends in Microbiology* **2000**, *8* (9), 402–410.

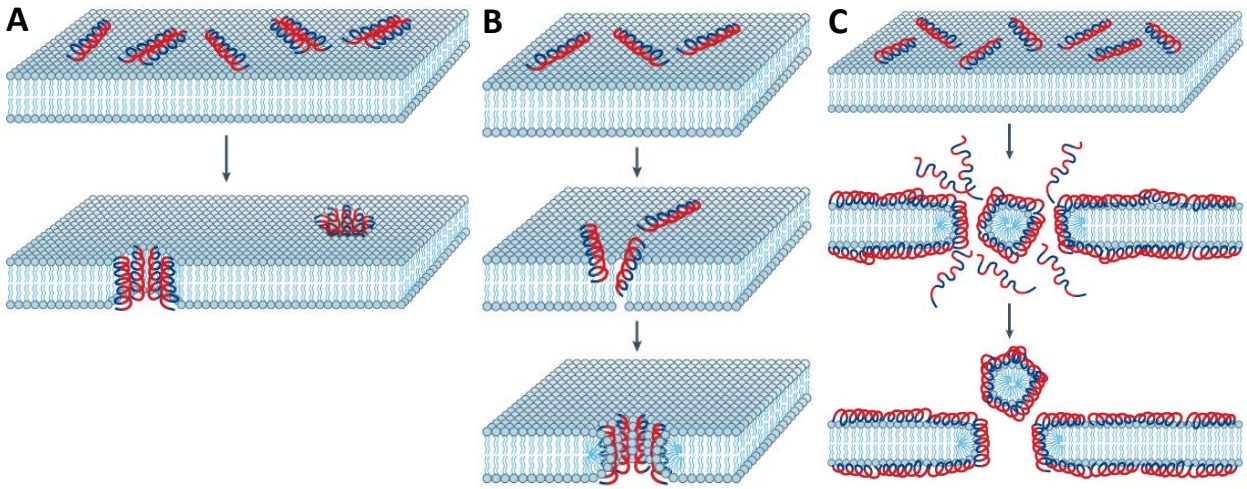

Figure 1-4: Membrane disrupting mechanisms of action of CAMPs. The barrel-stave (A), toroidal pore (B), and carpet (C) models of CAMP-induced bacterial killing. Adapted from Brogden, K. A. *Nat Rev Micro* **2005**, *3* (3), 238.

The majority of *S. aureus* phospholipids are anionic PG and CL, which attract CAMPs selectively to bacterial cells over the neutral mammalian cells.[11] However, as the membrane becomes more cationic with increasing Lys-PG amounts, the electrostatic interaction between the membrane and CAMPs is disrupted, leading to CAMP resistance via decreased membrane binding and activity (**Figure 1-5**).

1.5 Studies on Lys-PG Synthesis and CAMP Resistance

Although Lys-PG was first reported in the early 1960s[22–24], the enzyme responsible for its synthesis, multiple peptide resistance factor (MprF), was not discovered until 2001.[25,26] MprF is a transmembrane protein with two distinct functionalities: a soluble C-terminal Lys-PG synthase

domain and a transmembrane N-terminal flippase domain, which flips the newly synthesized Lys-PG from the inner leaflet to the outer leaflet.[27,28]

Lys-PG is correlated with an increased resistance to various antibiotics, especially CAMPs.[25,29,30] Up to a 30-fold decrease in minimum inhibitory concentration (MIC) of various CAMPs was observed in an *mprF* knockout *S. aureus* strain expressing no Lys-PG, in comparison to wild type *S. aureus*.[25] Subsequent studies have corroborated those results, displaying increased susceptibility of the *S. aureus* *mprF* knockout to antibiotics such as vancomycin[31], daptomycin[27], and methicillin[32], as well as CAMPs such as gallidermin.[27] Significantly lower antimicrobial MIC values *in vitro* and attenuated virulence in mice carrying a *mprF* knockout further demonstrate the importance of Lys-PG to *S. aureus* resistance and pathogenicity.[25]

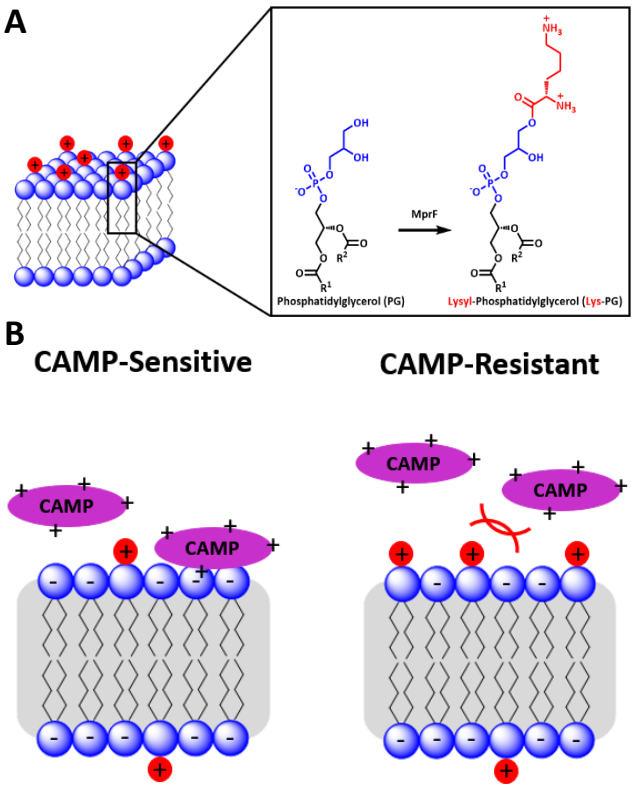

Figure 1-5: Depiction of Lys-PG on a bacterial membrane (A) and the different membrane compositions between cationic antimicrobial peptide (CAMP)-sensitive and CAMP-resistant bacteria (B).

Homologs of MprF have also been identified in a variety of other human pathogens, including *Pseudomonas aeruginosa*, *Bacillus subtilis*, *Enterococcus faecalis*, *Mycobacterium tuberculosis*, and *Mycobacterium leprae*.[25] In total, 347 homologous sequences have been identified in 31 Gram-positive genera, 59 Gram-negative genera, and three species of

archaea.[29] Lys-PG has also been identified in some of those bacteria species[25], as well as other aminoacyl-PG derivatives, such as Ala-PG and Arg-PG, suggesting that homologs from different species have different selectivities for which amino acid is loaded onto PG.[29,33]

1.6 Other Membrane Charge Altering Modifications Leading to CAMP Resistance

In addition to MprF-mediated lysyl modification of PG, staphylococci have also been found to modify teichoic acids with D-alanine through the *dlt* operon to reduce the negative charge of the cell wall, similarly modulating CAMP binding.[34] Teichoic acids are the carbohydrate-based polymers that comprise the *S. aureus* peptidoglycan layer outside of the cytoplasmic membrane. Moreover, amino-sugar glycosylation and phosphoethanolamine incorporation into the lipid A core of lipopolysaccharide in Gram-negative bacteria have also been shown to increase the overall charge of the outer membrane.[5]

In addition to cell surface charge modification, staphylococci have evolved other CAMP resistance mechanisms, including non-specific proteases, efflux pumps, and biofilm formation (**Figure 1-6**). Generally, CAMP resistance mechanisms are upregulated upon CAMP detection by sensing systems, such as the antimicrobial peptide sensor ApsSRX (*S. aureus* homolog is the glycopeptide resistance-associated sensor GraSRX) and vancomycin-resistance associated genes VraFG.[35] In the ApsSRX system, CAMP presence is detected via binding to a highly anionic 9 residue extracellular loop on ApsS, the transmembrane sensor kinase. ApsS phosphorylates ApsR, the response regulator, which causes a cascade resulting in upregulation of MprF and the *dlt* operon. ApsX is a cytosolic protein of unknown function known to interact with ApsS and required

for transduction of the CAMP signal from ApsS to ApsR. VraFG encodes an ABC transporter, which must act in conjunction with the ApsSRX system to detoxify CAMPs from bacteria. Specifically, the extracellular loop of the VraG permease has been shown to play an essential role in CAMP sensing.[36]

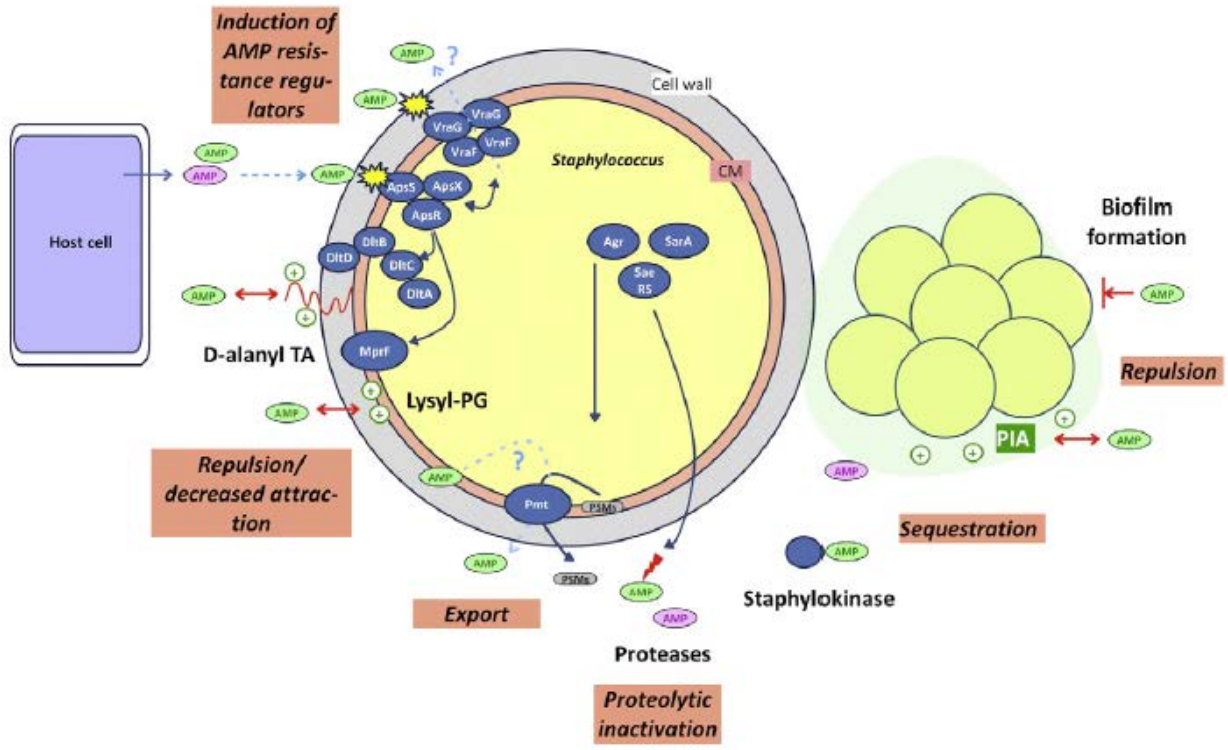

Figure 1-6: Various staphylococci CAMP sensing and resistance mechanisms. Adapted from Joo, H.-S.; Otto, M. *Biochimica et Biophysica Acta (BBA) - Biomembranes* **2015**, *1848* (11, Part B), 3055–3061.

1.7 Peptide-based Antibiotics and Antibiotic Adjuvants

CAMPs initially gained attention as potentially novel antibiotics because of their membrane-targeting antimicrobial activity, but recent studies have shown their antimicrobial

activity is significantly reduced in physiologically relevant salt concentrations, as well as in serum.[11,15] However, increasing evidence has shown that membrane disruption is only one of the mechanisms of antimicrobial activity that CAMPs possess, in addition to immune modulation[16], chemotactic activities, and inflammatory response management.[11,13] Having multiple mechanisms of action makes CAMPs more attractive for use as novel antibiotics due to a lower risk of developing resistance.[12]

CAMPs, especially host defense peptides, are not only being explored as novel antimicrobial drugs, but also as tunable innate antimicrobials.[17] The latter could be achieved by treatment with an antibiotic adjuvant, which would not kill the bacteria on its own, but increase the potency of the host CAMPs. Thus, bacteria could be rendered re-susceptible to host CAMPs through membrane manipulation to increase their net negative charge. This strategy is ideal as it would boost the host's own immune system without the need for administering an antibiotic and would theoretically avoid triggering resistance to the antibiotic adjuvant as it would not directly kill bacteria.

A few such co-treatments have been reported recently, involving anti-MprF antibodies to prevent Lys-PG expression in combination with antibiotics such as daptomycin and nisin in *S. aureus*[18], combinatorial β-lactam and daptomycin therapy to induce a cell surface charge reduction in clinical methicillin-resistant *S. aureus* (MRSA) strains[19,20], or non-lethal outer membrane-active small molecules with antibiotics such as vancomycin, rifampicin, and novobiocin in Gram-negative pathogens.[21]

1.8 Reversible Covalent Chemistries for Peptide Cyclization

Cyclic peptides represent complex yet synthetically accessible moieties which could be utilized to target bacterial membranes as novel antibiotics or non-lethal membrane modifiers. Accessing cyclic peptide scaffolds is advantageous as it provides preorganization and higher target binding affinity. Although there are many strategies for peptide cyclization, most are not reversible, excluding disulfide chemistry.[37] Reversibility is key as it could be used to tune the peptide activity to create responsive "smart" peptides, which could exert their own activity upon linearization or report on the presence of reactive metabolites. Discovering novel reversible covalent chemistries could be beneficial to developing peptide cyclization techniques.

Of the wide array of bioorthogonal reactions available[38,39], only a handful utilize reversible covalent chemistry, such as *ortho*-boronic acid functionalized iminoboronate formation.[8,40–43] Our lab previously demonstrated the rapid and reversible peptide cyclization between the ε-amine of a lysine residue and a novel amino acid containing a 2-acetylphenylboronic acid (APBA) moiety.[37] The *ortho*-boronic acid stabilizes the imine via formation of a dative bond upon condensation to form iminoboronates, allowing increased conjugate stability while maintaining rapid reversibility (**Figure 1-7A**). The iminoboronate-based peptide cyclization was found to be responsive to pH, oxidation, and small molecules, creating "smart" peptides that are stable to endogenous nucleophiles yet can be readily linearized upon orthogonal induction.

Taking advantage of the added reactivity of the aldehyde in 2-formylphenylboronic acid (FPBA) has enabled formation of iminoboronate-stabilized thiazolidines between free or N-terminal cysteine residues and FPBA, called thiazolidino boronates (TzB) (**Figure 1-7B**).[44] This strategy is advantageous because it utilizes an endogenous residue as one bioorthogonal reaction member while maintaining selectivity for the 1,2 aminothiol moiety over simple amines or thiols. Exploring the scope of FPBA-based reversible covalent chemistries could lead to more novel conjugation chemistries. Adding reversible reactions to the bioorthogonal "toolbox" enables expansion of possible applications.

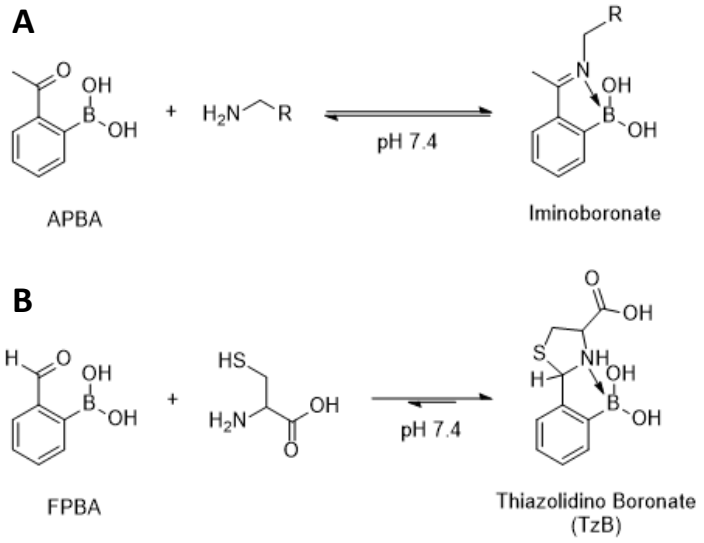

Figure 1-7: Reversible covalent chemistries between APBA with amines (A) and FPBA with cysteine (B).

1.9 Experimental Goals

In efforts to find novel antibiotic adjuvants, I have been exploring various ways to modulate *S. aureus* surface charge by targeting membrane amines, such as Lys-PG, with peptides and small molecules to increase bacterial susceptibility to CAMPs. This offers an advantage over genetic manipulations and knockout strains as we can study the electrostatic influence of CAMP effectiveness alone by directly manipulating the membrane surface charge. The reactivity of the Lys-PG headgroup's free amine can be utilized for peptide binding and small molecule

modification to neutralize the cationic charge and increase the membrane's net negative charge, with the goal of enabling more efficient CAMP activity.

A second project involves exploring novel FPBA-based reversible covalent chemistries for peptide cyclization applications. Expanding the repertoire of cyclization reactions is desirable as cyclic peptides possess enhanced biostability and binding affinity compared to linear peptides. These novel cyclic peptides could either be explored as antimicrobial drugs or non-lethal bacterial membrane-targeting antibiotic adjuvants.

1.10 References

(1) Lewis, K. *Nat. Rev. Drug Discov.* **2013**, *12* (5), 371–387.
(2) Blair, J. M. A.; Webber, M. A.; Baylay, A. J.; Ogbolu, D. O.; Piddock, L. J. V. *Nat. Rev. Microbiol.* **2015**, *13* (1), 42–51.
(3) Levy, S. B.; Marshall, B. *Nat. Med.* **2004**, *10*, S122–S129.
(4) Daugelavičius, R.; Bakiene˙, E.; Bamford, D. H. *Antimicrob. Agents Chemother.* **2000**, *44* (11), 2969–2978.
(5) Steinbuch, K. B.; Fridman, M. *Med. Chem. Commun.* **2016**, *7* (1), 86–102.
(6) Hurdle, J. G.; O'Neill, A. J.; Chopra, I.; Lee, R. E. *Nat. Rev. Microbiol.* **2011**, *9* (1), 62–75.
(7) van Meer, G.; Voelker, D. R.; Feigenson, G. W. *Nat. Rev. Mol. Cell Biol.* **2008**, *9* (2), 112–124.
(8) Bandyopadhyay, A.; McCarthy, K. A.; Kelly, M. A.; Gao, J. *Nat. Commun.* **2015**, *6*, 6561.
(9) Short, S. A.; White, D. C. *J. Bacteriol.* **1971**, *108* (1), 219–226.
(10) Haest, C. W. M.; De Gier, J.; Op Den Kamp, J. A. F.; Bartels, P.; Van Deenen, L. L. M. *Biochim. Biophys. Acta BBA - Biomembr.* **1972**, *255* (3), 720–733.
(11) Hancock, R. E. W.; Diamond, G. *Trends Microbiol.* **2000**, *8* (9), 402–410.
(12) Peschel, A.; Sahl, H.-G. *Nat. Rev. Microbiol.* **2006**, *4* (7), 529–536.
(13) Hilchie, A. L.; Wuerth, K.; Hancock, R. E. W. *Nat. Chem. Biol.* **2013**, *9* (12), 761–768.
(14) Brogden, K. A. *Nat. Rev. Microbiol.* **2005**, *3* (3), 238–250.
(15) Lai, J. R.; Epand, R. F.; Weisblum, B.; Epand, R. M.; Gellman, S. H. *Biochemistry (Mosc.)* **2006**, *45* (51), 15718–15730.
(16) Zerfas, B. L.; Gao, J. Recent Advances in Peptide Immunomodulators http://www.eurekaselect.com/132628/article (accessed Sep 25, 2017).
(17) Bastos, P.; Trindade, F.; da Costa, J.; Ferreira, R.; Vitorino, R. *Med. Res. Rev.* **2017**

(18) Ernst, C. M.; Peschel, A. P.; Kraus, A.; Tesar, M. Anti-Staphylococcal Antibodies. WO2014096333 (A1), June 26, 2014.
(19) Dhand, A.; Bayer, A. S.; Pogliano, J.; Yang, S. J.; Bolaris, M.; Nizet, V.; Wang, G.; Sakoulas, G. *Clin. Infect. Dis. Off. Publ. Infect. Dis. Soc. Am. Clin. Infect. Dis. Off. Publ. Infect. Dis. Soc. Am.* **2011**, *53*, *53* (2, 2), 158, 158–163.
(20) Mehta, S.; Singh, C.; Plata, K. B.; Chanda, P. K.; Paul, A.; Riosa, S.; Rosato, R. R.; Rosato, A. E. *Antimicrob. Agents Chemother.* **2012**, *56* (12), 6192–6200.
(21) Stokes, J. M.; MacNair, C. R.; Ilyas, B.; French, S.; Côté, J.-P.; Bouwman, C.; Farha, M. A.; Sieron, A. O.; Whitfield, C.; Coombes, B. K.; Brown, E. D. *Nat. Microbiol.* **2017**, *2*, 17028.
(22) Macfarlane, M. G. *Nature* **1962**, *196* (4850), 136–138.
(23) Gale, E.; Folkes, J. *Biochem. J.* **1965**, *94* (2), 390–400.
(24) Houtsmuller, U. M. T.; Deenen, L. L. M. van. *Biochim. Biophys. Acta BBA - Lipids Lipid Metab.* **1965**, *106* (3), 564–576.
(25) Peschel, A.; Jack, R. W.; Otto, M.; Collins, L. V.; Staubitz, P.; Nicholson, G.; Kalbacher, H.; Nieuwenhuizen, W. F.; Jung, G.; Tarkowski, A.; Kessel, K. P. M. van; Strijp, J. A. G. van. *J. Exp. Med.* **2001**, *193* (9), 1067–1076.
(26) Oku, Y.; Kurokawa, K.; Ichihashi, N.; Sekimizu, K. *Microbiology* **2004**, *150* (1), 45–51.
(27) Ernst, C. M.; Staubitz, P.; Mishra, N. N.; Yang, S.-J.; Hornig, G.; Kalbacher, H.; Bayer, A. S.; Kraus, D.; Peschel, A. *PLOS Pathog.* **2009**, *5* (11), e1000660.
(28) Ernst, C. M.; Kuhn, S.; Slavetinsky, C. J.; Krismer, B.; Heilbronner, S.; Gekeler, C.; Kraus, D.; Wagner, S.; Peschel, A. *mBio* **2015**, *6* (1).
(29) Roy, H. *IUBMB Life* **2009**, *61* (10), 940–953.
(30) Roy, H.; Dare, K.; Ibba, M. *Mol. Microbiol.* **2009**, *71* (3), 547–550.
(31) Ruzin, A.; Severin, A.; Moghazeh, S. L.; Etienne, J.; Bradford, P. A.; Projan, S. J.; Shlaes, D. M. *Biochim. Biophys. Acta BBA - Gen. Subj.* **2003**, *1621* (2), 117–121.
(32) Nishi, H.; Komatsuzawa, H.; Fujiwara, T.; McCallum, N.; Sugai, M. *Antimicrob. Agents Chemother.* **2004**, *48* (12), 4800–4807.
(33) Roy, H.; Ibba, M. *J. Biol. Chem.* **2009**, *284* (43), 29677–29683.
(34) Peschel, A.; Otto, M.; Jack, R. W.; Kalbacher, H.; Jung, G.; Götz, F. *J. Biol. Chem.* **1999**, *274* (13), 8405–8410.
(35) Li, M.; Cha, D. J.; Lai, Y.; Villaruz, A. E.; Sturdevant, D. E.; Otto, M. *Mol. Microbiol.* **2007**, *66* (5), 1136–1147.
(36) Falord, M.; Karimova, G.; Hiron, A.; Msadek, T. *Antimicrob. Agents Chemother.* **2012**, *56* (2), 1047–1058.
(37) Bandyopadhyay, A.; Gao, J. *J. Am. Chem. Soc.* **2016**, *138* (7), 2098–2101.
(38) Sletten, E. M.; Bertozzi, C. R. *Angew. Chem. Int. Ed.* **2009**, *48* (38), 6974–6998.
(39) Lang, K.; Chin, J. W. *ACS Chem. Biol.* **2014**, *9* (1), 16–20.
(40) Bandyopadhyay, A.; Gao, J. *Chem. – Eur. J.* **2015**, *21* (42), 14748–14752.
(41) Cal, P. M. S. D.; Vicente, J. B.; Pires, E.; Coelho, A. V.; Veiros, L. F.; Cordeiro, C.; Gois, P. M. P. *J. Am. Chem. Soc.* **2012**, *134* (24), 10299–10305.
(42) Schmidt, P.; Stress, C.; Gillingham, D. *Chem. Sci.* **2015**, *6* (6), 3329–3333.
(43) B. Draganov, A.; Wang, K.; Holmes, J.; Damera, K.; Wang, D.; Dai, C.; Wang, B. *Chem. Commun.* **2015**, *51* (82), 15180–15183.
(44) Bandyopadhyay, A.; Cambray, S.; Gao, J. *Chem. Sci.* **2016**.

CHAPTER 2: TARGETING AMINES ON THE *STAPHYLOCOCCUS AUREUS* MEMBRANE TO MODULATE CHARGE AND INCREASE ANTIBIOTIC SUSCEPTIBILITY

2.1 Lys-PG Binding Using Peptides

Previously in our lab, two peptides were discovered that bind potently to *S. aureus* or Lys-PG specifically: KAM-CT, a cyclic peptide containing three APBA moieties, which bind *S. aureus* surface amines through iminoboronate formation; and MAK3, a linear peptide containing two APBA moieties. KAM-CT is a potent *S. aureus* binder (K_d = 100-200 nM) while MAK3 specifically binds to Lys-PG potently (*S. aureus* K_d = 50-100 nM). MAK3 was identified as a specific Lys-PG binder through phage display by directly screening against Lys-PG. The potency of these peptides as antibiotic adjuvants was examined by treating *S. aureus* with each peptide followed by CAMP treatment of Gramicidin A3R, a cationic Gramicidin A mutant developed in our lab; Protegrin-1, a highly cationic porcine defensin; or Vancomycin, a slightly cationic glycopeptide (**Figure 2-1**).

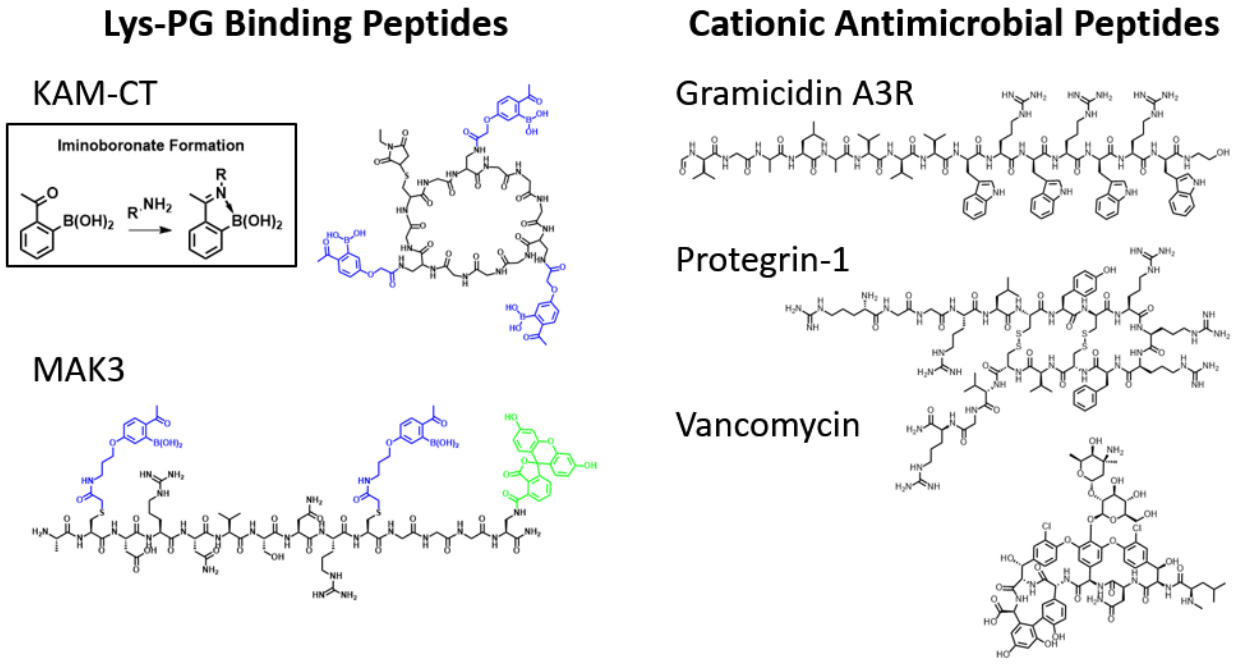

Figure 2-1: Structures of Lys-PG binding peptides and cationic antimicrobial peptides used for *S. aureus* treatment. Insert shows general iminoboronate formation between an amine and the APBA moiety on the Lys-PG binding peptides. APBA-functionalized side chains are indicated in blue.

2.1.1 Protegrin-1 Synthesis

While KAM-CT, MAK3, and Gramicidin A3R were provided by other lab members and Vancomycin was purchased, Protegrin-1 had to be synthesized. Based on previously reported syntheses[1–5], Protegrin-1 was synthesized using Fmoc-based SPPS. After N-terminal Fmoc deprotection and cleavage from resin, the crude peptide was reduced with dithiothreitol then purified using RP-HPLC. Air oxidation in PBS (pH 7.4) gave the oxidized peptide, which was purified via RP-HPLC (**Figure 2-2**).

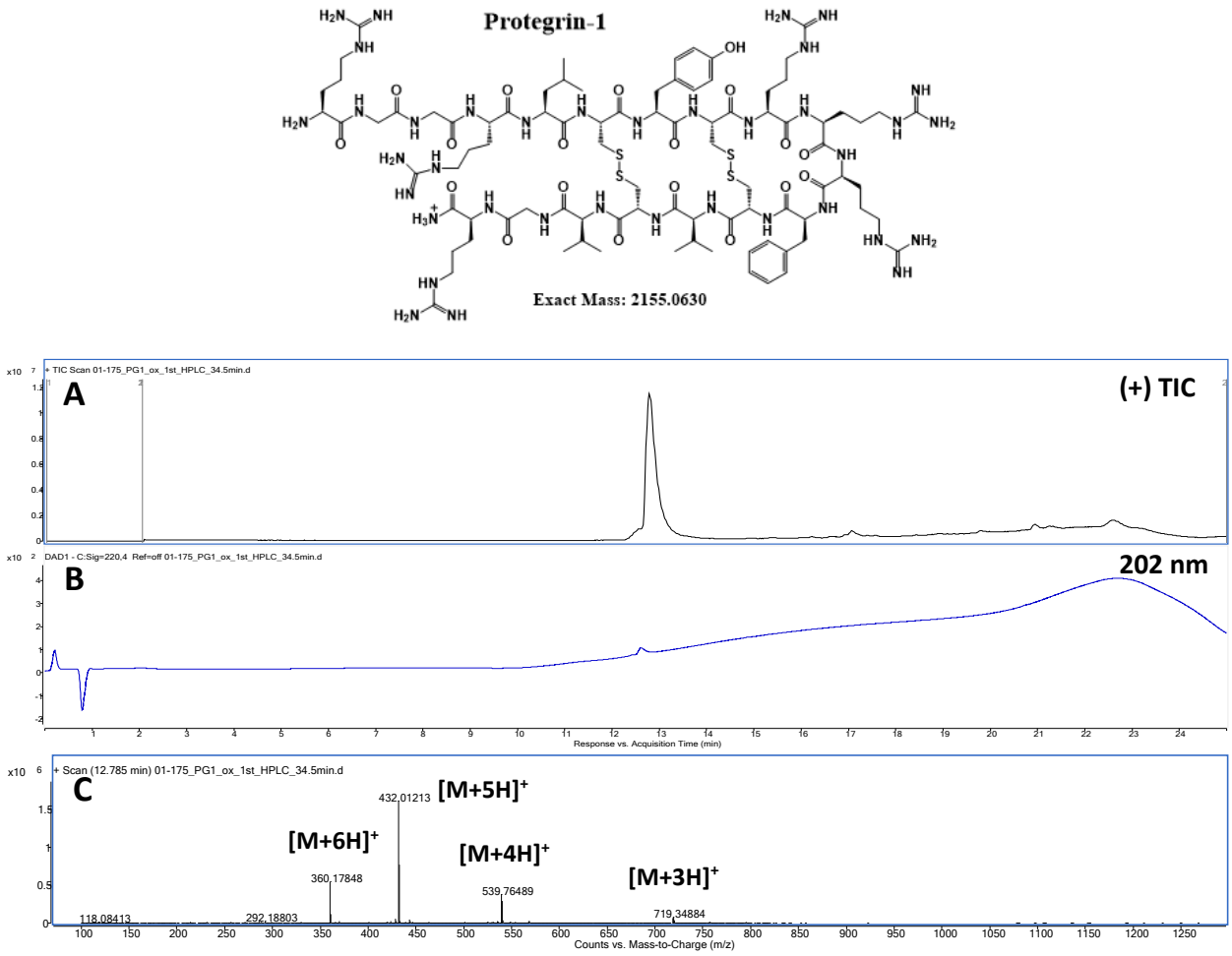

Figure 2-2: LC-MS TIC (A), UV trace (B), and mass-spec data (C) of oxidized Protegrin-1 (structure shown above).

Circular dichroism (CD) of pure oxidized Protegrin-1 was performed to verify the correct folding into a β-hairpin structure. The overall shape matches that expected of the correctly folded β-hairpin structure (**Figure 2-3**).[1]

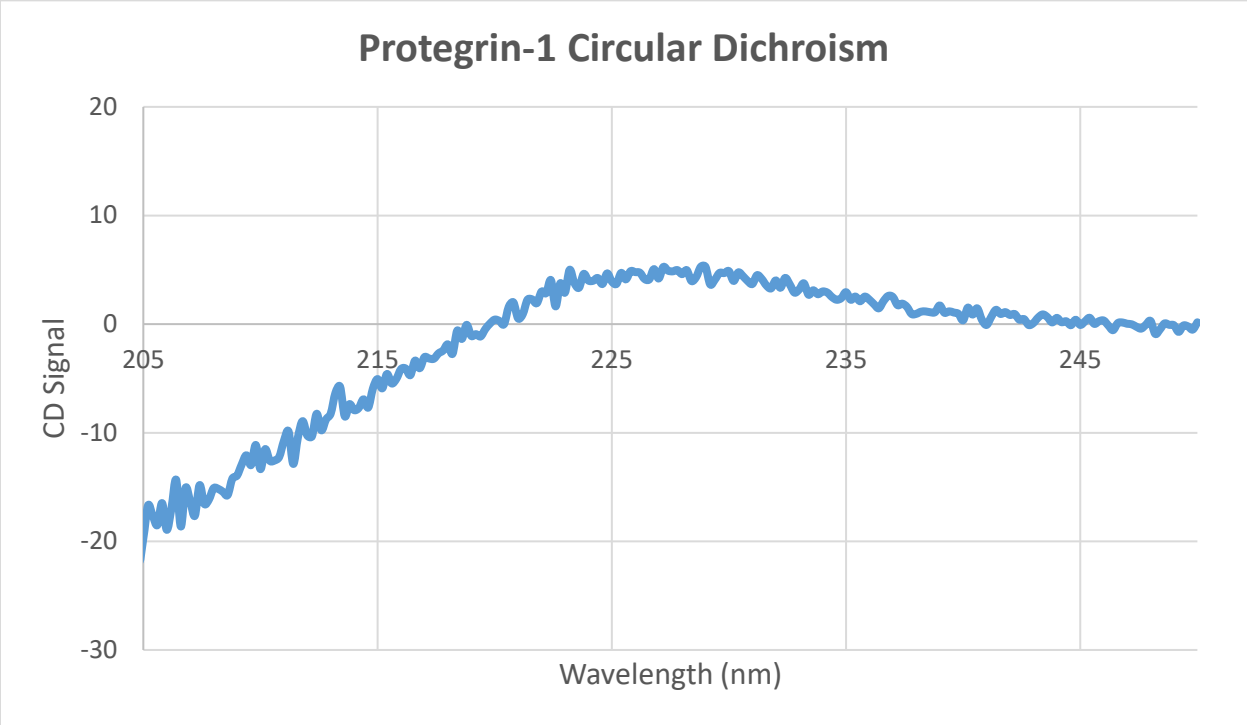

Figure 2-3: CD of oxidized Protegrin-1 to verify the correct β-hairpin structure.

2.1.2 Lys-PG Binding Peptide and CAMP Co-Treatments

Upon Lys-PG binding through iminoboronate formation, the positive charge on a Lys-PG headgroup amine will be removed, yielding an overall more anionic surface charge. This decrease in surface charge should cause increased activity of the CAMPs due to higher electrostatic attraction to the membrane.

Both KAM-CT (up to 10 µM) and MAK3 (up to 5 µM) alone did not kill *S. aureus*, meaning any additional killing with co-treatment compared to CAMP treatment alone is not due to killing

from the adjuvant peptide. Concentrations above *S. aureus* membrane saturation values were used for both peptides: above 1 µM and 500 nM for KAM-CT and MAK3, respectively.

Increased killing was seen after KAM-CT co-treatment with Gramicidin A3R and Protegrin-1 compared to each CAMP alone. However, there was no significant difference in killing with or without KAM-CT treatment with Vancomycin (**Figure 2-4**).

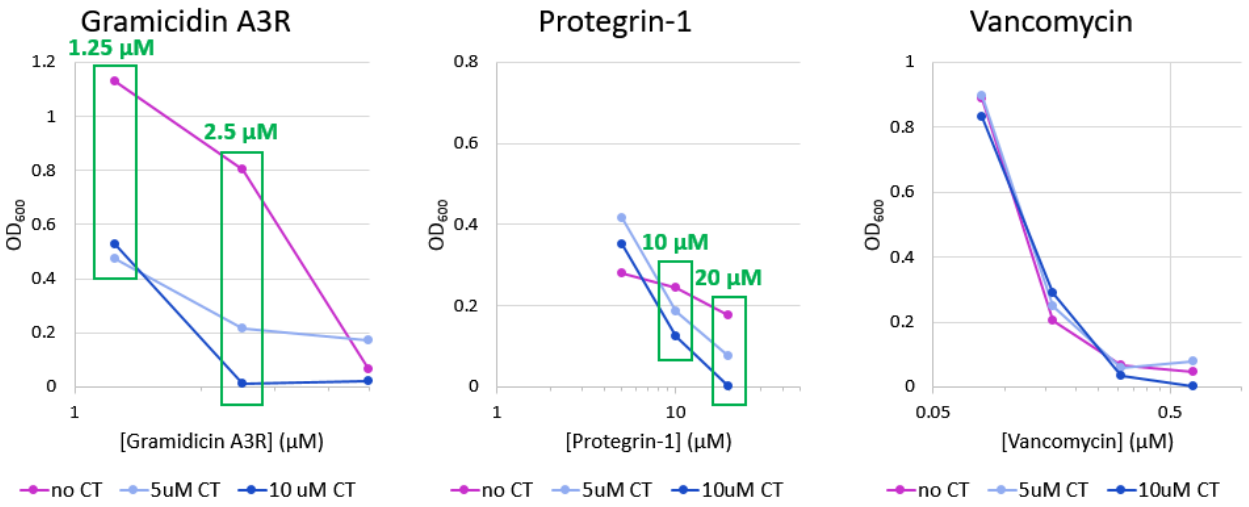

Figure 2-4: MIC assay results with KAM-CT and CAMP co-treatment plotted as concentration of CAMP (µM) versus OD_{600}. CAMP alone is purple, 5 µM KAM-CT is light blue, and 10 µM KAM-CT is dark blue. CAMP concentrations where a significant difference was seen after KAM-CT treatment are indicated by the green boxes and values. Gramicidin A3R data obtained by Breanna Zerfas.

Co-treatment with MAK3 did not cause any significant difference in *S. aureus* killing with any of the CAMPs. MAK3 has two cationic residues; therefore, upon binding two Lys-PG amines and diminishing the surface charge by two, it brings two additional charges with its residues, making the change in net surface charge zero. If the net surface charge did not change, the effectiveness of the CAMPs should not change either, which agrees with the experimental results.

2.2 Lys-PG Modification Using Small Molecules

Instead of binding Lys-PG with peptides, directly modifying Lys-PG was next explored using small molecules. Two modifications were employed: acetylation of Lys-PG headgroup amines with sulfo-NHS-acetate to reduce the net positive charge of the membrane; and cleavage of the lysine residue to regenerate the anionic PG headgroup (**Scheme 2-1**). Lysine cleavage would be more beneficial as it would regenerate an endogenous lipid as well as decrease the cationic charge of the membrane.

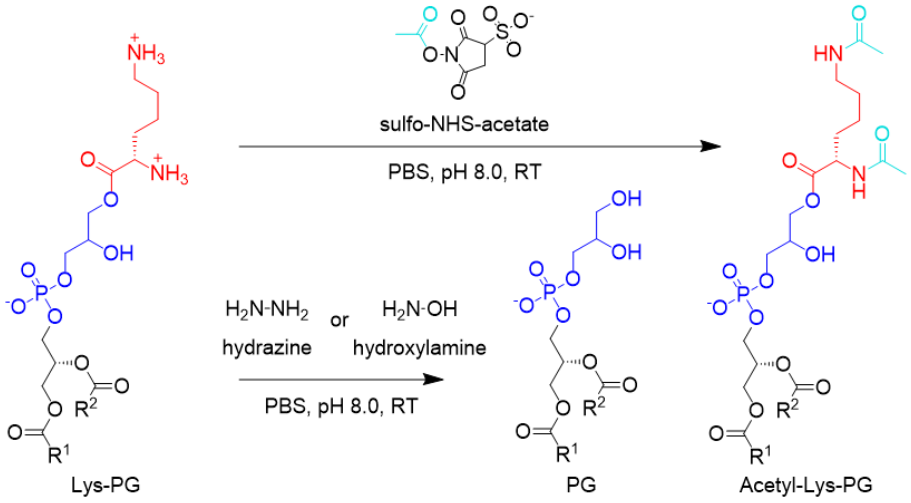

Scheme 2-1: Lys-PG modification via amine acetylation (top) or small molecule nucleophilic lysine cleavage to regenerate PG (bottom).

2.2.1 Lys-PG Acetylation

To quantify the extent of Lys-PG acetylation with various concentrations of sulfo-NHS-acetate, small unilamellar vesicle (SUV) liposomes composed of 3:1 PG:Lys-PG were used as models to mimic the phospholipid composition of *S. aureus*. After acetylation, the lipids were extracted and examined via negative ESI-MS, where the ion intensities were measured and used to calculate the percentage of Lys-PG that was acetylated. With 1 mM sulfo-NHS-acetate

treatment, about 30% of the Lys-PG was acetylated and 10mM treatment gave 65-80% Lys-PG acetylation. For *S. aureus* treatment, 10 mM sulfo-NHS-acetate was chosen to achieve the most acetylation.

S. aureus acetylation without CAMP treatment was shown to cause 35% killing, which was taken into consideration when calculating the increase in killing seen with CAMP treatment (**Figure 2-5A**). Wild type Gramicidin A (gA WT) was used as a positive control to ensure complete bacterial killing. Acetylation followed by Gramicidin A3R or Protegrin-1 treatment gave an average of 2.5x and 10x increased killing compared to each CAMP treatment alone, respectively (**Figure 2-5B**). These results agree with the Lys-PG binding peptide-induced increase in CAMP activity seen previously. Therefore, altering *S. aureus* membrane charge to be less cationic can modulate CAMP activity by exploiting an increased electrostatic interaction.

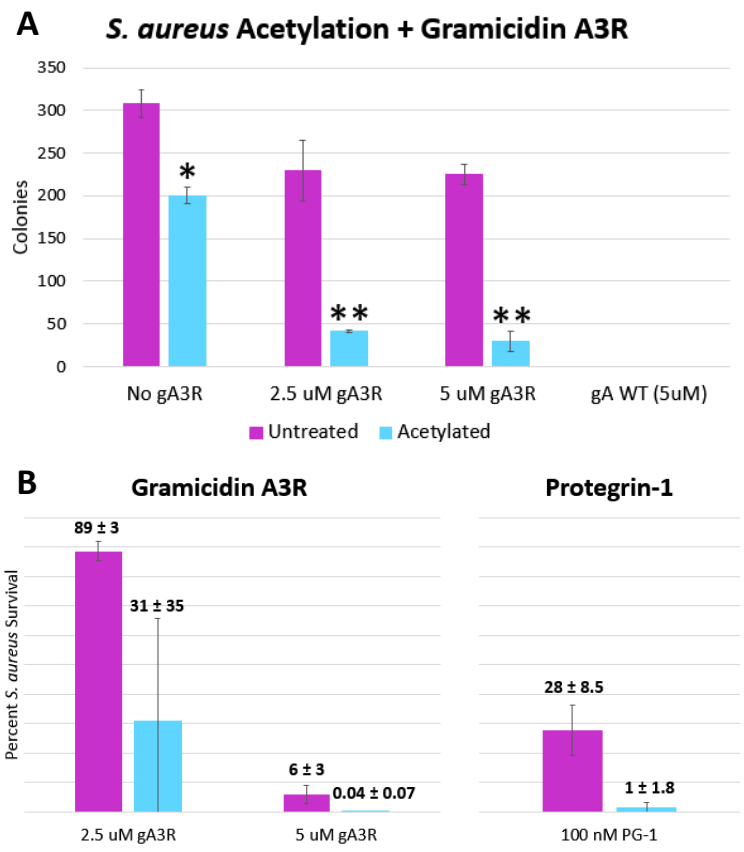

Figure 2-5: *S. aureus* acetylation followed by Gramicidin A3R and Protegrin-1 treatment. A) Treatment with 10 mM sulfo-NHS-acetate followed by triplicate Gramicidin A3R treatment. * Indicates killing caused by acetylation alone. ** Indicates a synergistic increase in killing seen with co-treatment compared to additive Gramicidin A3R and acetylation killing. B) Percent *S. aureus* survival with (blue) and without (purple) acetylation treatment followed by Gramicidin A3R or Protgerin-1 treatment.

2.2.2 Lys-PG Cleavage with Pig Liver Esterase

First, specific Lys-PG cleavage was explored using pig liver esterase to selectively cleave the lysine ester bond of the Lys-PG headgroup. 3:1 PG:Lys-PG liposomes were treated with a range of esterase concentrations and the lipids were extracted with chloroform. No lipid masses were seen from the lipid extracts upon ESI-MS analysis, making esterase treatment inconclusive.

2.2.3 Lys-PG Cleavage with Hydrazine- and Hydroxylamine-based Nucleophiles

Lys-PG cleavage was next explored using non-specific small molecule nucleophiles. A panel of hydrazine- and hydrazide-based nucleophiles were evaluated for Lys-PG cleavage efficiency using liposome models and ESI-MS analysis. Initial screening involved harsh conditions of 1 M nucleophile with overnight liposome treatment to identify sufficiently active nucleophiles, ideally ones that would cause complete Lys-PG cleavage under those conditions. Acetyl hydrazide, semicarbazide, and *p*-carboxy-phenylhydrazine showed increasing Lys-PG cleavage, corresponding to increase nucleophilicity, but did not cause enough cleavage to be meaningful (less than 60% Lys-PG cleavage). The most nucleophilic small molecules, hydrazine and hydroxylamine, both showed complete Lys-PG hydrolysis (**Figure 2-6A**). To explore their reactivity at more biologically relevant conditions, 10 mM, 100 mM, and 1 M of each were incubated with liposomes for 1 hour. Significant Lys-PG cleavage was only seen at the 1 M concentration (**Figure 2-6B**). That was not ideal as 1 M is too concentrated to be biologically relevant, however hydroxylamine was chosen to move forward with as it caused the most Lys-PG cleavage.

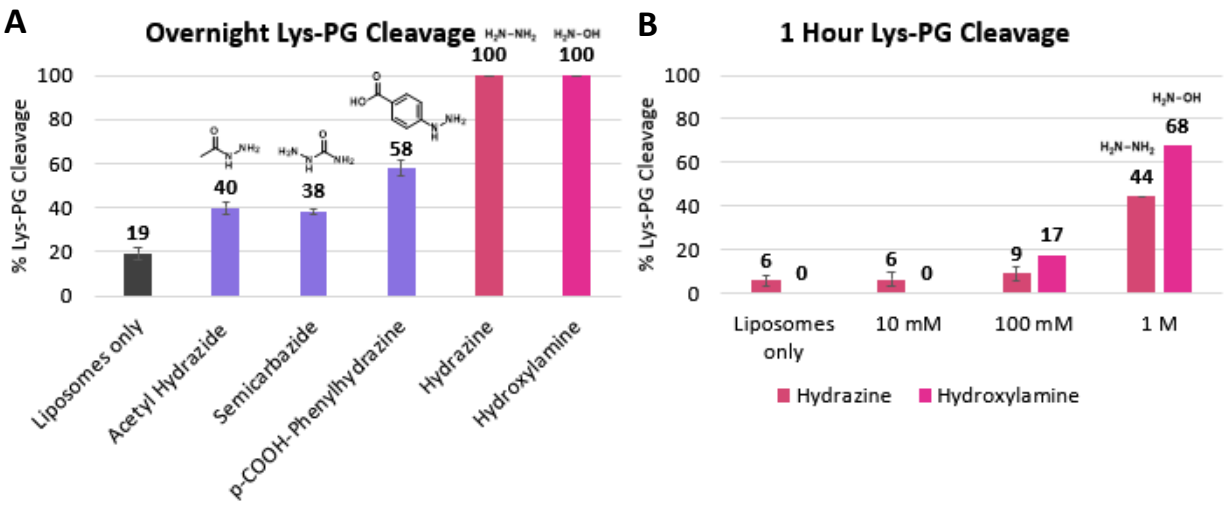

Figure 2-6: Lys-PG Cleavage with Small Molecule Nucleophiles. A) Overnight incubation of 1 M of each small molecule with 3:1 PG:Lys-PG liposomes. B) 1-hour incubation with 10 mM to 1 M hydrazine or hydroxylamine with 3:1 PG:Lys-PG liposomes. Percent Lys-PG cleavage measured by the relative ion intensity of DOPG produced from Lysyl-DOPG via negative ESI-MS. 1-hour liposome incubation with hydroxylamine only performed once (no error bars).

2.2.4 Hydrazine or Hydroxylamine-Induced Cleavage of Lys-OMe

The speed of hydrazine- and hydroxylamine-induced ester cleavage was examined using lysine methyl ester as a model of the Lys-PG headgroup. The kinetics of 10 mM lysine methyl ester cleavage with 1 M hydrazine or hydroxylamine was studied using ^{1}H NMR in PBS (pH 8.0). The disappearance of the lysine ester methyl peak and appearance of the methanol methyl peak was monitored over time to determine the amount of methanol present. The percent methanol was plotted against time to generate a curve from which t_1 values of 3.88 and 3.16 hours were calculated for hydrazine and hydroxylamine, respectively (**Figure 2-7**).

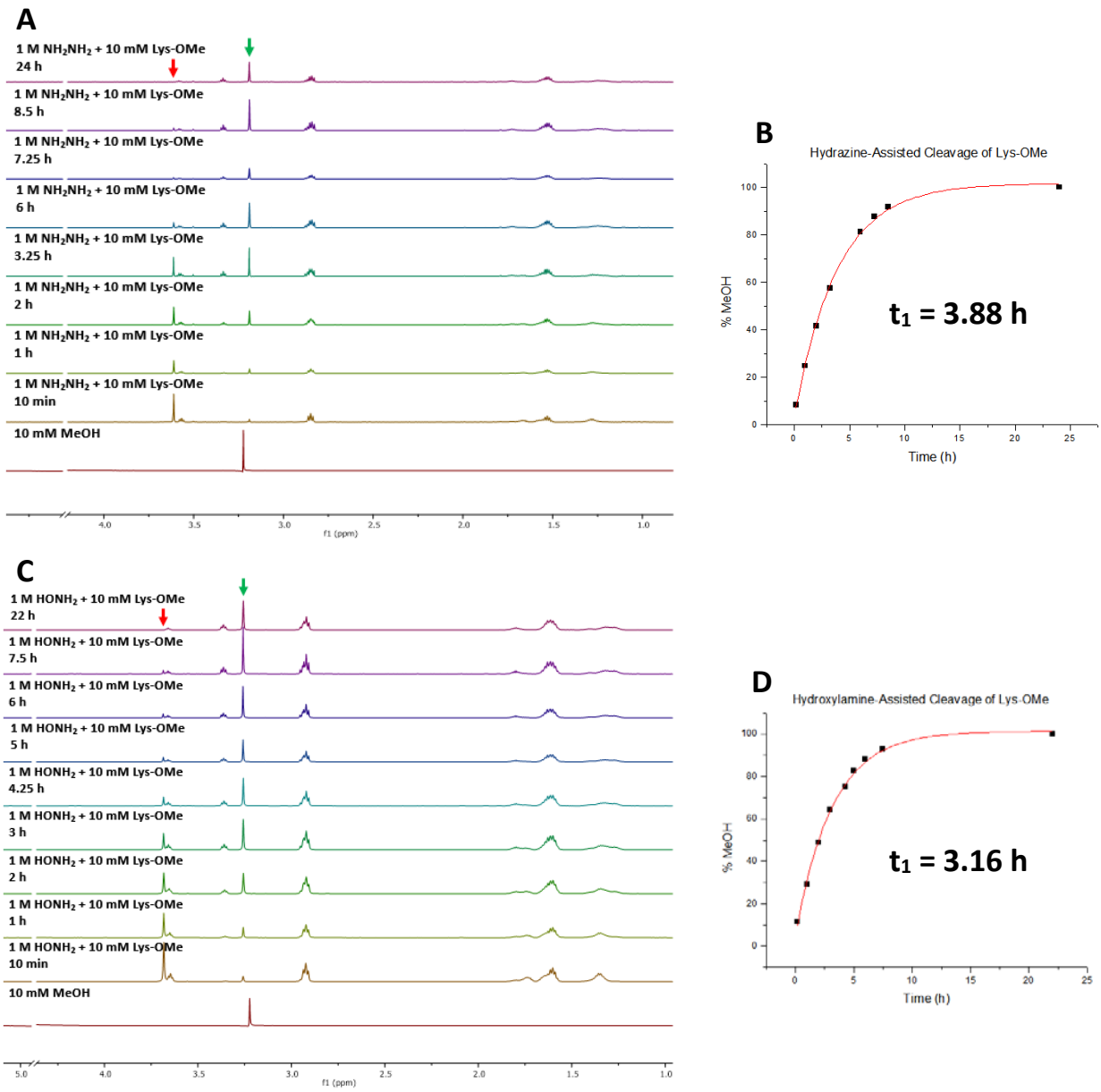

Figure 2-7: Lysine Methyl Ester Cleavage with 1 M Hydrazine (A) or Hydroxylamine (C) via ^{1}H NMR. The percent cleavage was calculated by integrating and comparing the ester methyl (red arrow) and methanol methyl (green arrow) peaks. The percent methanol was plotted against time to generate a curve, which was fit with an exponential equation to generate the t_1 values (B, D).

Because the cleavage kinetics is slow, increasing the concentration of hydroxylamine at the membrane surface would increase cleavage potency. Hydroxylamine could be conjugated to a membrane-binding peptide, which would decrease the concentration of hydroxylamine-

conjugated peptide required for sufficient activity. This was examined by directly conjugating hydroxylamine to a small CAMP.

2.3 Activity of a Hydroxylamine-Functionalized CAMP: AOA-Hlys

A 9-residue fragment of human lysozyme, called Hlys, was chosen as a model CAMP due to its staphylocidal activity[6] and the ease of its synthesis and modification. A glycine linker was added to the N-terminus and the hydroxylamine was installed via amide bond formation between the N-terminal amine and the carboxylic acid of aminooxyacetic acid (AOA) (**Figure 2-8A**).

The Lys-PG cleavage efficacy of the peptide conjugate, called AOA-Hlys, compared to hydroxylamine and Hlys alone were compared using 3:1 PG:Lys-PG liposome models. After lipid extraction and ESI-MS analysis, the AOA-Hlys peptide conjugate showed about 2-fold increase in Lys-PG cleavage compared to hydroxylamine alone. Surprisingly, Hlys also displayed Lys-PG cleavage activity greater than hydroxylamine, but less than AOA-Hlys (**Figure 2-8B**). Hlys was not anticipated to have cleavage ability as there are no nucleophilic residues; it was just anticipated to bind and insert into the membrane.

The cell killing capability of the AOA-Hlys conjugate was compared to Hlys in the hopes of showing increased killing with the conjugate due to nucleophilic cleavage of Lys-PG and regeneration of PG. However, Hlys showed greater *S. aureus* killing activity than AOA-Hlys (**Figure 2-6C**). The only difference between Hlys and AOA-Hlys is the AOA moiety on the N-terminus, indicating that it may cause a deleterious effect on the staphylocidal activity of Hlys.

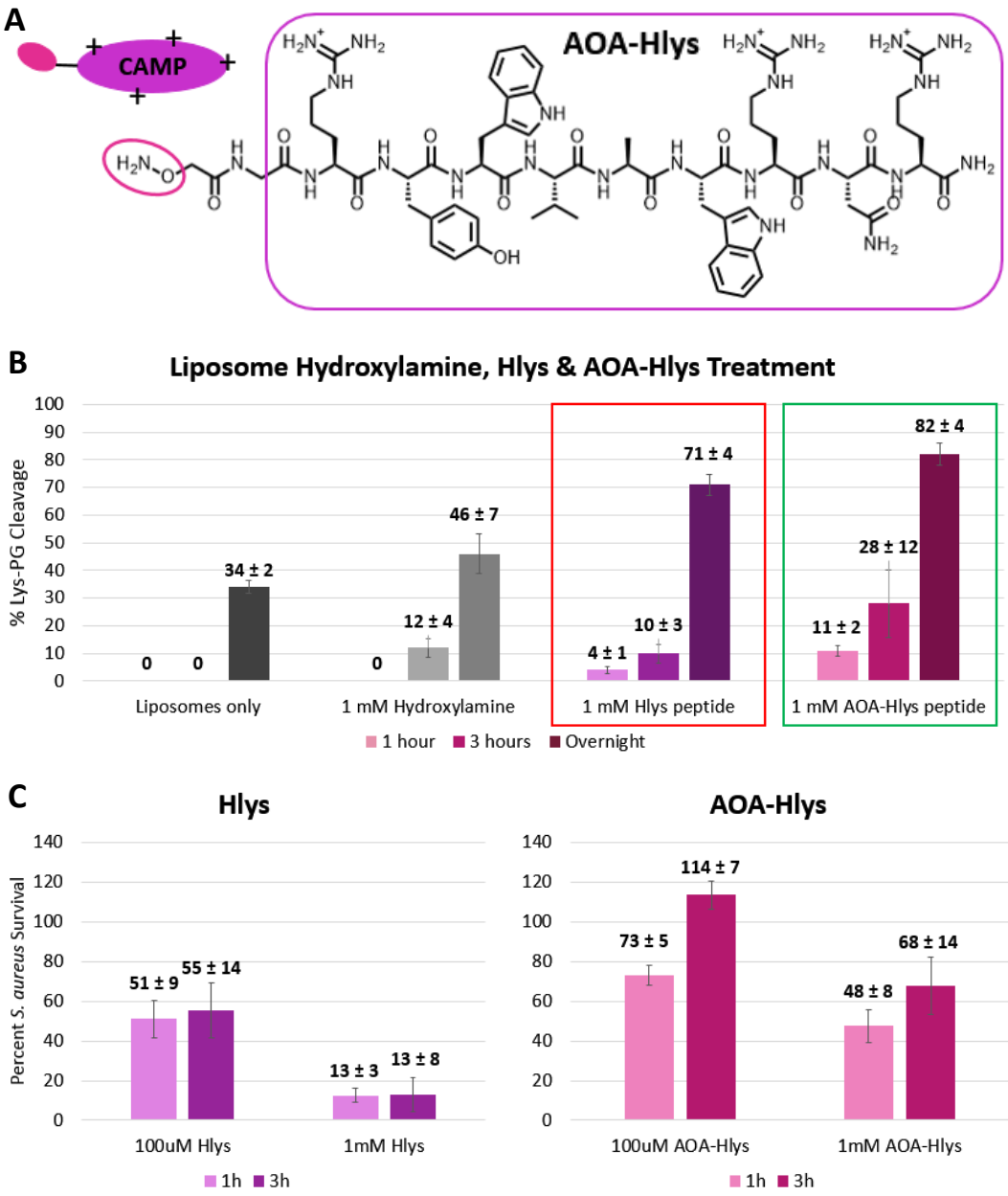

Figure 2-8: A) Cartoon (inset) and structure of the hydroxylamine-Hlys peptide conjugate, AOA-Hlys. B) Liposomes treated with 1 mM hydroxylamine, Hlys, and AOA-Hlys to examine Lys-PG cleavage at 1 h, 3 h and overnight incubations. C) *S. aureus* killing comparing Hlys (purple) to the AOA-Hlys conjugate (pink), each at 100 µM or 1 mM.

To study what is happening to the membrane more closely, evaluation of peptide membrane binding and quantification of Lys-PG following various treatments is desirable.

2.4 Hlys and AOA-Hlys Liposome Binding

Binding of Hlys and AOA-Hlys peptides to 3:1 PG:Lys-PG liposomes was examined via tryptophan (Trp) fluorescence, which was previously used to study peptide-membrane interactions.[7–10] After excitation at 280 nm, Trp emits between 340-350 nm with a blue shift and increase in fluorescence intensity occurring as the side chain moves into a more hydrophobic environment.[7] The binding of Hlys (1 µM) with increasing the concentrations of liposomes (25-100 µM) showed the characteristic blue shift and fluorescence intensity increase (**Figure 2-9**). Both Hlys and AOA-Hlys displayed comparable binding to liposomes.

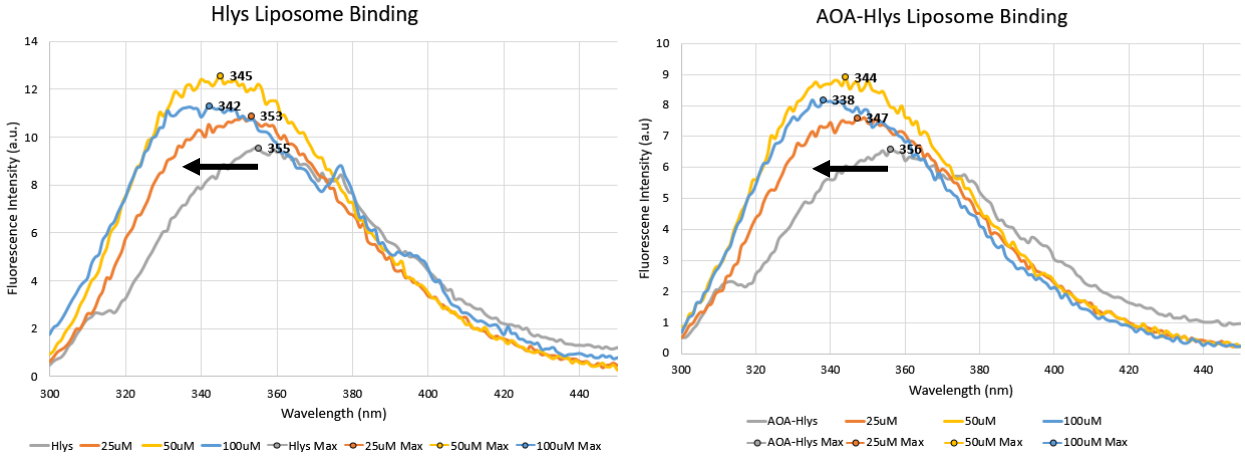

Figure 2-9: Binding of Hlys and AOA-Hlys peptides to 3:1 PG:Lys-PG liposomes in phosphate buffer, pH 7.4. Tryptophan fluorescence was recorded with increasing concentrations of liposomes (25-100 µM) with 1 µM Hlys or AOA-Hlys. The wavelengths with the maximum fluorescence with each liposome concentration are indicated as the data point on each spectrum.

2.5 Lys-PG Quantification

Phospholipids can be extracted from bacteria using a modified Bligh and Dyer method[11] then separated and visualized using two main methods. First, 1D or 2D thin layer chromatography

(TLC) of the phospholipid extracts can be stained with a phosphate-specific molybdenum stain or an amine-specific ninhydrin stain.[12,13] Second, normal-phase high performance liquid chromatography (NP-HPLC) can be used to detect phospholipids via absorbance at a non-specific wavelength, such as 200-210 nm[14,15], or the more sensitive evaporative light scattering detection (ELSD) method.[16,17] For lipid quantification, bacteria can be grown in the presence of a radioactive metabolite, such as ^{32}P, and extracted to obtain the phospholipids. After TLC separation, the radioactivity of each spot, corresponding to a specific type of phospholipid, can be measured. Alternatively, the area under the peaks from the HPLC trace can be quantified and the concentrations of each lipid could be estimated using the known concentration of an internal standard.

2.5.1 Phospholipid 1D TLC

Following lipid extraction, the isolated phospholipids from the chloroform layer were spotted onto TLC plates and developed in 65% chloroform : 30% methanol : 5% acetic acid until the solvent front reached the top of the plate (less than 10 minutes). Lipids were visualized using the amine-specific stain ninhydrin or the phosphate-specific stain ceric ammonium molybdate (CAM) (**Figure 2-10**). Although the phospholipids were successfully isolated, separated, and identified using lipid standards, they were not easily quantified. Previous quantification using TLC studied the Lys-PG differences between wild type *S. aureus* and gene knockouts producing no Lys-PG, allowing the relative Lys-PG concentration difference to be easily discernable.[18,19]

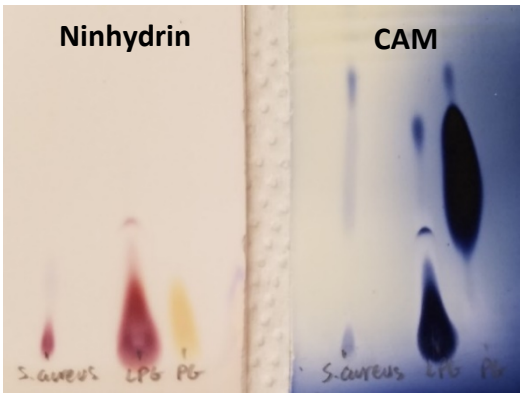

Figure 2-10: Example 1D TLC of phospholipids extracted from *S. aureus* stained with amine-specific ninhydrin (left) or phosphate-specific CAM (right). Lys-PG and PG standards are included.

2.5.2 Phospholipid Normal-Phase Analytical HPLC

To expand the possible detection methods, normal-phase HPLC was attempted on phospholipid extracts with various detection methods. Although previous reports indicated phospholipid separation and visualization using absorbance at 205 nm, neither lipid extracts nor phospholipid standard solutions could be visualized at that wavelength.

Taking advantage of the amine reactivity of the Lys-PG headgroup and the sensitivity of the carboxyfluorescein (FAM) fluorophore, Lys-PG can be specifically fluorophore-labeled, and the conjugate can be detected at 495nm. Optimal fluorophore labeling conditions were found to be lipids reacted with excess NHS-FAM (1 mM) and triethylamine (1 µL) in chloroform (50 µL total reaction volume) for 2 hours at room temperature. Ethylenediamine (EDA, 10 mM) was added to quench the remaining NHS-FAM because the retention time of NHS-FAM was very close to that of FAM-Lys-PG. The EDA-FAM adduct has a much more delayed retention time, allowing for easy peak integration. That adduct peak can be used as an internal standard for compare with the FAM-Lys-PG peak. A range of Lys-PG concentrations were used (50 µM – 500 µM), all of which were successfully labeled. FAM-Lys-PG (10 µL) from the 50 µM reaction could be detected as a

clear peak on the analytical HPLC, indicating a detection limit of approximately 2-3 pmol FAM-Lys-PG at 495 nm.

The ability to detect and quantify phospholipids extracted from *S. aureus* was assessed using this fluorophore-labeled HPLC method. After lipid extraction, NHS-FAM labeling, and ethylenediamine NHS-FAM quenching, the crude labeling reaction was analyzed directly via NP-HPLC (**Figure 2-11A**). Each peak was collected and analyzed via positive and negative MS loop injections. Both major peaks around 34-35 min corresponded to FAM-Lys-PG with the major ion being derived from Lys-PG with two 16:0 acyl chains ($[M+H]^+$ = 1209.6 and $[M-H]^-$ = 1207.6). Differences of 14 mass units correlate with the addition or loss of a methylene (CH_2) from the acyl chain of the Lys-PG lipid (**Figure 2-11B,C**).

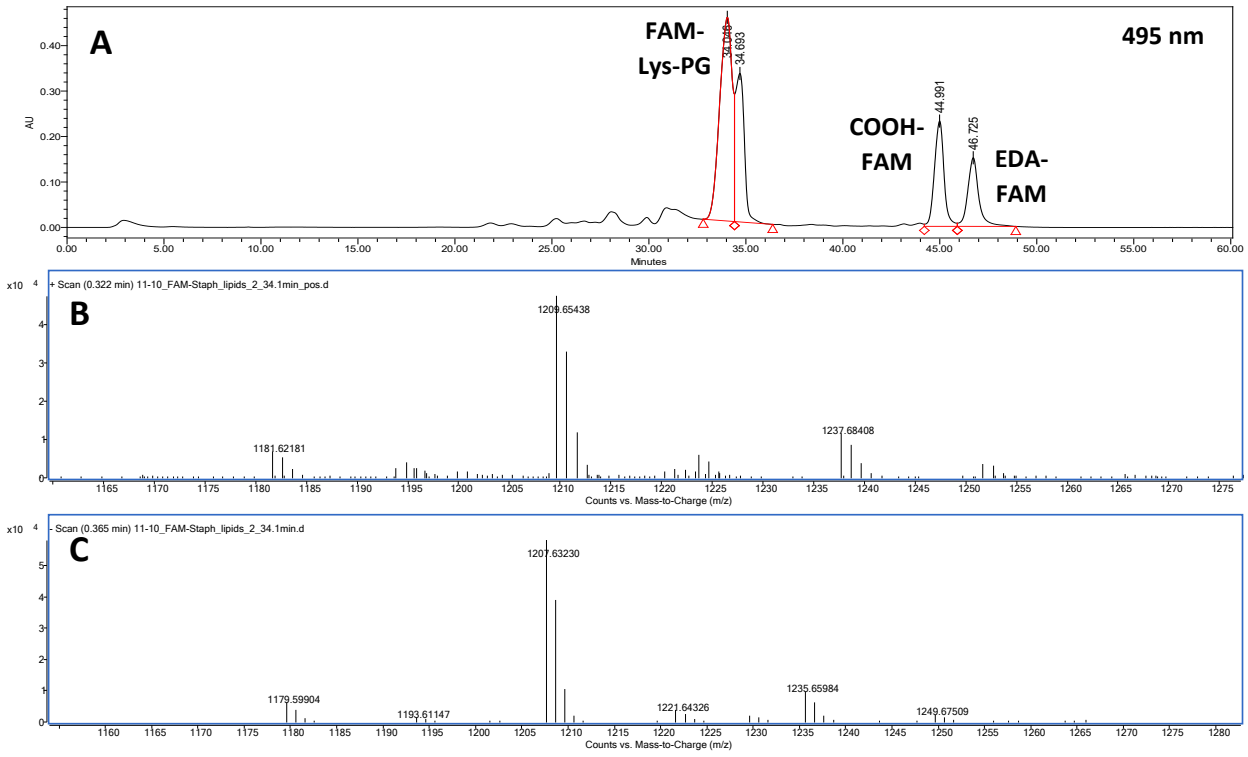

Figure 2-11: Example analytical NP-HPLC of fluorescein-labeled Lys-PG after extraction from untreated *S. aureus* (A). Positive (B) and negative (C) MS of the main peak at 34 min show the masses of FAM-Lys-PG species, with differences of 14 corresponding to a methylene addition or loss in the acyl chain.

This HPLC protocol was used to study the unmodified Lys-PG content found in *S. aureus* after acetylation with 10 mM sulfo-NHS-acetate, as previously studied using liposome modification and *S. aureus* cell killing. After 10 mM sulfo-NHS-acetate treatment, lipid extraction, NHS-FAM labeling, and ethylenediamine NHS-FAM quenching, the amount of FAM-Lys-PG was quantified (**Figure 2-12A,B**). The percent of FAM-Lys-PG was calculated by dividing the area under the FAM-Lys-PG peaks by the total area under the FAM-Lys-PG and EDA-FAM peaks, representing the total amount of NHS-FAM originally present (**Figure 2-12C**). After acetylation, there was 58% the amount of FAM-Lys-PG present from untreated *S. aureus*, indicating approximately 40% of the bacterial Lys-PG was acetylated and unable to react with NHS-FAM. This complemented the liposome MS analysis, which indicated 65-80% acetylation with 10 mM sulfo-NHS-acetate. Therefore, both the MS analysis and this HPLC method were reliable ways to probe the reactivity of sulfo-NHS-acetate with Lys-PG.

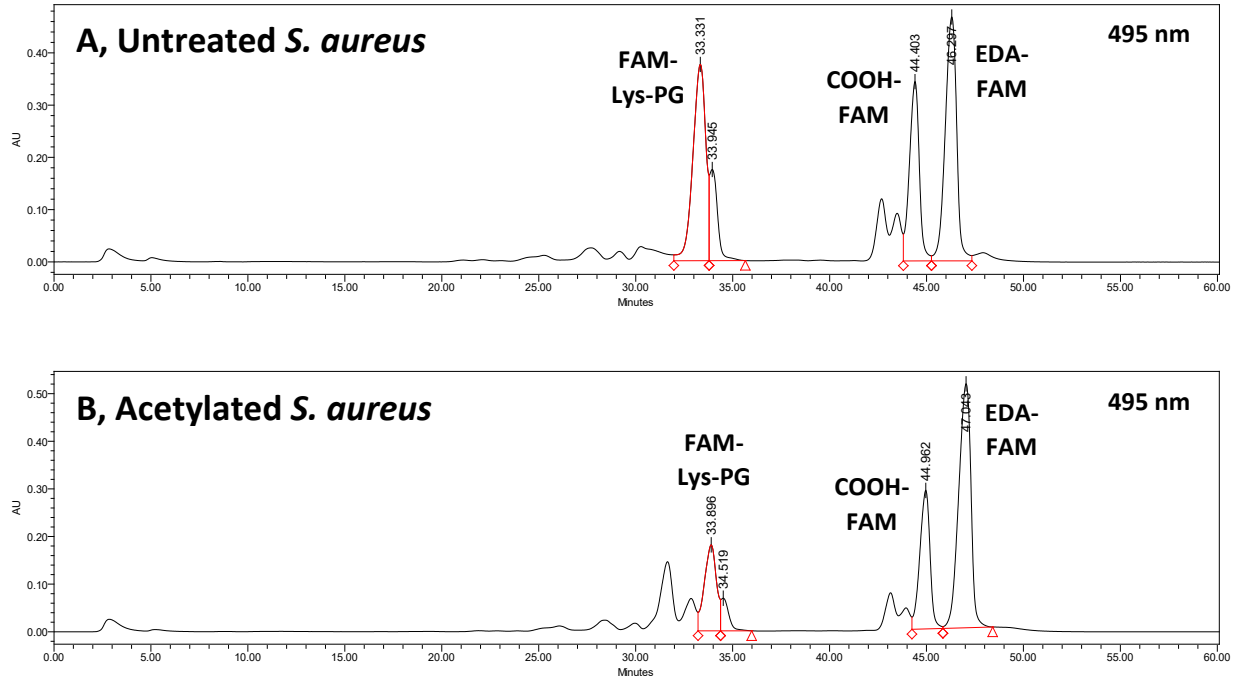

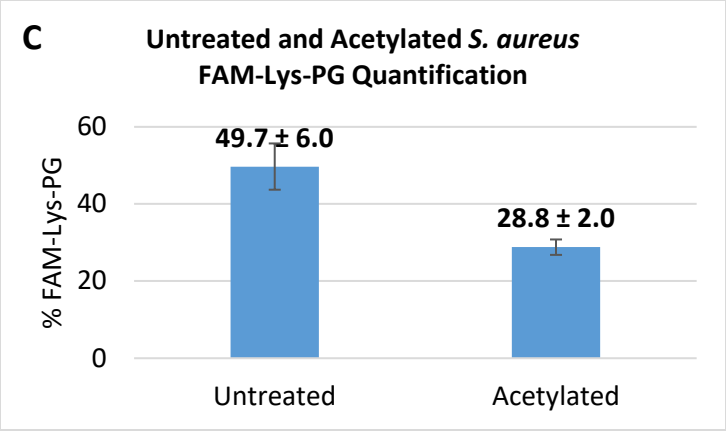

Figure 2-12: Example analytical HPLC of fluorescein-labeled Lys-PG after extraction from untreated *S. aureus* (A) or *S. aureus* treated with 10 mM sulfo-NHS-acetate (B). The peaks corresponding to FAM-labeled Lys-PG (2 peaks, 33-34 min), hydrolyzed NHS-FAM (COOH-FAM, 44.5 min), and the ethylenediamine-FAM adduct (EDA-FAM, 46 min) are labeled. Percent FAM-Lys-PG was determined by comparing the peak areas under the FAM-Lys-PG peaks and the EDA-FAM peak (C).

The Lys-PG cleavage ability of Hlys with liposomes was also explored using this HPLC protocol. 3:1 PG:Lys-PG liposomes were treated with Hlys (10 and 100 µM) overnight at room temperature. After lipid extraction, NHS-FAM labeling, and ethylenediamine NHS-FAM quenching, there was no significant difference in the amount of FAM-Lys-PG: untreated *S. aureus* gave 10.1 ± 0.5% FAM-Lys-PG and *S. aureus* treated with 100 µM Hlys gave 8.9 ± 2.4% FAM-Lys-PG. This is not surprising as Hlys was not expected to cause Lys-PG cleavage, but this contrasts the data from ESI-MS analysis. Knowing this, the data from ESI-MS analysis can be interpreted with caution and this HPLC protocol can be used to verify (or refute) the ESI-MS data.

2.6 Conclusions

Modulating the bacterial membrane charge allows for increased susceptibility to certain CAMPs. Binding surface amines with iminoboronate-forming peptides caused a concentration-

dependent inhibition of *S. aureus* growth after Gramicidin A3R and Protegrin-1 treatments. This is presumably due to increased CAMP activity resulting from the lowering of surface charge by elimination of cationic free amines through iminoboronate formation.

Sulfo-NHS-acetate was used to acetylate Lys-PG, as demonstrated through model liposome labeling analyzed via ESI-MS and labeling of *S. aureus* analyzed via fluorophore labeling the lipid extracts followed by NP-HPLC. Acetylating surface amines to remove their cationic charge caused *S. aureus* to become 2.5 and 10 times more susceptible to Gramicidin A3R and Protegrin-1, respectively.

Nucleophilic Lys-PG cleavage was achieved by hydroxylamine and a hydroxylamine-functionalized CAMP, AOA-Hlys. The AOA-Hlys conjugate increased Lys-PG cleavage by about 2-fold in liposomes compared to hydroxylamine alone, as determined via ESI-MS. However, Hlys killed *S. aureus* more effectively than the AOA-Hlys conjugate, contrary to the hypothesis that the hydroxylamine would promote Lys-PG cleavage and regenerate a more anionic membrane surface. Analysis of Hlys and AOA-Hlys liposome binding via Trp fluorescence revealed comparable binding. ESI-MS analysis of Lys-PG cleavage from liposomes treated with either Hlys or AOA-Hlys revealed that Hlys also caused Lys-PG cleavage, which was unexpected as it does not contain any nucleophilic residues. However, fluorophore labeling and NP-HPLC analysis revealed no significant difference in FAM-Lys-PG levels between untreated *S. aureus* and *S. aureus* treated with 100 μM Hlys. Therefore, the results from the ESI-MS analysis should be interpreted with caution as error caused by ionization or fragmentation cannot be ruled out. The HPLC analysis protocol is more reliable as it uses a well-established NHS-based fluorophore labeling chemistry and analytical method.

2.7 Experimental Procedures

2.7.1 General Methods

1-palmitoyl-2-oleoyl-*sn*-glycero-3-phospho-(1'-*rac*-glycerol) (sodium salt) (POPG) and 1,2-dioleoyl-*sn*-glycero-3-[phospho-*rac*-(3-lysyl(1-glycerol))] (chloride salt) (Lysyl-DOPG) were purchased from Avanti Polar Lipids (Alabaster, AL). Vancomycin hydrochloride was purchased from Chem-Impex International (Wood Dale, IL). All other chemicals were purchased from Fisher Scientific (Pittsburgh, PA) or Sigma Aldrich (St. Louis, MO), unless otherwise indicated. Gram-positive *Staphylococcus aureus* (ATCC 6538) were purchased as lyophilized cell pellets from Microbiologics (Cloud, MN). Peptide synthesis was carried out on a Tribute peptide synthesizer (Protein Technologies, Tucson, AZ). Peptide purification was performed on a Waters PrepLC system using a Phenomenex Jupiter C_{18} column (Torrance, CA). MIC data was obtained using a SpectraMax M5 microtiter plate reader (Molecular Devices, Sunnyvale, CA). 1x (10 mM) PBS buffer was used for all experiments at the indicated pH values. The peptide concentrations of all peptides used in MIC assays were determined by measuring their absorbance at a specified wavelength (below) on a NanoDrop 2000c UV-vis spectrometer either by cuvette or 1µL NanoDrop measurements. The extinction coefficients were either calculated by the number of Trp residues (ε = 5,560 $M^{-1}cm^{-1}$), APBA moieties (ε = 9,795.5 $M^{-1}cm^{-1}$), or FAM fluorophores (ε = 80,000 $M^{-1}cm^{-1}$) present or found in the literature, as indicated in the following table.

Peptide	Wavelength (nm)	Extinction Coefficient ($M^{-1}cm^{-1}$)
KAM-CT	280	29,386.5 (3 APBA moieties)
MAK3	495	80,000 (1 FAM fluorophore)
Gramicidin A3R	280	22,240 (4 Trp residues)
Protegrin-1	278	1520 (1 Tyr, 1 Phe, 2 disulfide bonds)[1]
Vancomycin	280	5942.8

2.7.2 Peptide Synthesis and Characterization

All peptides were synthesized using standard Fmoc-based SPPS on Rink Amide MBHA resin. They were carried out on a 0.05 mmol scale using 5 equivalents of each amino acid and 4.75 equivalents of HBTU for each coupling reaction. All peptides had a purity of 90% or higher. KAM-CT and MAK3 were synthesized and provided by Kelly McCarthy and Michael Kelly, respectively. Gramicidin A3R synthesis was previously reported[20] and provided by Breanna Zerfas.

Protegrin-1 Synthesis

After Fmoc SPPS and N-terminal Fmoc deprotection, the crude peptide was cleaved off resin and globally deprotected with 90% trifluoroacetic acid : 5% water : 5% thioanisole treatment for 2.5 hours. Cold ether precipitation yielded crude peptide, which was dissolved in water and lyophilized. The crude lyophilized peptide (35 mg, 0.016 mmol) was dissolved in 5 mg/mL urea (7 mL) and reduced with dithiothreitol (14 eq, 0.227 mmol) via stirring overnight at room temperature.[1] The reduced peptide was purified using RP-HPLC, monitoring at 214 nm (amide bonds), and lyophilized. The lyophilized reduced peptide was dissolved in PBS (pH 7.4) and stirred open to the atmosphere for approximately 36 hours at room temperature. Oxidation was complete at 8 hours, as indicated by LC-MS analysis. Crude oxidized peptide was purified using RP-HPLC, monitoring at 214 nm, and lyophilized. Peptide purity was assessed by LCMS. For oxidized Protegrin-1, the calculated *m/z* $[M+H]^+$ is 2155.0630 and observed *m/z* $[M+3H]^+$ is 719.3488, respectively.

Circular dichroism (CD) was performed to verify the correct oxidation of the disulfide bonds. Oxidized Protegrin-1 (68 µM) in PBS (pH 7.4) was scanned from 190 to 250 nm at 25°C. A PBS buffer blank was subtracted to generate the final CD spectrum.

Hlys & AOA-Hlys Synthesis

After SPPS and N-terminal Fmoc deprotection, Hlys was globally deprotected and cleaved off resin via Reagent K (82.5% trifluoroacetic acid : 5% water : 5% thioanisole : 5% phenol : 2.5% 1,2-ethanedithiol) treatment for 2 hours. The peptide was precipitated with cold ether then purified via RP-HPLC and lyophilized.

The hydroxylamine moiety was added to the free N-terminus of Hlys on resin via addition of aminooxyacetic acid. Boc-aminooxyacetic acid (5 eq) was activated with HBTU (4.7 eq) in 0.4 M NMM in DMF for 5 min then added to the on-resin peptide, stirring for 1.5 hours. AOA-Hlys was globally deprotected and cleaved off resin via Reagent K (82.5% trifluoroacetic acid : 5% water : 5% thioanisole : 5% phenol : 2.5% 1,2-ethanedithiol) treatment for 3 hours. The peptide was precipitated with cold ether then purified via RP-HPLC and lyophilized. Due to the known reactivity of the hydroxylamine moiety with acetonitrile[21], the HPLC samples were prepared and purified immediately.

2.7.3 Minimal Inhibitory Concentration (MIC) Assay

S. aureus growth in the presence of membrane binding peptides and CAMPs were assessed using the standard microbroth dilution method.[22] A single colony was selected from an LB agar plate and grown in LB media overnight at 37°C with agitation. The next morning, the culture was diluted 100 times into fresh LB media and grown until an OD_{600} value between 0.5 and 0.6 was

reached. The culture was diluted to approximately 5 x 10^5 colony forming units per mL (cfu/mL) using a previously calculated factor. Diluted culture (200 µL) was added to each well of a sterile 96-well plate. Either KAM-CT (stock in water) or MAK3 (stock in water/DMSO mixture) were added to final concentrations of either 5 or 10 µM. Finally, 2µL of 2-fold serially diluted Gramicidin A3R (stock in DMSO), Protegrin-1 (stock in DMSO), or Vancomycin (stock in water) were added in triplicates. The plate was incubated at 37°C in a microtiter plate reader overnight. The OD_{600} value was recorded every 10 minutes after 15 seconds of shaking. The time when untreated *S. aureus* began to reach stationary phase was chosen to compare OD_{600} values of each treated sample.

2.7.4 Cell Killing Assay

S. aureus survival after sulfo-NHS-acetate and CAMP co-treatment was assessed. A single colony was selected from an LB agar plate and grown in LB media overnight at 37°C with agitation. The next morning, the culture was diluted 100 times into fresh LB media and grown until an OD_{600} value between 0.5 and 0.6 was reached. The bacteria were pelleted via centrifugation at 5,000 rcf for 5 min, washed with PBS twice, and re-centrifuged. Approximately 1 x 10^7 cfu/mL of bacteria were treated with 10 mM sulfo-NHS-acetate in PBS (pH 8.5, 1 mL total reaction volume) for 1 hour at room temperature. The bacteria were pelleted via centrifugation, washed with PBS, and resuspended in PBS (pH 8.5, 1 mL). PBS (pH 8.5, 95 µL) was added to each well of a sterile 96-well plate. The culture in PBS (5 µL, approximately 5 x 10^5 cfu/mL) and CAMP stock (in DMSO) or DMSO (1 µL) were added to the wells to give the desired CAMP concentrations. The plate was incubated at 37°C for 1 hour with shaking. The bacteria were directly diluted to approximately 2.5 x 10^4 cfu/mL (7.5 µL reaction in 142.5 µL PBS, pH 8.5) and aliquoted (100 µL) onto LB agar

plates. After overnight growth at 37°C, the colonies on each plate were counted. Triplicate acetylation reactions and CAMP treatments were performed. To calculate the percent survival, the average number of colonies for each treatment condition was divided by the average number of colonies for comparable blank samples (either acetylated *S. aureus* or untreated *S. aureus*) and multiplied by 100. Percent killing is defined as 100 minus the percent survival.

This protocol was also used to study *S. aureus* survival after Hlys or AOA-Hlys treatment at 100 µM or 1 mM concentrations.

2.7.5 Small Molecule and Peptide Liposome Treatment

SUV Liposomes were prepared by aliquoting the desired amount of POPG and Lysyl-DOPG stocks (in chloroform) into a small glass vial and evaporating the chloroform. The lipid film was dissolved in PBS (pH 8.0) and immediately ultra-sonicated at 65% amplitude in short pulses until the solution was uniformly cloudy. Liposomes were used immediately after preparation.

Acetylation

3:1 PG:Lys-PG liposomes (50 µM total lipids per reaction) were prepared in PBS (pH 8.0, 200 µL total volume per reaction). Sulfo-NHS-acetate stock (in deionized water) was added to make either 1 mM or 10 mM final concentrations. Reactions were stirred for 1 hour at room temperature then the lipids were extracted with chloroform (200 µL, twice). Lipids were analyzed via negative ESI-MS.

Pig Liver Esterase

3:1 PG:Lys-PG liposomes (50 μM total lipids per reaction) were prepared in PBS (pH 8.0, 200 μL total volume per reaction). Esterase stock (in deionized water) was added to give 1 to 10 U of enzyme activity. Reactions were stirred for 45 min at room temperature then the lipids were extracted with chloroform (200 μL, twice). Lipids were analyzed via negative APPI-MS.

Hydrazine-based Small Molecules

3:1 PG:Lys-PG liposomes (50 μM total lipids per reaction) were prepared in PBS (pH 8.0, 200 μL total volume per reaction). Stocks of each of the following small molecules (in PBS) were tuned to pH 8.0 and added to liposomes to give the final concentration (1 mM – 1 M): acetic hydrazide (acetyl hydrazide), semicarbazide hydrochloride, 4-hydrazinobenzoic acid (*p*-carboxy-phenylhydrazine), hydrazine monohydrate, and hydroxylamine hydrochloride. Reactions were stirred for 1-3 hours or overnight at room temperature then the lipids were extracted with chloroform (200 μL, twice). Lipids were analyzed via negative ESI-MS.

Hlys and AOA-Hlys Peptides

3:1 PG:Lys-PG liposomes (50 μM total lipids per reaction) were prepared in PBS (pH 8.0, 100 μL total volume per reaction). Hlys or AOA-Hlys stocks (in PBS) were tuned to pH 8.0 and added to each reaction to make a final concentration of 1 mM. Reactions were stirred for 1-3 hours or overnight at room temperature then the lipids were extracted with chloroform (200 μL, twice). Lipids were analyzed via negative ESI-MS.

2.7.6 Lipid ESI-Mass Spectrometry Analysis

Lipid extracts from liposomes were analyzed via negative ESI-MS by comparing the ionization of POPG compared to DOPG and/or Lysyl-DOPG. Lipids were either used directly after chloroform extraction or dissolved in minimal chloroform (at least 20 µL). 10 µL of lipid sample was injected into the MS via loop injection and analyzed using an isocratic solvent of 99.9% methanol : 0.1% ammonium hydroxide over 2 minutes. Negative ion mode was used for all analyses as both PG and Lys-PG were able to be seen, although Lys-PG (cationic) did not ionize as well as PG (anionic). The discrepancy between the calculated molar ratio of PG to Lys-PG (3:1) and actual ion intensity seen (10:1) lead to a correction factor (0.3) being applied to PG ionization. The corrected PG ion intensity and raw Lys-PG ion intensity values were summed to get the total ion intensity. The percent of each lipid is defined as the following: (lipid ion intensity)/(total ion intensity) * 100.

To determine the extent of Lys-PG acetylation, the percentage of mono-Ac-Lysyl-DOPG, di-Ac-Lysyl-DOPG, and Lysyl-DOPG were summed to obtain the original amount of Lys-PG. The percent Lys-PG acetylation is defined as (% mono-Ac-Lysyl-DOPG + % di-Ac-Lysyl-DOPG)/(original amount of Lys-PG) * 100.

To determine the extent of Lys-PG cleavage, the percent of DOPG produced from Lysyl-DOPG was calculated by summing the percent DOPG and percent Lysyl-DOPG to obtain the original amount of Lys-PG. The percent Lys-PG cleavage is defined as (% DOPG)/(original amount of Lys-PG) * 100.

2.7.7 Hydrazine or Hydroxylamine-Induced Lys-OMe Cleavage NMR Kinetic Study

A 600 µL NMR sample of either 1 M hydrazine or hydroxylamine in 20% D_2O/PBS was prepared and tuned to pH 8.0. 6 µL of a 1 M Lys-OMe stock in PBS (pH 8.0) was added to the NMR sample to give a final concentration of 10 mM. The ^1H NMR was recorded immediately and at certain intervals over 22 or 24 hours. The methyl peak of methanol and the methyl peak of Lys-OMe were integrated and compared to determine the percent cleavage (reported as percent methanol). The percent methanol was calculated as the following: (methanol methyl peak area)/(methanol methyl peak area + Lys-OMe methyl peak area) * 100. After plotting the time versus percent methanol, the points were fit to an exponential association curve, from which a t_1 value could be extracted.

2.7.8 Tryptophan Fluorescence

A 3:1 PG:Lys-PG liposome stock (100 µM total lipids) was prepared as described above in PBS (pH 8.0). 0.55 mM Hlys and AOA-Hlys stocks (in PBS) were made and tuned to pH 8.0. For each fluorescence sample, 600 µL of liposomes (25, 50, or 100 µM final liposome concentrations) was aliquoted into a quartz microcuvette. Hlys or AOA-Hlys stock (1.1 µL) was added (1 µM final peptide concentration) and gently inverted to mix directly in the cuvette. The sample was excited at 280 nm and the fluorescence emission spectrum was recorded from 300 to 450 nm with 5 nm steps.[7,8,10] The liposome alone emission spectra were recorded prior to adding the peptide stock and subtracted from each sample. The emission spectra of Hlys and AOA-Hlys samples (1.1 µL stock in 600 µL PBS, pH 8.0) were also recorded.

2.7.9 *S. aureus* Lipid Extraction

A single *S. aureus* colony was selected from an LB agar plate and grown in LB media overnight at 37°C with agitation. The next morning, the culture was diluted 100 times into fresh LB media and grown until an OD_{600} value between 0.5 and 0.6 was reached. The bacteria were pelleted via centrifugation at 5,000 rcf for 5 min, washed with PBS (pH 8.0) twice, and re-centrifuged. The bacteria were either treated with a small molecule (such as acetylation with 10 mM sulfo-NHS-acetate, as described previously) or directly used for lipid extraction. To have enough bacteria for HPLC analysis, 7 mL of subculture at an OD_{600} value of 0.5 were used (~5 x 10^9 cfu/mL).

Following the Bligh and Dyer method[11], the bacteria pellet was resuspended in 0.8 mL of 0.12 M sodium acetate buffer, pH 4.8. Chloroform (1 mL) and methanol (2.2 mL) were added and the solution was vortex until homogeneous. The suspension was shaken at room temperature for 1 hour, then centrifuged to pellet the cell debris. The supernatant was removed and put into a clean Falcon tube. Chloroform (1 mL) and deionized water (1 mL) were added and vortexed to mix well. The bottom chloroform layer was removed, placed into a clean glass vial and evaporated. The lipids were then either analyzed via TLC or fluorescein labeled then analyzed via analytical NP-HPLC.

2.7.10 Lipid TLC Analysis

Lipids dissolved in chloroform were spotted onto a silica gel 60 F_{254} TLC plates (Merck, Darmstadt, Germany) and developed in 65% chloroform : 30% methanol : 5% acetic acid until the solvent front was 1 mm from the top of the plate. The plates were stained with either ninhydrin or ceric

ammonium molybdate (CAM) and heated until spots became visible: purple spots with ninhydrin or dark blue spots with CAM. Lipid standards from Avanti Polar Lipids were spotted on each plate.

2.7.11 Lipid Fluorescein Labeling

10 mM 5/6-carboxyfluorescein succinimidyl ester (NHS-fluorescein) stock in DMF (5 µL) and triethylamine (1 µL) were added to lipids dissolved in chloroform (44 µL). The dark orange mixture was stirred at room temperature for 2 hours. To quench the remaining NHS-fluorescein, 30 mM ethylenediamine stock in chloroform (25 µL) was added and allowed to react for 5 mins until the solution was a fluorescent pink/yellow color. The crude reaction was directly analyzed via analytical NP-HPLC.

2.7.12 Lipid Analytical HPLC Analysis

Crude fluorescein-labeled lipids (10 µL) were injected onto an Atlantis HILIC Silica (3 µm 2.1 x 150 mm) analytical column (Waters, Milford, MA). The flow rate was 0.3 mL/min throughout. Solvent A was 80% chloroform : 19.5% methanol : 0.5% ammonium hydroxide and Solvent B was 60% chloroform : 34% methanol : 5.5% water : 0.5% ammonium hydroxide. The gradient used was as follows: isocratic 100% A for 5 min, gradient from 0% to 85% over 30 min, gradient 85% to 100% B over 2 min, isocratic 100% B for 5 min, gradient from 100% to 0% B over 5 min, and isocratic 100% A for 13 min. Wavelengths were monitored at 254 and 495 nm.

2.8 References

(1) Gottler, L. M.; de la Salud Bea, R.; Shelburne, C. E.; Ramamoorthy, A.; Marsh, E. N. G. *Biochemistry (Mosc.)* **2008**, *47* (35), 9243–9250.

(2) Harwig, S. S. L.; Waring, A.; Yang, H. J.; Cho, Y.; Tan, L.; Lehrer, R. I. *Eur. J. Biochem.* **1996**, *240* (2), 352–357.

(3) Yamaguchi, S.; Hong, T.; Waring, A.; Lehrer, R. I.; Hong, M. *Biochemistry (Mosc.)* **2002**, *41* (31), 9852–9862.

(4) Steinberg, D. A.; Hurst, M. A.; Fujii, C. A.; Kung, A. H.; Ho, J. F.; Cheng, F. C.; Loury, D. J.; Fiddes, J. C. *Antimicrob. Agents Chemother.* **1997**, *41* (8), 1738–1742.

(5) Roumestand, C.; Louis, V.; Aumelas, A.; Grassy, G.; Calas, B.; Chavanieu, A. *FEBS Lett.* **1998**, *421* (3), 263–267.

(6) González, R.; Albericio, F.; Cascone, O.; Iannucci, N. B. *J. Pept. Sci.* **2010**, *16* (8), 424–429.

(7) Breukink, E.; van Kraaij, C.; van Dalen, A.; Demel, R. A.; Siezen, R. J.; de Kruijff, B.; Kuipers, O. P. *Biochemistry (Mosc.)* **1998**, *37* (22), 8153–8162.

(8) Christiaens, B.; Symoens, S.; Vanderheyden, S.; Engelborghs, Y.; Joliot, A.; Prochiantz, A.; Vandekerckhove, J.; Rosseneu, M.; Vanloo, B. *Eur. J. Biochem.* **2002**, *269* (12), 2918–2926.

(9) Zhao, H.; Kinnunen, P. K. J. *J. Biol. Chem.* **2002**, *277* (28), 25170–25177.

(10) Hunter, H. N.; Jing, W.; Schibli, D. J.; Trinh, T.; Park, I. Y.; Kim, S. C.; Vogel, H. J. *Biochim. Biophys. Acta BBA - Biomembr.* **2005**, *1668* (2), 175–189.

(11) Bligh, E. G.; Dyer, W. J. *Can. J. Biochem. Physiol.* **1959**, *37* (8), 911–917.

(12) Griffiths, K. k.; Setlow, P. *J. Appl. Microbiol.* **2009**, *106* (6), 2064–2078.

(13) Fuchs, B.; Süß, R.; Teuber, K.; Eibisch, M.; Schiller, J. *J. Chromatogr. A* **2011**, *1218* (19), 2754–2774.

(14) Patton, G. M.; Fasulo, J. M.; Robins, S. J. *J. Lipid Res.* **1982**, *23* (1), 190–196.

(15) Kaduce, T. L.; Norton, K. C.; Spector, A. A. *J. Lipid Res.* **1983**, *24* (10), 1398–1403.

(16) Descalzo, A. M.; Insani, E. M.; Pensel, N. A. *Lipids* **2003**, *38* (9), 999–1003.

(17) Narváez-Rivas, M.; Gallardo, E.; Ríos, J. J.; León-Camacho, M. *J. Chromatogr. A* **2011**, *1218* (22), 3453–3458.

(18) Peschel, A.; Jack, R. W.; Otto, M.; Collins, L. V.; Staubitz, P.; Nicholson, G.; Kalbacher, H.; Nieuwenhuizen, W. F.; Jung, G.; Tarkowski, A.; Kessel, K. P. M. van; Strijp, J. A. G. van. *J. Exp. Med.* **2001**, *193* (9), 1067–1076.

(19) Oku, Y.; Kurokawa, K.; Ichihashi, N.; Sekimizu, K. *Microbiology* **2004**, *150* (1), 45–51.

(20) Wang, F.; Qin, L.; Pace, C. J.; Wong, P.; Malonis, R.; Gao, J. *ChemBioChem* **2012**, *13* (1), 51–55.

(21) Haney, C. M.; Loch, M. T.; Horne, W. S. *Chem. Commun.* **2011**, *47* (39), 10915–10917.

(22) Wiegand, I.; Hilpert, K.; Hancock, R. E. W. *Nat Protoc.* **2008**, *3* (2), 163–175.

CHAPTER 3: 2-FORMYLPHENYLBORONIC ACID-BASED REVERSIBLE COVALENT CHEMISTRIES AS A NOVEL PEPTIDE CYCLIZATION STRATEGY

3.1 Reversible Bioorthogonal Chemistries

As bioorthogonal chemistries continue to be discovered[1,2], faster and more potent conjugations which do not require metal catalysts have become sought after. Reversible conjugation, especially covalent binding, is gaining increasing attention due to its high potency and selectivity. Reversible covalent chemistries have been utilized in dynamic combinatorial chemistry[3], to design ligands that target biomolecules[4], and as potential enzyme inhibitor drugs, which have decreased toxicity compared to irreversible covalent inhibitors.[5] Specific reversible covalent conjugations include formation of boronate esters to target saccharides[6–8], Michael addition of thiols to create covalent kinase inhibitors[9,10], and modification of glutathione to generate specific sensors.[11,12]

Our group and others have exploited the reactivity of amines to form iminoboronates through N-B dative bond stabilization when a 2-acetylphenylboronic (APBA) acid is used to bind proteins and lipids[13,14] or promote peptide cyclization with an amine-containing residue.[15,16] The potent reversible covalent interaction between APBA and amines has highlighted the utility of iminoboronate-stabilized conjugations as novel bioorthogonal reactions.

3.2 Previous Work: Thiazolidino Boronate (TzB) Formation

Our lab and the Gois lab previously reported a novel conjugation chemistry between 2-formylphenyl boronic acid (FPBA) and free cysteine (Cys) to form an iminoboronate-stabilized thiazolidine, named a thiazolidino boronate (TzB)[17,18] (**Scheme 3-1A**). TzB complex formation is very potent (K_d = ~50 nM) and quick ($t_{1/2}$ = 18 ± 2 sec) with a rate constant on the order of 10^3 M^{-}

$^{1}s^{-1}$, which is as fast as some of the quickest reported bioorthogonal reactions.[19] The TzB complex between FPBA and Cys gives two characteristic ^{1}H NMR shifts around 6.1 and 6.25 ppm, both representing the allylic hydrogen. There are two peaks because two TzB isomers form at neutral pH: the multicyclic mixed anhydride form and the open free carboxylic acid form (**Figure 3-1A**).

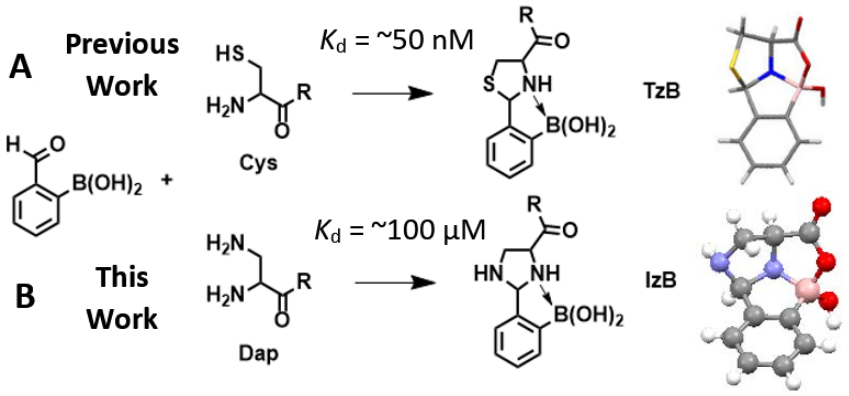

Scheme 3-1: Comparison of previous thiazolidino boronate (TzB) conjugation to the current imidazolidino boronate (IzB) small molecule conjugation. X-ray crystal structures of both conjugates are shown on the right.

3.3 Imidazolidino Boronate (IzB) Formation

3.3.1 IzB Formation Between Dap and FPBA

To explore other related conjugation chemistries, the reactivity of FPBA with the short chain lysine homolog 2,3-diaminopropionic acid (Dap) was explored. Dap is also a Cys analog, with a 1,2-diamino moiety instead of a 1,2-aminothiol moiety, allowing for similar types of reactivity. The FPBA-Dap conjugate, called an imidazolidino boronate (IzB), is structurally very similar to the TzB complex as an iminoboronate-stabilized imidazolidine (**Scheme 3-1B**). The rate constant was on the same order of magnitude as TzB formation (10^3 $M^{-1}s^{-1}$), however, the conjugate formation was less potent (K_d = ~100 µM), but slightly quicker (t_1 = 6.2 ± 0.4 sec) than TzB formation (**Figure 3-2**). The IzB complex between FPBA and Dap also gives two characteristic ^{1}H NMR shifts around 5.7 and 5.8 ppm, representing the allylic hydrogen of the two IzB isomers (**Figure 3-1B**).

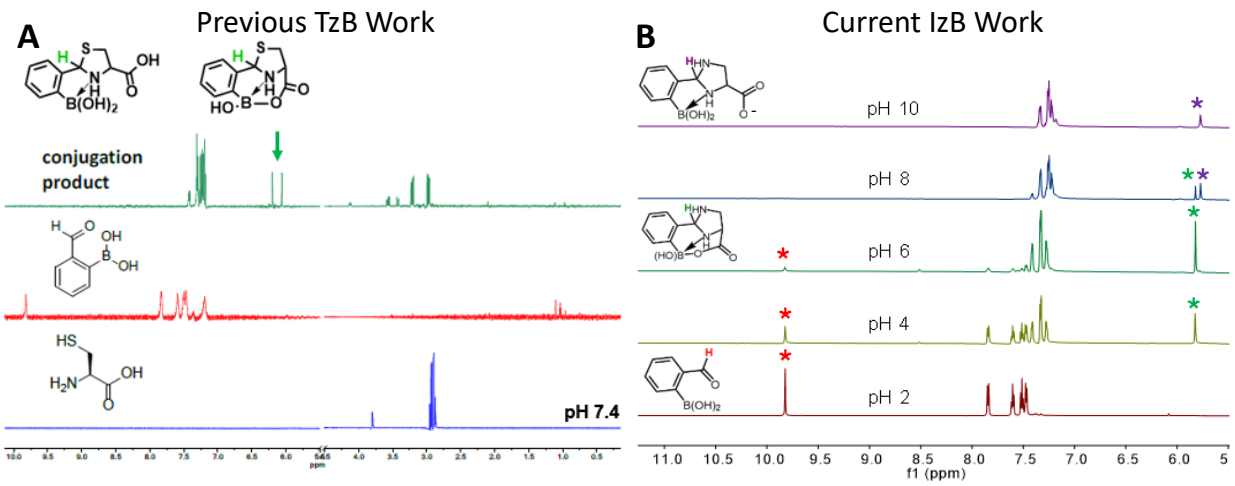

Figure 3-1: Small molecule TzB and IzB Conjugate NMR Spectra. A) Previously reported [1]H NMR of TzB formation between FPBA and Cys in neutral, aqueous solution, displaying the characteristic conjugate peaks around 6.1 and 6.25 ppm (green arrow).[17] B) From this work, [1]H NMR illustrating IzB formation as a function of pH, displaying two characteristic allylic H peaks around 5.7 and 5.8 ppm. Like TzB formation, there are two isomers seen at neutral pH, with the mixed anhydride assumed to be predominant at acidic pH values and the open free carboxylic acid isomer assumed to be predominant at basic pH values. Colored * correspond to the colored hydrogens.

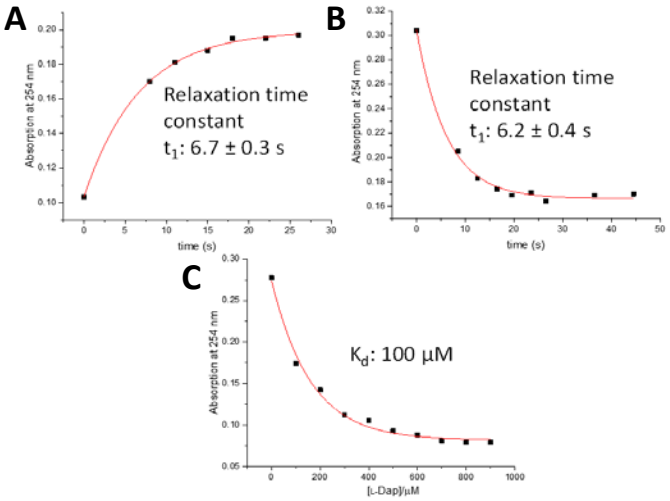

Figure 3-2: Kinetics of IzB Formation Between FPBA and Dap. Reaction kinetics of IzB complex dissociation (A) and formation (B) with a t_1 of about 6 seconds. Titration curve of IzB complex formation with increasing Dap concentrations (C). All monitored the appearance or disappearance of FPBA via UV-Vis absorption at 254 nm.

The crystal structure of the FPBA-Dap IzB was obtained at pH 7.4. The full structure was a tetramer of IzB complexes around a central NaCl molecule (**Figure 3-3**). The multicyclic monomer structure is highlighted in **Scheme 3-1B**. Structural data can be found in **Table 3-1** and **Table 3-2**.

Table 3-1: Crystal data and structure refinement for the FPBA-Dap IzB complex. Structure Seen as a tetramer around a central NaCl molecule.

Identification code	C40H44B4ClN8NaO12	
Empirical formula	C40 H44 B4 Cl N8 Na O12	
Formula weight	930.51	
Temperature	100(2) K	
Wavelength	1.54178 Å	
Crystal system	Tetragonal	
Space group	I4	
Unit cell dimensions	a = 17.4670(5) Å	a= 90°.
	b = 17.4670(5) Å	b= 90°.
	c = 6.7244(2) Å	g = 90°.
Volume	2051.59(13) $Å^3$	
Z	2	
Density (calculated)	1.506 Mg/m^3	
Absorption coefficient	1.580 mm^{-1}	
F(000)	968	
Crystal size	0.250 x 0.220 x 0.140 mm^3	
Theta range for data collection	5.064 to 66.529°.	
Index ranges	-20<=h<=11, -20<=k<=19, -7<=l<=7	
Reflections collected	5002	
Independent reflections	1718 [R(int) = 0.0245]	
Completeness to theta = 66.529°	99.3 %	
Absorption correction	Semi-empirical from equivalents	
Max. and min. transmission	0.7528 and 0.6716	
Refinement method	Full-matrix least-squares on F^2	
Data / restraints / parameters	1718 / 1 / 163	
Goodness-of-fit on F^2	1.039	
Final R indices [I>2sigma(I)]	R1 = 0.0227, wR2 = 0.0577	
R indices (all data)	R1 = 0.0232, wR2 = 0.0580	
Absolute structure parameter	0.032(8)	
Extinction coefficient	n/a	
Largest diff. peak and hole	0.305 and -0.156 $e.Å^{-3}$	

Table 3-2: Atomic coordinates (x 10^4) and equivalent isotropic displacement parameters ($Å^2x10^3$) for the FPBA-Dap IzB complex. U(eq) is defined as one third of the trace of the orthogonalized U^{ij} tensor.

	x	y	z	U(eq)
Na(1)	5000	5000	2511(3)	15(1)
Cl(1)	5000	5000	6570(1)	14(1)
O(1)	6341(1)	5315(1)	2576(2)	13(1)
O(2)	7024(1)	5597(1)	5578(2)	13(1)
O(3)	6905(1)	5644(1)	8865(2)	16(1)
N(1)	6699(1)	4269(1)	5014(3)	12(1)
N(2)	7501(1)	3290(1)	6337(3)	17(1)
B(1)	6941(1)	5046(1)	3834(4)	12(1)
C(1)	6914(1)	5280(1)	7325(3)	12(1)
C(2)	6810(1)	4422(1)	7171(3)	14(1)
C(3)	7529(1)	3942(1)	7708(4)	17(1)
C(4)	7248(1)	3617(1)	4474(4)	15(1)
C(5)	7877(1)	4011(1)	3306(3)	13(1)
C(6)	8536(1)	3643(1)	2655(3)	16(1)
C(7)	9065(1)	4057(1)	1550(4)	20(1)
C(8)	8937(1)	4828(1)	1137(3)	18(1)
C(9)	8280(1)	5192(1)	1808(3)	14(1)
C(10)	7735(1)	4783(1)	2899(3)	12(1)

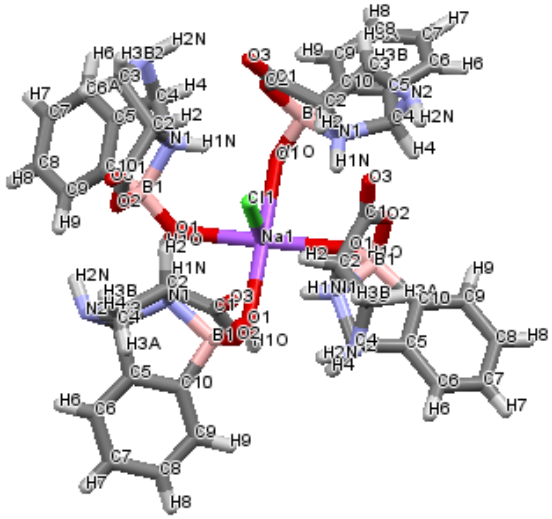

Figure 3-3: Crystal structure of the tetrameric NaCl salt IzB complex between FPBA and Dap.

3.3.2 The Bioorthogonality of IzB Conjugation

The stability of the FPBA-Dap IzB complex towards biologically relevant moieties, such as amines (Lys), thiols (glutathione), diol boron chelators (glucose), 1,2-aminoalcohols (Ser), and 1,2-aminothiols (Cys), was examined via ^{1}H NMR (**Figure 3-4**). Glutathione, glucose, and Ser did not interfere with the IzB complex, so biological thiols, diol boron chelators, and 1,2-aminoalcohols should not compete with IzB complexes. As expected, Cys at either an equimolar or 10-fold excess ratio to the IzB complex competed to form the TzB complex, as indicated by the disappearance of the two IzB peaks at 5.7 and 5.8 ppm (pink arrows) and the appearance of the TzB conjugate peaks at 6.1 and 6.25 ppm (green arrows). Lys caused slight competition via iminoboronate formation with the FPBA, as indicated by the appearance of an imine peak around 8.4 ppm (blue asterisk).

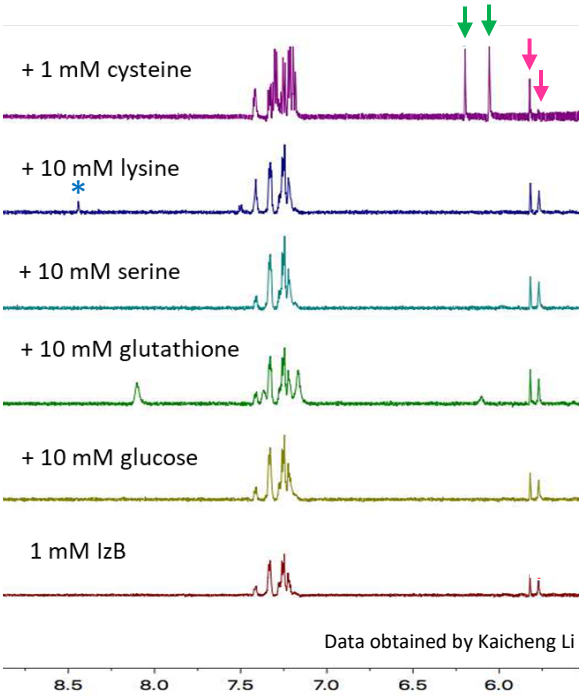

Figure 3-4: Small Molecule Competition with Dap/FPBA IzB. ^{1}H NMR spectra of the IzB (1 mM) with a variety of potential biologically relevant small molecule inhibitors. Cys competed the IzB peaks around 5.7 and 5.8 ppm (pink arrows) away to form a TzB conjugate, as indicated by the peaks around 6.1 and 6.25 ppm (green arrows). Lysine also caused minimal competition via iminoboronate formation with FPBA, forming an imine peak around 8.4 ppm (blue asterisk).

3.4 Attempts at TzB-Mediated Peptide Cyclization

FPBA was previously shown to form a TzB with the N-terminal Cys of a short peptide, CAL, at neutral pH.[17] To study intramolecular TzB formation, peptides containing an N-terminal Cys residue and a C-terminal FPBA-containing residue were synthesized in the hopes of using TzB formation as a novel peptide cyclization strategy. The peptide names and sequences are listed in **Table 3-3**.

Peptide Name	Sequence
CW1	CAAAAGDap(FPBA)
CW2	SAAAAGDap(FPBA)
CW3	CAVWAGDap(FPBA) – using Cys(Acm)
CW4	CAVWAGDap(FPBA) – using Cys(Fm)
CW5	CAVWAGC(FPBA)
CW6	DapAVWAGC(FPBA)
KL21	DapAAAAGDap(FPBA)
KL22	DapAAGAAAGDap(FPBA)

Table 3-3: Peptide names and sequences used for TzB and IzB peptide cyclization studies.

3.4.1 Initial Peptide Synthetic Scheme

In the first synthetic strategy, the orthogonal Alloc protecting group was selectively deprotected using palladium after Fmoc-based SPPS to reveal the free side chain amine of Dap at the C-terminus. A carboxylic acid derivative of FPBA was activated using HBTU and coupled to the Dap side chain amine under standard amide bond formation conditions. After on-resin Fmoc removal, the peptide was globally deprotected and cleaved from resin using a TFA and water mixture followed by HPLC purification. If an orthogonal protecting group was used on the side chain thiol of Cys, that would be selectively removed last and re-purified via HPLC (**Scheme 3-2**).

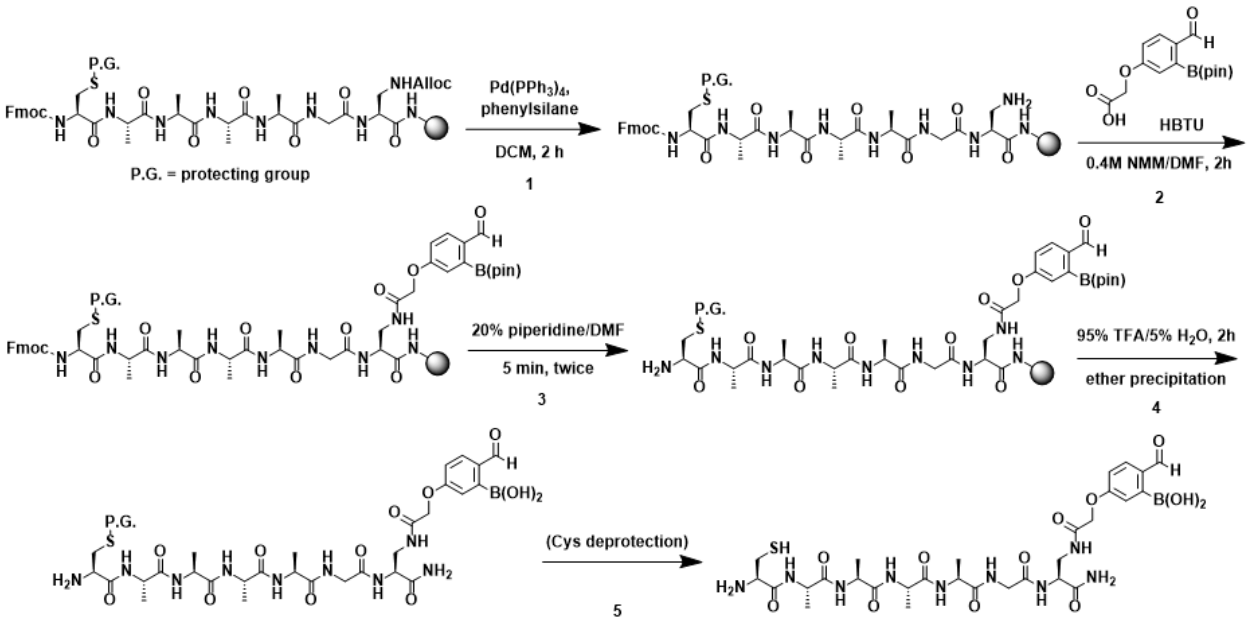

Scheme 3-2: Initial N-terminal Cys and FPBA-containing peptide synthetic strategy. Used to make CW1 through CW4 (CW1 shown). P.G. represents the Cys protecting group.

3.4.2 CW1 Peptide Synthesis

First, the acid-labile Trt protecting group was used for the side chain thiol of Cys to make a short peptide containing an N-terminal Cys and a C-terminal FPBA-modified Dap residue: CAAAAGDap(FPBA), named CW1 (**Table 3-3**). After step 2, a small-scale acidic cleavage and peptide deprotection was performed to check peptide quality (**Scheme 3-2**). LCMS analysis of Fmoc-CW1 gave multiple peaks, corresponding to either peptide intermediates (Alloc-protected peptide and Alloc-deprotected but not FPBA coupled peptide) or the expected peptide mass minus one or two water molecules (**Figure 3-5A**). The presence of peptide intermediates indicated that the Alloc deprotection and FPBA coupling steps were not clean. The expected peptide mass minus one or more water molecules could be due to water loss from the boronic acid of FPBA, which has been reported before[13,15]. The peptide was not anticipated to be this

messy, as the N-terminal Fmoc protection should prevent TzB cyclization. After step 4, the deprotected peptide mass was not detectable via LC-MS.

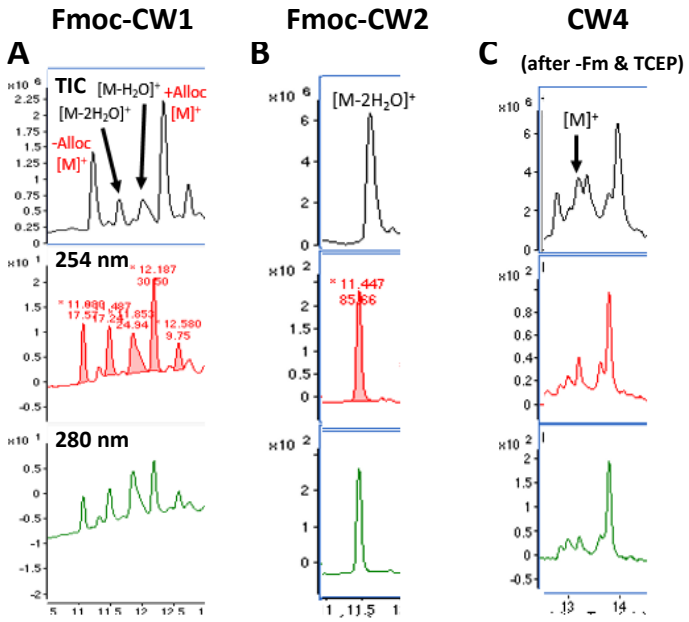

Figure 3-5: Initial Peptide Synthesis Attempts. LC-MS trace after acidic cleavage and deprotection of the Trt-protected Fmoc-CW1 peptide (A), displaying multiple peaks corresponding to intermediate peptides (in red) and the expected peptide mass minus one or two water molecules; the Fmoc-CW2 peptide (B), displaying a single peak corresponding to the expected peptide mass minus two water molecules; and the CW4 peptide after Fm deprotection and TCEP reduction (C), displaying the expected peptide mass among multiple peaks.

3.4.3 Serine Analog CW2 Peptide Synthesis

Given the messiness of CW1, the N-terminal serine (Ser) analog CW2 was made, which was not expected to react with FPBA, due to the high side chain pK_a of Ser. This would allow us to examine the peptide synthetic strategy to ensure that FPBA could be cleanly incorporated into a peptide via Dap side chain modification.

After step 2, small scale acidic cleavage and LC-MS analysis gave only one peak, corresponding to the expected peptide mass of Fmoc-CW2 minus two water molecules (**Figure 3-5B**). The water loss is most likely from the boronic acid, as the peptide was not expected to cyclize. After step 4, the expected mass of the deprotected peptide was readily seen via LC-MS. Therefore, the peptide synthesis was not the issue.

3.4.4 CW3 and CW4 Peptide Synthesis

The sequence was modified slightly to incorporate more hydrophobic residues, increasing the retention time on a reverse-phase HPLC column and allowing for easier LC-MS analysis. To keep the Cys side chain thiol protected during acidic cleavage, a few orthogonally protected Cys residues were explored. The acetamidomethyl (Acm) protecting group was initially used, but the Acm-protected CW3 peptide was difficult to purify after Fmoc deprotection. A variety of Acm deprotection conditions were used, including $Hg(OAc)_2$[20], AgOAc[21], AgOTf[22], and $PdCl_2$,[23] of which AgOAc cleanly deprotected the Fmoc-Cys(Acm)-OH amino acid. After Acm deprotection with AgOAc, multiple peaks were seen for CW3 upon LC-MS analysis. Two peaks corresponded with the desired peptide mass minus two water molecules, but it was too messy to purify.

Next, the 9-fluorenylmethyl (Fm) protecting group was chosen as its deprotection conditions (50% piperidine in DMF for 2h) were better tolerated. Fm-protected CW4 was synthesized and purified very cleanly. However, the LC-MS trace became messy upon Fm removal, although the dimer mass was seen. This was expected as the Fm deprotection conditions are known to given oxidized Cys thiols.[24] HPLC purification did not yield a significantly more pure peptide. TCEP reduction did give the reduced monomer peptide mass, but made the LC-MS trace even messier (**Figure 3-5C**).

Overall, selective deprotection of the Cys residue did not yield cleanly or easily synthesized peptides. Those are essential to make a novel peptide cyclization strategy meaningful. Therefore, another strategy for incorporation of the FPBA moiety was investigated in attempts to create the N-terminal Cys and FPBA-containing peptide cleanly.

3.4.5 Modified Peptide Synthetic Scheme

The order of FPBA addition and Cys deprotection steps were reversed so that FPBA was added last to reduce possible side reactions. Instead of using a carboxylic acid FPBA derivative to amidate a Dap residue in DMF, an iodoacetamide FPBA derivative was used to alkylate a Cys residue in aqueous solution. The peptide was synthesized using standard Fmoc SPPS protocols and all acid-labile protecting groups, including an N-terminal Boc. After acidic resin cleavage and deprotection using Reagent K, the crude free peptide was dissolved in neutral PBS and reacted with FPBA for 5-10 minutes. This allows the N-terminal Cys to be protected as a TzB complex and not be available for alkylation with the iodoacetamide small molecule, which would react with any free thiol. After TzB protection, the iodoacetamide FPBA derivative is added and reacted overnight. The TzB complex is dissociated by acidifying the reaction before HPLC purification, yielding the free N-terminal Cys and FPBA modified peptide (**Scheme 3-3**).

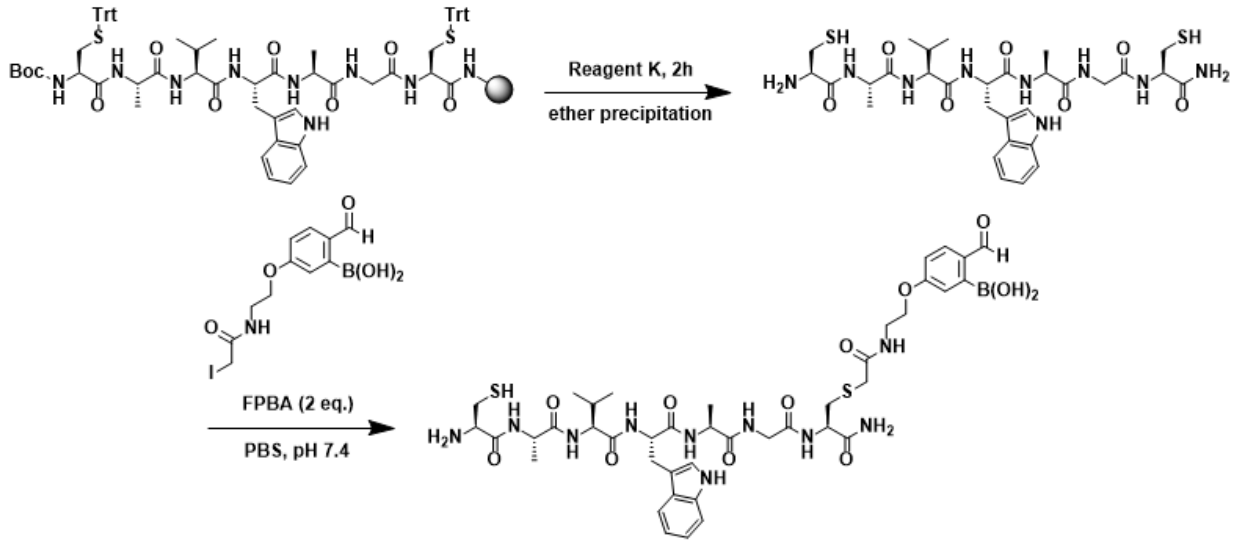

Scheme 3-3: Modified N-terminal Cys and FPBA-containing peptide synthetic strategy used to make CW5 and CW6 (CW5 shown).

3.4.6 CW5 Peptide Synthesis

After synthesis using the modified iodoacetamide method, CW5 was a single peak during HPLC purification but multiple peaks on the LC-MS trace, all corresponding to the expected peptide mass (linear) or the mass minus one (cyclic) or multiple water molecules (cyclic peptide with boronic acid water loss) (**Figure 3-6B**). Given that this peptide was the cleanest N-terminal Cys and FPBA-containing peptide made, the multiple peaks were determined to be due to an intrinsic intramolecular reactivity of an N-terminal Cys residue and FPBA.

3.4.7 CW6 Peptide Synthesis

To examine a less reactive analogous peptide, an N-terminal Dap residue was used in place of Cys to induce IzB-mediated peptide cyclization (**Figure 3-6A**). IzB formation is less potent than TzB formation, so peptide cyclization was anticipated to be cleaner. After synthesis using the modified method and HPLC purification, CW6 gave a single peak on the HPLC and LC-MS trace, corresponding to the expected peptide mass (linear), the mass minus one water molecule (cyclic), and the mass minus two water molecules (cyclic peptide with boronic acid water loss) (**Figure 3-6C**). The single peak displaying the collection of masses related to the expected peptide mass indicated that there was one species present in multiple forms, whereas the multiple peaks of CW5 indicated that multiple species were present.

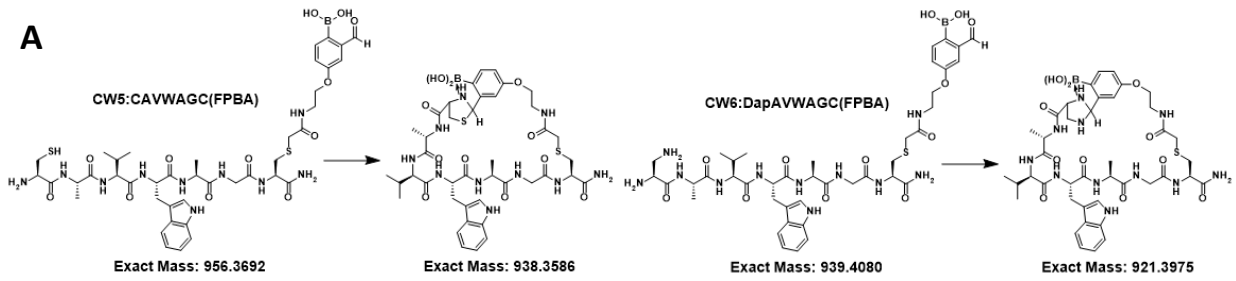

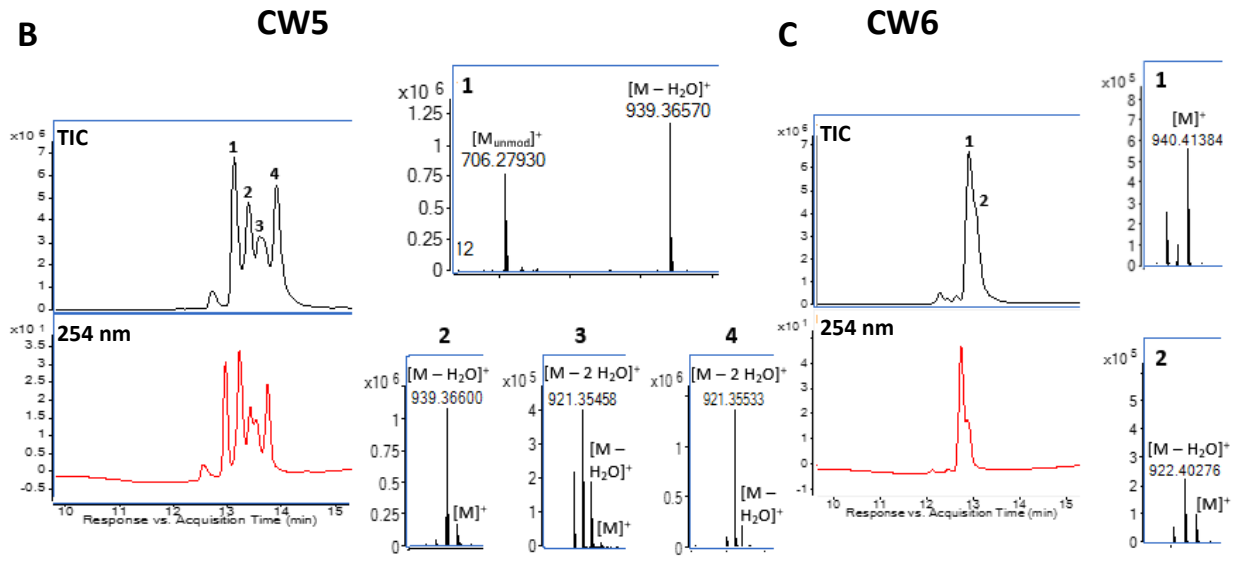

Figure 3-6: TzB- and IzB-Cyclized Peptides. Structures of liner and cyclic CW5 and CW6 (A). LC-MS traces of pure TzB-cyclized CW5 (B), displaying multiple peaks corresponding to the expected peptide mass minus one or two water molecules; and pure IzB-cyclized CW6 (C), displaying one peak of the expected peptide mass with a shoulder of the desired mass minus one water molecule.

3.5 IzB-Mediated Peptide Cyclization with KL21 and KL22

3.5.1 KL21 and KL22 Peptide Synthesis

Given the success of IzB-cyclized CW6, IzB-mediated peptide cyclization was further studied in a joint effort with Kaicheng Li. KL21 and KL22, N-terminal Dap and FPBA-containing peptides of various lengths, were synthesized using standard Fmoc-based SPPS and C-terminal Dap amidation method to install the FPBA moiety (**Scheme 3-4**). A simple sequence of alanine and glycine residues were used to simplify NMR analysis. Peptide synthesis with an N-terminal Dap residue was much easier than an N-terminal Cys residue and gave a clean peptide as seen via LC-MS (**Figure 3-7**).

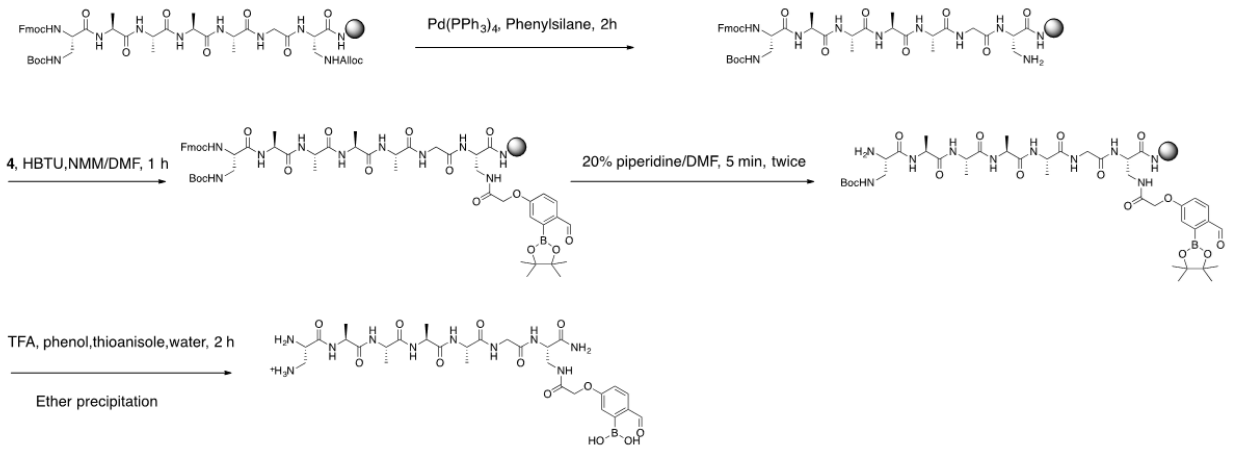

Scheme 3-4: Synthetic route for KL21 and KL22 peptides (KL21 shown).

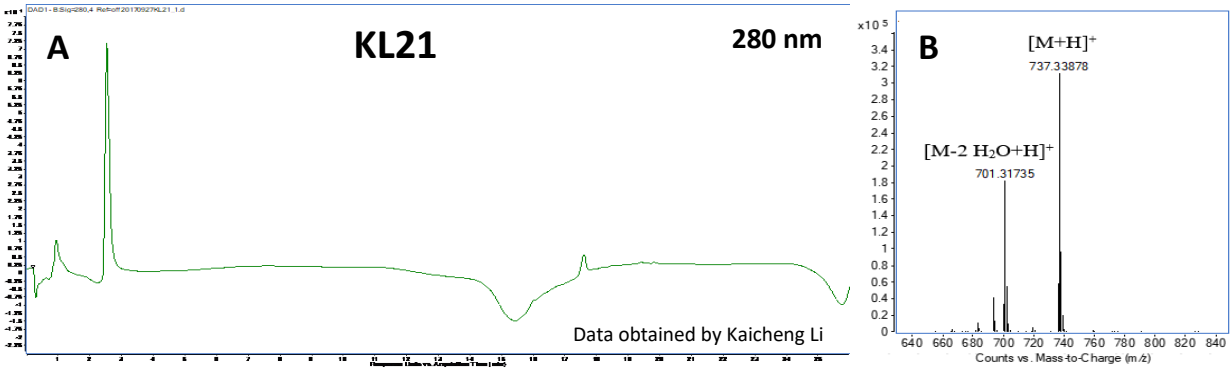

Figure 3-7: LC UV trace (A) and mass spec data (B) of KL21.

3.5.2 pH-Dependent Peptide Cyclization

Intramolecular IzB cyclization was examined via ^{1}H NMR of KL21 and KL22 at various pH values in PBS buffer (**Figure 3-8**). Both peptides are completely linear at acidic pH (pH < 3), as indicated by the presence of the characteristic FPBA aldehyde peak around 9.8 ppm. Above pH 5, the aldehyde peak begins to disappear and the IzB conjugate peak around 5.7 ppm appears. Lack of the aldehyde peak at neutral pH indicates complete cyclization of both peptides.

Intramolecular cyclization results in one IzB conjugate peak because only one IzB isomer can form, as the amide bond of the N-terminal Dap residue prevents formation of the mixed anhydride isomer.

Given their pH profiles, both KL21 and KL22 should be stable and remain cyclic under physiologic conditions. The pH-dependent reversibility of IzB cyclization would allow such cyclic peptides to act as "smart" peptides, able to become linear in slightly acidic environments, such as the endosome (pH 4.5-6.5).[25]

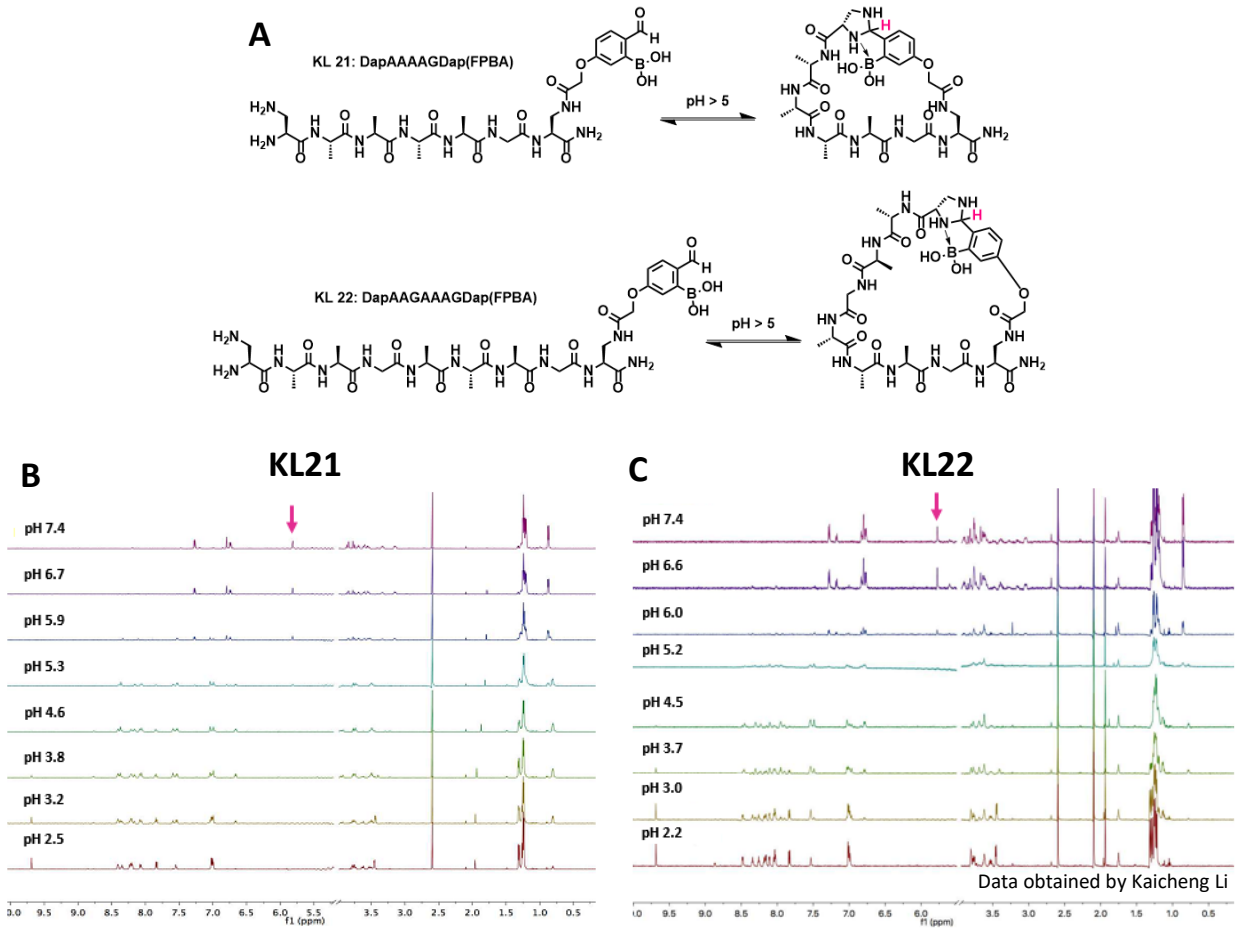

Figure 3-8: pH-Dependent IzB Cyclization of KL21 and KL22 Peptides. Structures of IzB-cyclized KL21 and KL22 peptides with the characteristic allylic H indicated in pink (A). ^{1}H NMR spectra of KL21 (B) or KL22 (C) (500 µM) in buffer at increasing pH values. Cyclization is monitored via appearance of the IzB peak around 5.7 ppm (pink arrow). Cyclization is complete at neutral pH for both KL21 and KL22.

3.5.3 Stability of IzB-Cyclized KL21 Peptide

Due to the specific FPBA reactivity with either 1,2-aminothiol or 1,2-diamino moieties, no interference from other biologically relevant small molecules is expected. Cyclic KL21 at neutral pH was subjected to biologically relevant small molecules to probe intramolecular IzB stability towards amines (Lys), thiols (glutathione), diol boron chelators (glucose), and 1,2-aminoalcohols (Ser) (**Figure 3-9**). The IzB peak around 5.7 ppm persisted with all small molecule treatment, indicating IzB-cyclized peptides are stable to all the small molecules tested.

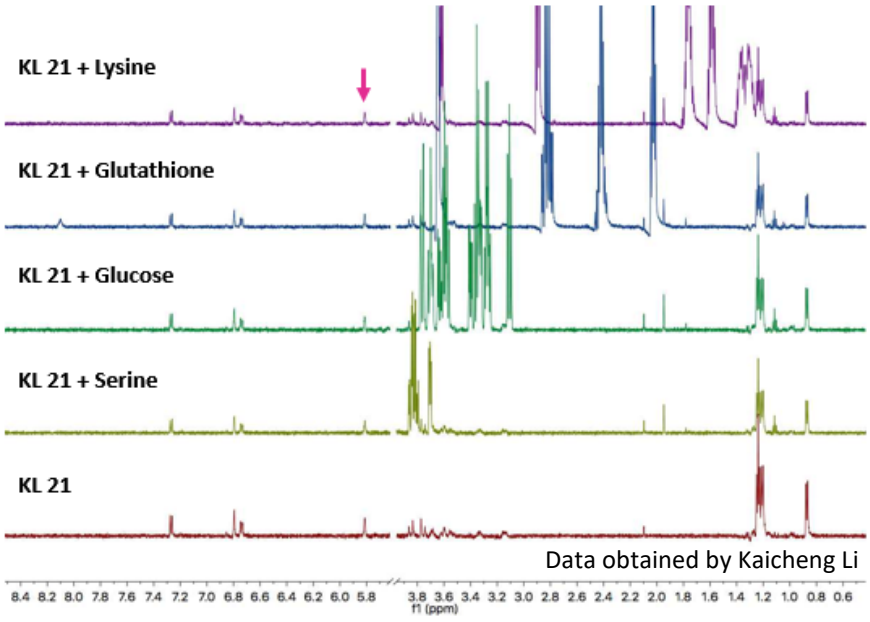

Figure 3-9: Biologically Relevant Small Molecule Competition with an IzB-Cyclized Peptide. ^{1}H NMR spectra of the KL21 peptide (200 μM) with a variety of potential biologically relevant small molecule IzB inhibitors (2 mM). None of the small molecules inhibited IzB formation, as indicated by the presence of the IzB conjugate around 5.8 ppm (pink arrow).

3.6 Potential Application: Cysteine Sensing

Previously, TzB formation between FPBA and a short model peptide containing an N-terminal Cys residue showed competition between free Cys and the peptide for TzB formation with FPBA.[17] We also showed that the IzB complex between Dap and FPBA is in equilibrium with

the TzB complex upon addition of Cys. Therefore, it was hypothesized that an IzB-cyclized peptide could be linearized with Cys treatment (**Scheme 3-5**). Thus, an IzB-cyclized "smart" peptide could be used to respond to Cys, potentially acting as a Cys sensor.

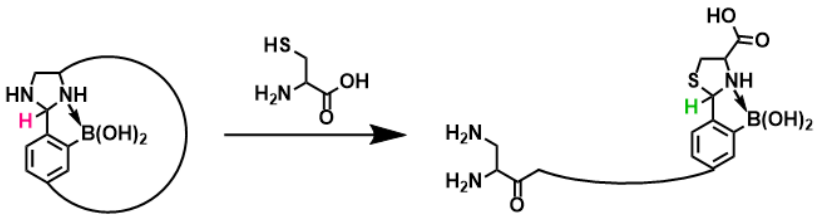

Scheme 3-5: Cartoon depicting "smart" Cys-mediated peptide linearization via TzB formation.

3.6.1 Cysteine Reactivity of IzB-Cyclized Peptides

The extent of Cys sensitivity of IzB-cyclized KL21 and KL22 was examined via ^{1}H NMR. As expected, the TzB complex formed in a Cys concentration-dependent manner, as indicated by the appearance of the two IzB peaks around 6.1 and 6.25 ppm (green arrows) (**Figure 3-10A, B**). Linearization began around 0.3 mM and 2 mM Cys for KL21 and KL22, respectively. Upon plotting the integration of the TzB peaks compared to the IzB peak and curve fitting, EC_{50} values of 2.0 mM and 1.5 mM for KL21 and KL22, respectively, could be determined (**Figure 3-10C, D**).

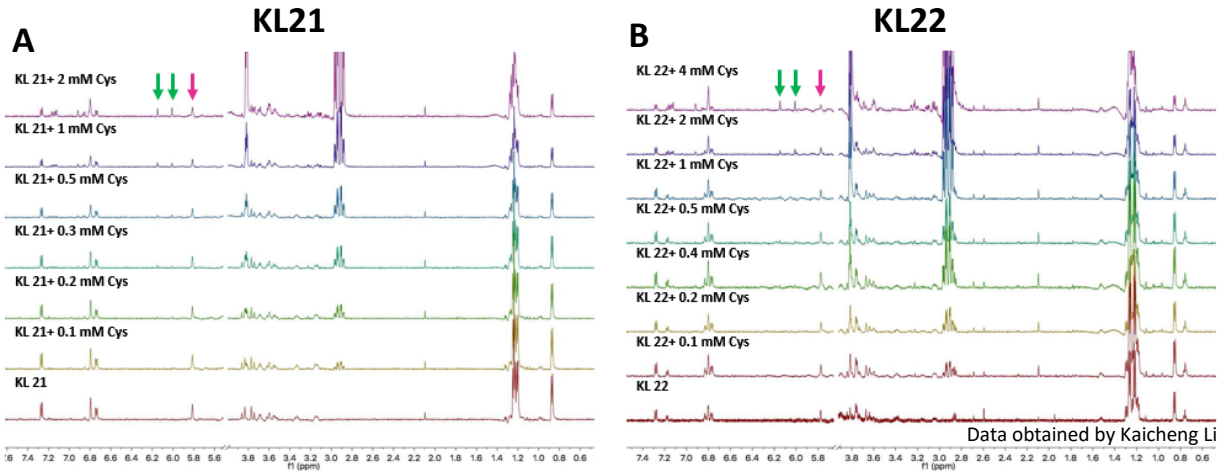

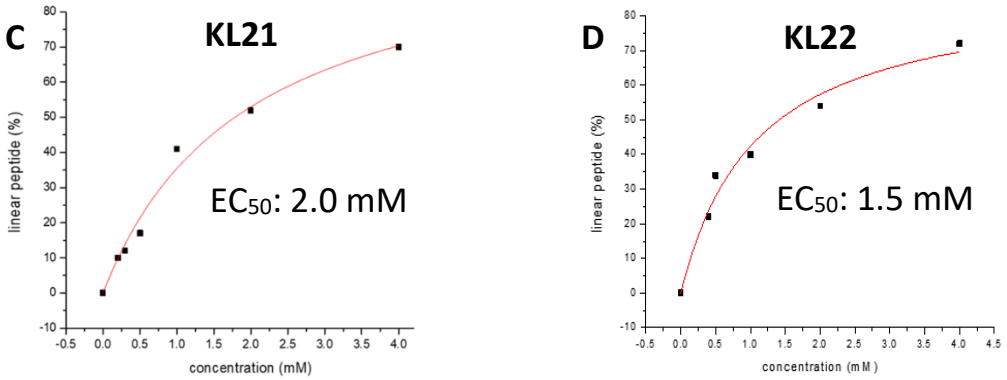

Figure 3-10: Cysteine Titration Competitions with IzB-Cyclized Peptides KL21 and KL22. ^{1}H NMR spectra of cyclic KL21 (A) or cyclic KL22 (B) (200 µM) in neutral buffer with increasing Cys concentrations. Linearization is monitored via appearance of the two TzB isomer peaks around 6.0 and 6.2 ppm (green arrows) and disappearance of the IzB peak around 5.8 ppm (pink arrow). Titration curves of TzB complex formation of KL21 (C) and KL22 (D) with increasing Cys concentrations.

3.6.2 Cys-Dependent Linearization and Cys Oxidation of KL21 in FBS

To ensure the applicability of IzB-mediated peptide cyclization in biological applications, IzB-cyclized peptides must be stable in complex mixtures, such as a fetal bovine serum (FBS) solution. The cysteine sensing ability must also not be altered in the presence of a complex mixture.

Upon ^{1}H NMR analysis, 10% FBS did not affect the cyclization of KL21 nor the ability of Cys linearize KL21 in a concentration-dependent manner (EC_{50} = 2.1 mM, **Figure 3-11A**). However, upon incubation at room temperature over 20 h, Cys oxidized to cystine, which could no longer form the TzB complex, as evident by the disappearance of the TzB peaks at 6.1 and 6.25 ppm. This allowed KL21 to re-cyclize, as seen by the re-appearance of the IzB benzylic peak around 5.8 ppm (**Figure 3-11B**).

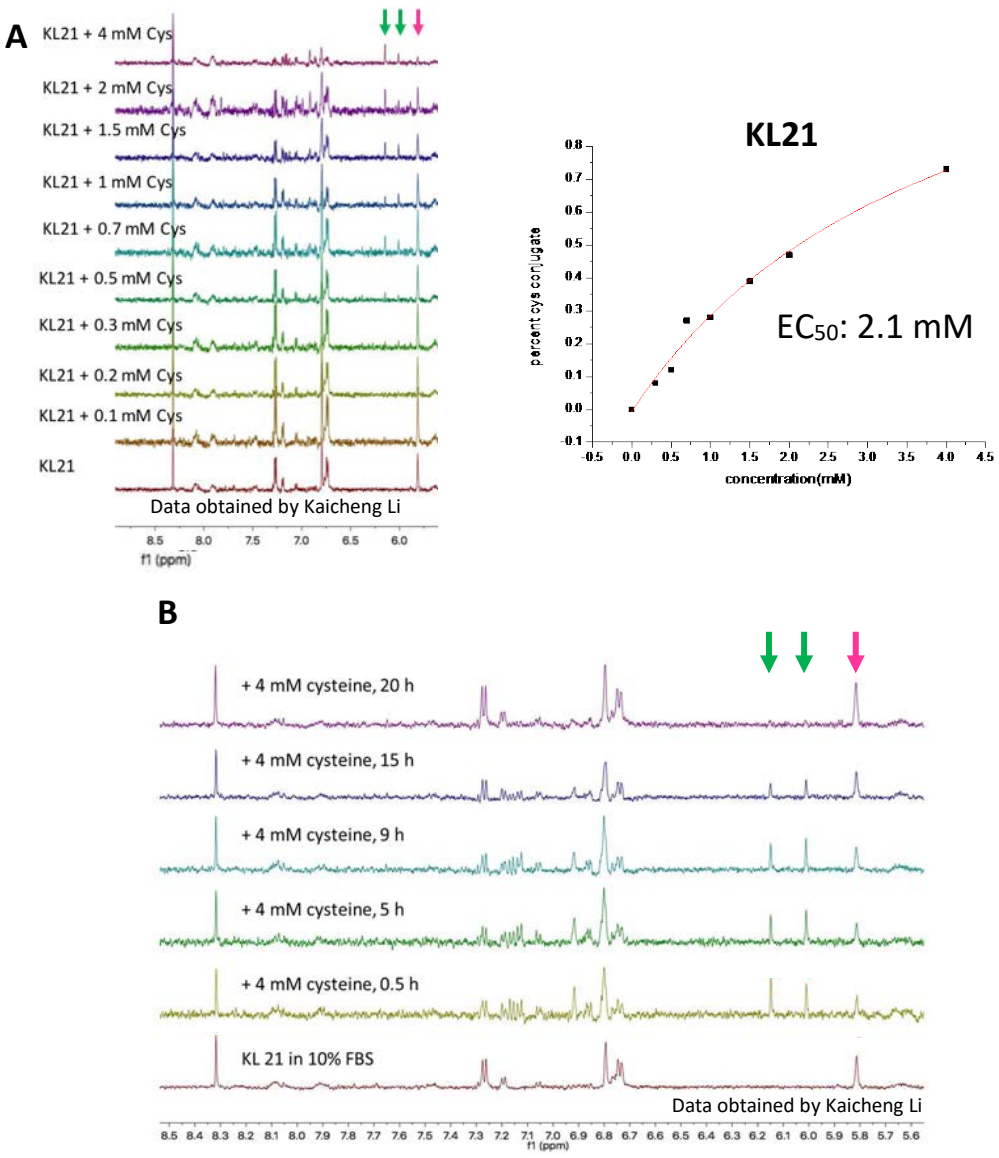

Figure 3-11: Cysteine Responsiveness of IzB-Cyclized KL21 Peptide in FBS. (A) ^{1}H NMR spectra of the Cys titration of KL21 (200 µM) in the presence of 10% FBS. There is no interference from FBS, as the IzB conjugate peak (pink arrow) becomes the TzB conjugate peaks (green arrows) with increasing Cys concentration. Integration of the TzB peaks relative to the IzB peak and curve fitting gave an EC_{50} value for Cys-induced peptide linearization. (B) Time resolved ^{1}H-NMR spectra measuring Cys oxidation in 10% FBS. As the Cys is oxidized over time, KL21 recyclizes, as indicated by the reappearance of the IzB peak.

3.7 Conclusions

Inspired by our previously discovered reversible covalent TzB chemistry, TzB-cyclized peptides were pursued by incorporating an N-terminal Cys residue and C-terminal FPBA moiety. After multiple attempts using orthogonal Cys protecting groups and introduction of the FPBA at various synthetic steps, it was determined that intramolecular TzB formation yielded messy peptides for reasons yet to be understood. A few N-terminal Cys and FPBA-containing peptides were synthesized to give the expected masses via LC-MS analysis, but gave multiple peaks on the TIC trace corresponding to the correct mass or the mass minus one or multiple water molecules. Given the complications with TzB-mediated peptide cyclization, another related reversible covalent chemistry was characterized and explored.

We have contributed a novel reversible covalent chemistry between Dap and FPBA to form an IzB complex. IzB conjugation is quickly reversible under physiological conditions and quite potent, with a K_d of approximately 100 μM. There is little interference from most biologically relevant small molecules, except Cys, which is known to readily form a TzB complex with FPBA. This conjugation can be utilized for rapid peptide cyclization at neutral pH, yielding a "smart" peptide that is able to linearize in both pH- and Cys-dependent manners. An IzB-cyclized peptide was also shown to be stable in the presence of FBS. Given the biocompatibility and chemoselectivity, IzB conjugation should be useful in the development of molecular probes and other "smart" materials.

3.8 Experimental Procedures

3.8.1 General Methods

Fmoc-Rink Amide MBHA resin and HBTU were purchased from Novabiochem (San Diego, CA). All Fmoc-protected amino acids and L-2,3-diaminopropionic acid (Dap) were purchased from either Chem-Impex International (Wood Dale, IL) or Advanced Chemtech (Louisville, KY). All other chemicals were purchased from Fisher Scientific (Pittsburgh, PA) or Sigma Aldrich (St. Louis, MO), unless otherwise indicated. IzB association and dissociation kinetics were studied using a NanoDrop 2000c UV-vis spectrometer. Peptide synthesis was carried out on a Tribute peptide synthesizer (Protein Technologies, Tucson, AZ). Peptide purification was performed on a Waters PrepLC system using a Phenomenex Jupiter C_{18} column (Torrance, CA). ^{1}H NMR spectra were collected using a VNMRS 600 MHz NMR spectrometer with 256 scans at 25°C. NMR data were processed using MestReNova 11.0 software. Mass spectrometry data were collected using an Agilent 6230 LC TOF mass spectrometer. PBS buffer (1 mM) was used for all experiments.

3.8.2 NMR Studies of FPBA Conjugation with Dap

To prepare the IzB complex, 315 µL each of 22.2 mM FPBA and Dap stock solutions (in PBS) were mixed with 70 µL D_2O (10 mM each final concentration, 10% D_2O). The pH was tuned from 1 to 10 incrementally.

3.8.3 IzB Complex Crystallographic Information

300 mM solutions of FPBA (22.5 mg in 500 µL) and Dap (21.1 mg in 500 µL) in water were prepared and combined. 1 mL of MeOH was added to that mixture and the pH was tuned to 7.4.

The solution was filtered through a 0.45 µm PTFE membrane filter (Phenomenex) and allowed to slowly evaporate from a loosely capped 5 mL glass vial at room temperature. After a few days, crystal aggregates were observed and redissolved in pure MeOH. After slow recrystallization at room temperature over a week, single crystals were observed.

3.8.4 Kinetic and Thermodynamic Studies of the IzB Complex Formation

Both the association and dissociation kinetics were examined via UV-vis absorption. The disappearance or appearance of the characteristic FPBA absorbance at 254 nm was used to measure the formation or breakdown of the IzB complex, respectively. Data were collected after blank subtraction using PBS (pH 7.4). The reactions were performed in a quartz cuvette (10 mm path length, total volume ~1 mL) using PBS at room temperature. All stock solutions were prepared in PBS (pH 7.4).

For the dissociation reaction, an equimolar mixture of FPBA and Dap (1 mM) was created by mixing 90 µL of FPBA stock (10 mM) and 18 µL of Dap stock (50 mM) with 792 µL PBS. The mixture was incubated at room temperature for 15 minutes to allow the IzB complex to form completely. The mixture was diluted 16.7x to a final concentration of 60 µM and quickly mixed via pipetting. The absorbance profile was recorded approximately every 3 seconds. The initial absorbance value of the IzB complex was obtained from a separate equimolar mixture of FPBA and Dap (600 µM) pre-incubated for 15 minutes. The absorbance at 254 nm was obtained via NanoDrop reading. A 600 µM solution measured using a 1 mm path length (NanoDrop) would be equivalent to a 60 µM solution measured using a 10-mm path length (cuvette). A rapid increase in absorbance at 254 nm was seen as FPBA was generated upon dissociation of the IzB complex.

Plotting the absorbance at 254 nm against time followed by curve fitting gave the relaxation time constant of the backward reaction.

For the association reaction, 6 µL of FPBA stock (10 mM) was added to 994 µL PBS in the cuvette and mixed to make a 60 µM FPBA solution. The absorbance spectrum was recorded as the initial time point. 1.2 µL of Dap stock (50 mM) was added to the cuvette and quickly mixed via pipetting. The absorbance profile was recorded approximately every 3 seconds. A rapid decrease in absorbance at 254 nm was seen as the FPBA was converted to the IzB complex, which does not have an absorbance maximum at 254 nm. Plotting the time versus absorbance at 254 nm followed by curve fitting gave the forward reaction time constant. As the reactants were used at equal concentrations, the forward reaction kinetics data were fitted according to the equations of second order relaxation kinetics (details can be found on Page 369 of *Physical Chemistry: Principles and Applications in Biological Sciences*, Fourth Edition, by Tinoco et al., Prentice Hall PTR, 2001).

For the equilibrium binding study, increasing amounts of a Dap stock (100 mM) was added to an FPBA solution (50 µM) to give final Dap concentrations of 100 µM to 900 µM. The decrease in absorbance at 254 nm was measured as the FPBA was converted to the IzB complex. Plotting the absorbance at 254 nm against the concentration of Dap gave the binding curve. Fitting the data to a hyperbolic equation ($y = A + Bx/(C+x)$) yielded the apparent K_d value ($K_d = C$).

3.8.5 Probing Small Molecule Interference of IzB Formation via NMR

100 µL of FPBA-Dap IzB complex (10 mM) was diluted in 400 µL PBS (pH 7.4, 20% D_2O). The solution was mixed with 500 µL stock solutions of lysine (20 mM), serine (20 mM), glutathione (20 mM), glucose (20 mM), and cysteine (2 mM) in phosphate buffer (**Figure 3-3**). The pH of the mixtures was tuned to 7.4. All samples were incubated for 30 minutes before the ^{1}H-NMR spectra were taken.

3.8.6 Peptide Synthesis and Characterization

All peptides were synthesized using standard Fmoc-based SPPS on Rink Amide MBHA resin. They were carried out on a 0.05 mmol scale using 5 equivalents of each amino acid and 4.75 equivalents of HBTU for each coupling reaction.

CW1 through CW4

$Pd(PPh_3)_4$ (100 mg) and phenylsilane (600µL) in DCM (2 mL) was added to the resin and stirred for 1-2 hours to selectively deprotect the Alloc group. A second Alloc removal was done if LCMS analysis shown incomplete deprotection upon small scale cleavage from resin. The FPBA functionality was installed by activating **4** (5 eq) with HBTU (4.7 eq) in 0.4 M NMM in DMF for about 5 minutes, then adding the solution to the peptide on-resin and mixing for 1-2 hours. The N-terminal Fmoc was deprotected with two 20% piperidine in DMF treatments for 5 min each. The peptide was cleaved off resin and globally deprotected with 95% trifluoroacetic acid : 5% water treatment for 2 hours. Cold ether precipitation yielded crude peptide, which was purified using RP-HPLC and lyophilized. For CW3 and CW4, the orthogonal Cys protecting group was

deprotected as described below. Peptide purity was assessed by LCMS. The calculated and observed *m/z* $[M+H]^+$ values are listed below**.**

Peptide	Calculated $[M+H]^+$	Observed $[M+H]^+$
Fmoc-CW1	976.3677	958.3557 $[M-H_2O+H]^+$
Fmoc-CW2	960.3905	924.3701 $[M-2H_2O+H]^+$
C(Acm)-CW3	968.4102	968.4078
CW3	897.3731	861.3520 $[M-2H_2O+H]^+$
C(Fm)-CW4	1075.4513	1075.4266
CW4	897.3731	897.3767
CW5	957.3765	939.3657 $[M-H_2O+H]^+$
CW6	940.4153	940.4138
KL21	737.3384	737.3388
KL22	865.3970	865.3965

Acm Deprotection: $Hg(OAc)_2$ & β-Mercaptoethanol[20]

CW3 (5-10 mg/mL) was dissolved in 10% (v/v) aqueous acetic acid and the pH was adjusted to 3-4. $Hg(OAc)_2$ (10 eq) was added and the reaction was stirred under Ar at room temperature for 1 hour. β-Mercaptoethanol (40 eq) was added and the reaction was allowed to sit at room temperature for 5 hours. The reaction was centrifuged to remove the Hg salts and the supernatant was analyzed for deprotection completion via LC-MS.

Acm Deprotection: AgOAc & Dithiothreitol (DTT)[21]

CW3(1 mg/mL) was dissolved in 1:1 acetic acid:water and AgOAc (35 eq) was added. The reaction was stirred at room temperature overnight. DTT (200 eq) added to the reaction and stirred for 20 min at room temperature. The reaction was centrifuged to remove the Ag salts and the

supernatant was analyzed for deprotection completion via LC-MS. This was the cleanest and easiest to analyze deprotection condition.

Acm Deprotection: AgOTf & DTT[22]

CW3 (1 mg/mL) was dissolved in 99% TFA : 1% anisole and chilled over ice. AgOTf (100 eq) was added and the reaction was stirred on ice for 2 hours. After cold ether precipitation and centrifugation, the peptide-Ag salt was dried and dissolved in 1 M aqueous acetic acid (1 mg/mL). DTT (40 eq) was added and the reaction was stirred at room temperature for 3 hours. The reaction was centrifuged to remove the Ag salts and the supernatant was analyzed for deprotection completion via LC-MS.

Acm Deprotection: $PdCl_2$ & DTT[23]

CW3 (2 mM) was dissolved in water and $PdCl_2$ (10 eq) was added as a water solution. The reaction was incubated at 37°C for 50 minutes, then treated with DTT (20 eq) for 10-15 min at room temperature. The reaction was centrifuged to remove the Pd salts and the supernatant was analyzed for deprotection completion via LC-MS.

Fm Deprotection[24]

CW4 (1 mg) was dissolved in 50% piperidine in DMF (30 µL) and stirred at room temperature for 2 hours. The crude peptide was directly RP-HPLC purified and LC-MS analysis revealed the peptide was oxidized. After lyophilization, CW4 (<0.5 mg) was dissolved in 95% water : 5% acetonitrile : 0.1% TFA (10 µL). Excess TCEP was added and incubated at room temperature for 1 hour to reduce the peptide, then the solution was analyzed via LC-MS.

CW5 and CW6

Directly after SPPS, the N-terminal Fmoc was deprotected with two 20% piperidine in DMF treatments for 5 min each. The peptide was cleaved off resin and globally deprotected with 85% TFA : 5% water : 5% phenol : 5% thioanisole for 2 hours. Cold ether precipitation yielded crude peptide, which was dried and immediately dissolved in PBS (1X, pH 7.4) and 95% water : 5% acetonitrile : 0.1% TFA (38% (v/v)) for peptide solubility. The FPBA moiety was installed through iodoacetamide reaction of an FPBA-iodoacetamide derivative with the C-terminal Cys side chain. FPBA (2 eq) was added to the crude peptide solution to form a complex with the N-terminal Cys or Dap residue, rendering it unreactive. The FPBA iodoacetamide derivative (1.5 eq) was added and the mixture was stirred overnight at room temperature. Acidification by adding TFA dissociated the FPBA from the N-terminal residue. The reaction was purified using RP-HPLC and peptide purity was assessed by LCMS. The calculated and observed *m/z* $[M+H]^+$ values are listed above.

KL21 and KL22

Kaicheng Li performed the synthesis, purification, and most of the work involving KL21 and KL22. $Pd(PPh_3)_4$ (100 mg) and phenylsilane (600µL) in dichloromethane (2 mL) was added to the resin and stirred for 2 hours to selectively deprotect the Alloc group. The FPBA functionality was installed by activating **4** (4 eq) with HBTU (3.8 eq) in 0.4 M NMM in DMF for 5 min, then adding the solution to the peptide on-resin and mixing for 1h. After N-terminal Fmoc deprotection with 20% piperidine in DMF, the peptide was cleaved off resin and globally deprotected with 85% TFA: 5% water : 5% phenol : 5% thioanisole treatment for 2 hours. Cold ether precipitation yielded

crude peptide, which was purified using RP-HPLC and lyophilized. Peptide purity was assessed by ^{1}H NMR and LCMS. The calculated and observed *m/z* $[M+H]^+$ values are listed above.

For LCMS analysis, an Agilent Extend C18 (1.8 µm, 2.1 x 50 mm) analytical column was used with a water-acetonitrile mobile phase at a flow rate of 0.2 mL/min. The gradient used was as follows: isocratic 5% CH_3CN for 5 min, gradient from 5% to 95% CH_3CN in 10 min, isocratic 95% CH_3CN for 5 min, gradient from 95% to 5% CH_3CN in 1 min, then isocratic 5% CH_3CN for 5 min.

3.8.7 pH-Dependent Cyclization of KL21 and KL22

A solution of KL21 or KL22 (500 µM) in PBS (20% D_2O) was prepared. The pH was tuned from 2.5 to 7.4 incrementally. Cyclization was monitored by the disappearance of the FPBA aldehyde peak at 9.8 ppm and the appearance of the IzB benzylic hydrogen peak around 5.8 ppm.

3.8.8 Probing Small Molecule Interference of Kl21 Cyclization via NMR

KL21 (0.15 mg) was dissolved in 900 µL PBS (pH 7.4, 20% D_2O, final KL21 concentration 200 µM). The solution was mixed with 100 µL stock solutions of lysine (20 mM), serine (20 mM), glutathione (20 mM), and glucose (20 mM) in PBS. The pH of the mixtures was tuned to 7.4. The samples were incubated for 30 minutes before the NMR spectra were taken.

3.8.9 Cysteine-Induced KL21 Linearization

KL21 (0.15 mg) or KL22 (0.18 mg) were dissolved in 800 µL PBS (pH 7.4, 20% D_2O, final peptide concentration 200 µM). Increasing amounts of a cysteine stock (100 mM) in PBS was added to give final Cys concentrations of 100 µM to 4 mM. To ensure the Cys remained reduced, iTCEP (25 µL) was added to the NMR tube. The pH of the mixture was tuned to 7.4. Titration curves were

generated by plotting the area of the two TzB benzylic proton peaks against Cys concentration. Fitting these titration curves using a hyperbolic equation gave the EC_{50} value for Cys-induced peptide linearization.

3.8.10 Cysteine-Induced KL21 Linearization in Fetal Bovine Serum (FBS)

To a solution of KL21 (200 µM) in 900 µL PBS (pH 7.4, 20% D_2O) and 100 µL FBS (10% FBS (v/v)), increasing amounts of a Cys stock (100 mM) in phosphate buffer was added to give final Cys concentrations of 100 µM to 4 mM. To ensure the Cys remains reduced, iTCEP (25 µL) was added to the NMR tube. The pH of the mixtures was tuned to 7.4. All samples were incubated for 30 minutes before the ^{1}H-NMR spectra were taken. Titration curves were generated by plotting the area of the two TzB benzylic proton peaks against Cys concentration. Fitting these titration curves using a hyperbolic equation gave the EC_{50} value for Cys-induced peptide linearization.

3.8.11 KL21 Cysteine Oxidation in FBS

A solution of KL21 (200 µM) and Cys (4 mM) in 1.8 mL PBS (pH 7.4, 20% D_2O) with 200 µL FBS (10% FBS (v/v)) was made and a ^{1}H-NMR spectrum was recorded as soon as possible (~30 minutes). The solution (~2 mL total volume) was incubated at 25°C in a scintillation vial open to air to allow gradual Cys oxidation over time. The ^{1}H-NMR spectrum was recorded occasionally over the course of a few days.

3.8.12 Synthesis and Characterization of the Carboxylic Acid Derivative of FPBA (**4**)

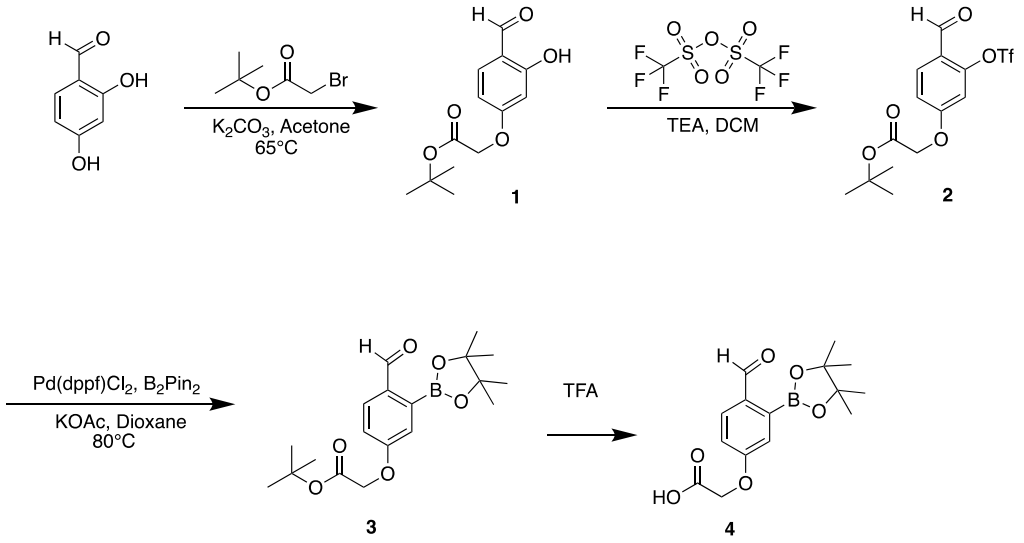

*Synthesis of **1***

2,4-dihydroxylbenzaldehyde (3.00 g, 21.74 mmol) was dissolved in 10 mL acetone, to which tert-butyl 2-bromoacetate (4.24 g, 21.43 mmol) and potassium carbonate (5 g, 36.23 mmol) was added. The reaction was stirred at 65 °C for 16 h then cooled down to room temperature. 150 mL of water was added to the reaction mixture and extracted with ethyl acetate (3 x 150 mL). The organic layers were combined, washed with brine (150 mL) and dried over sodium sulfate. Ethyl acetate was evaporated, and the crude product was purified by silica column using ethyl acetate: hexane (1:10) to yield a white solid (2.90 g, 53%).

^{1}H-NMR (500 MHz, Chloroform-*d*) δ 11.42 (s, 1H), 9.72 (s, 1H), 7.44 (d, *J* = 8.7 Hz, 1H), 6.56 (d, *J* = 11.1 Hz, 1H), 6.36 (d, *J* = 2.4 Hz, 1H), 4.55 (s, 2H), 1.48 (s, 9H).

^{13}C-NMR (126 MHz, Chloroform-*d*) δ 194.47, 166.81, 164.88, 164.25, 135.37, 115.70, 108.45, 101.45, 82.97, 65.48, 28.00.

MS-ESI^{+}: *m/z* calculated for $C_{13}H_{17}O_5$ $[M+H]^{+}$ 253.1076, observed 253.1055.

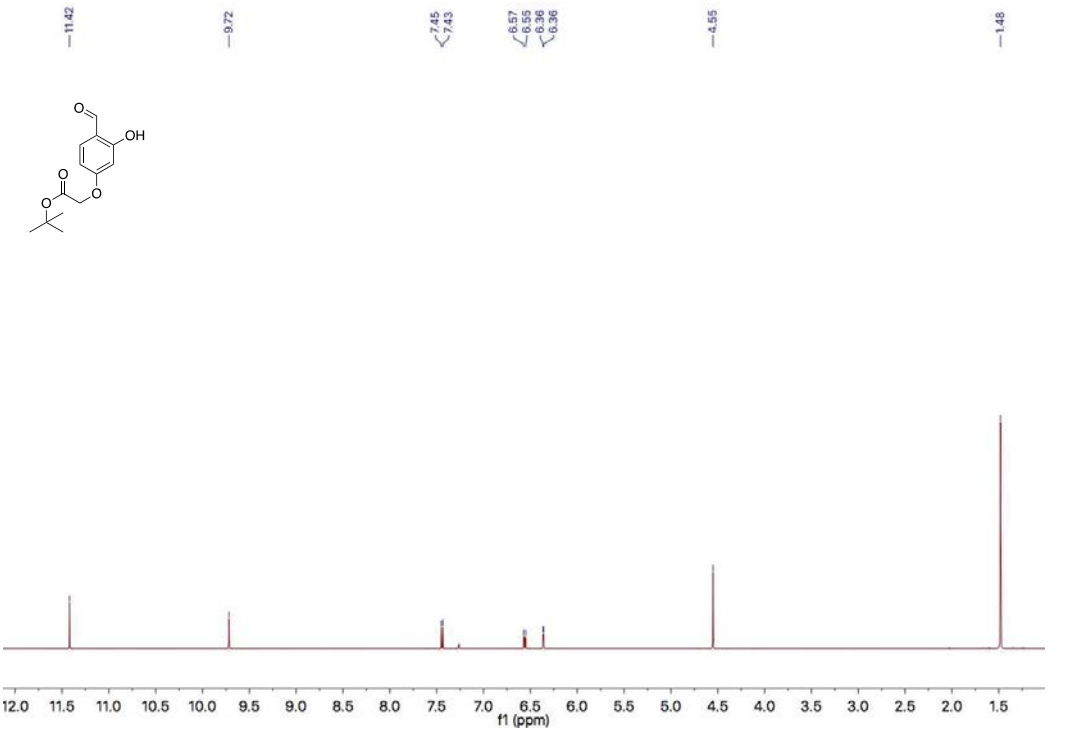
11.42
9.72
7.45
7.43
6.57
6.55
6.36
6.36
4.55
1.48
OH
O
O
O
O
12.0 11.5 11.0 10.5 10.0 9.5 9.0 8.5 8.0 7.5 7.0 6.5 6.0 5.5 5.0 4.5 4.0 3.5 3.0 2.5 2.0 1.5
f1 (ppm)

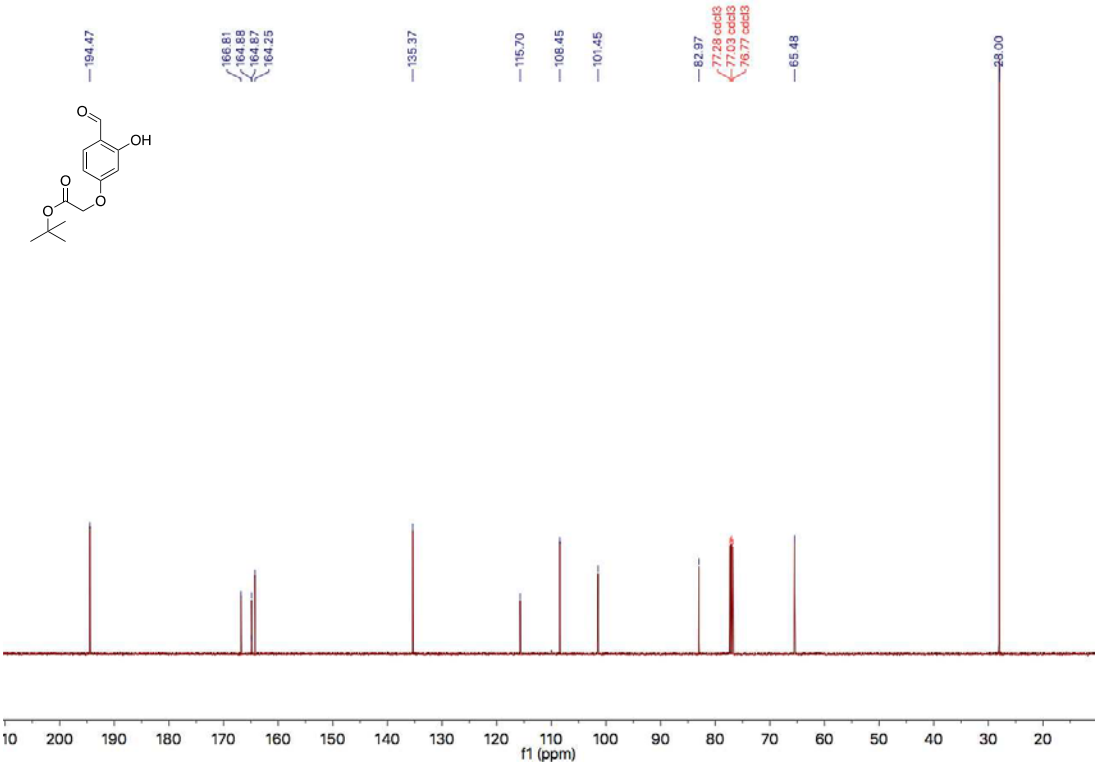
194.47
166.81
164.88
164.87
164.25
135.37
115.70
106.45
101.45
82.97
77.28 cdcl3
77.03 cdcl3
76.77 cdcl3
65.48
28.00
OH
O
O
O
O
210 200 190 180 170 160 150 140 130 120 110 100 90 80 70 60 50 40 30 20
f1 (ppm)

*Synthesis of **2***

1 (1.51 g, 6.00 mmol) and triethylamine (3.03 g, 30.00 mmol) were dissolved in 15 mL of dichloromethane and stirred at -78 °C for 5 min. Trifluoromethanesulfonic anhydride (3.39 g, 12.00 mmol) was added slowly into the mixture over 1 min. The reaction was then allowed to stir at room temperature for 1 h under argon and quenched with 50 mL of saturated sodium bicarbonate. The mixture was stirred for 5 min and then extracted with dichloromethane (3 x 100 mL). The combined organic layer was washed with brine (100 mL) and dried over sodium sulfate. After solvent removal, the crude product was purified by silica column using ethyl acetate: hexane (1:9) to yield a light yellow solid (1.90 g, 83%).

^{1}H-NMR (600 MHz, Chloroform-*d*) δ 10.13 (s, 1H), 7.94 (d, *J* = 8.7 Hz, 1H), 7.00 (dd, *J* = 8.7, 2.3 Hz, 1H), 6.88 (d, *J* = 2.3 Hz, 1H), 4.61 (s, 2H), 1.49 (s, 9H).

^{13}C-NMR (151 MHz, Chloroform-*d*) δ 187.90, 168.90, 166.14, 153.79, 134.82, 125.08, 121.24, 117.31, 111.52, 86.14, 68.56, 30.66.

MS-ESI^{+}: *m/z* calculated for $C_{14}H_{16}F_3O_7S$ $[M+H]^{+}$ 385.0569, observed 385.0515.

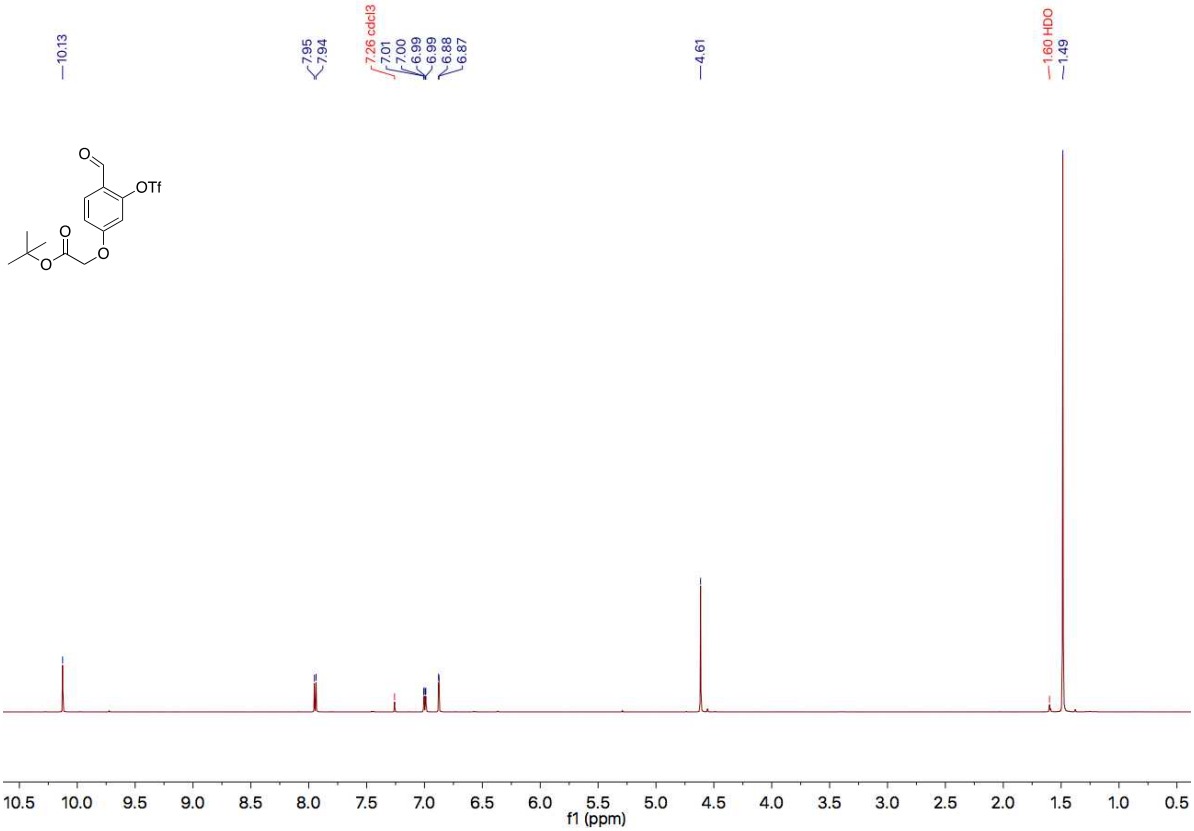

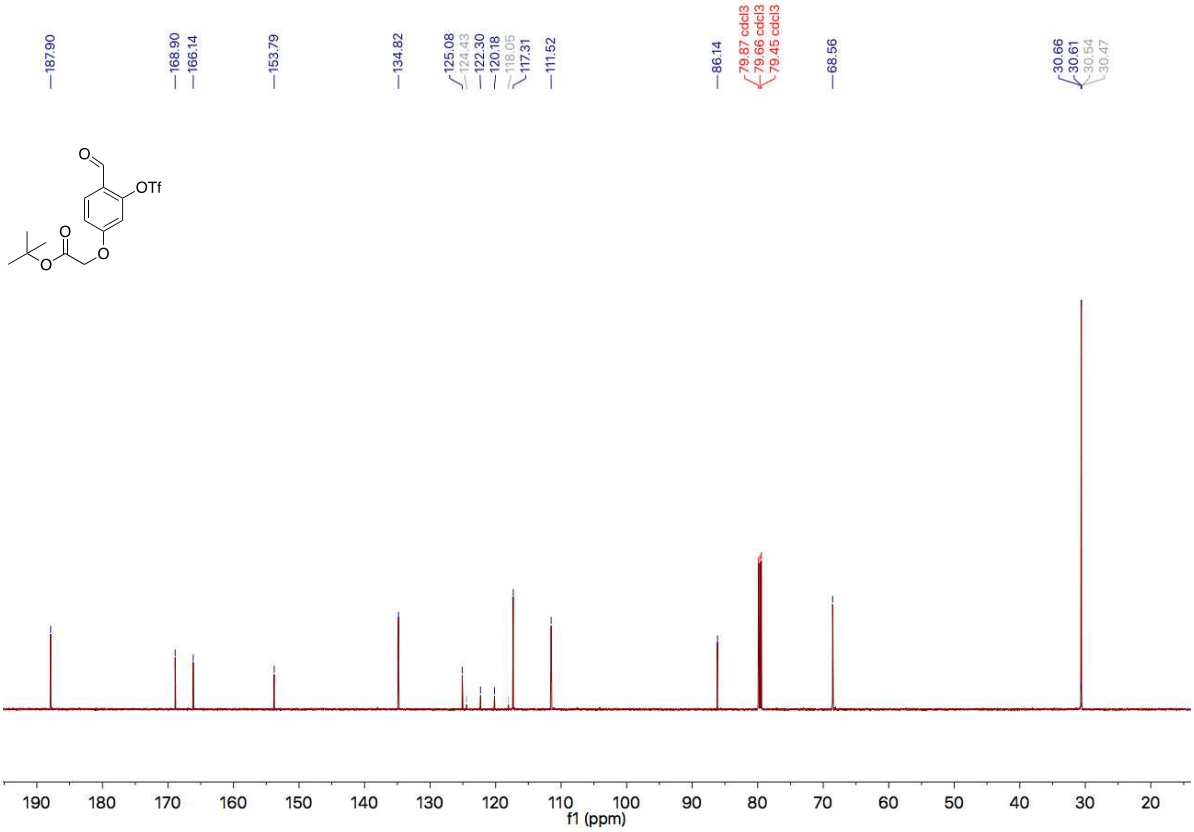

*Synthesis of **3***

2 (1.50g, 3.90 mmol), B_2pin_2 (2.57g, 10.12 mmol), $Pd(dppf)Cl_2$ (300 mg, 0.41 mmol) and potassium acetate (2.00 g, 21.01 mmol) were dissolved in 10 mL of anhydrous dioxane, to which ~100 mg of 3 Å molecular sieves were added. The reaction was flushed with argon for 15 min and allowed to stir for 1 h at 80 °C. The reaction was cooled down to room temperature and water (50 mL) was added to the reaction. The product was extracted with ethyl acetate (3 x 100 mL). The combined organic layer was washed with brine (100 mL) and dried over sodium sulfate. Ethyl acetate was removed, and the product was purified on silica gel column using ethyl acetate: hexane (3:17) to give the desired product a white solid (0.54 g, 38% yield).

^{1}H-NMR (600 MHz, Chloroform-*d*) δ 10.40 (s, 1H), 7.93 (d, *J* = 8.6 Hz, 1H), 7.28 (d, *J* = 2.6 Hz, 1H), 7.03 (dd, *J* = 8.6, 2.7 Hz, 1H), 4.59 (s, 2H), 1.48 (s, 9H), 1.37 (s, 12H).

^{13}C-NMR (151 MHz, Chloroform-*d*) δ 195.67, 169.89, 164.09, 138.03, 132.95, 123.06, 119.73, 87.11, 85.40, 68.22, 30.65, 27.50.

MS-ESI^{+}: *m/z* calculated for $C_{13}H_{16}BO_5$ $[M\text{-}Pin\text{-}H_2O+H]^{+}$ 263.1091, observed 263.1221.

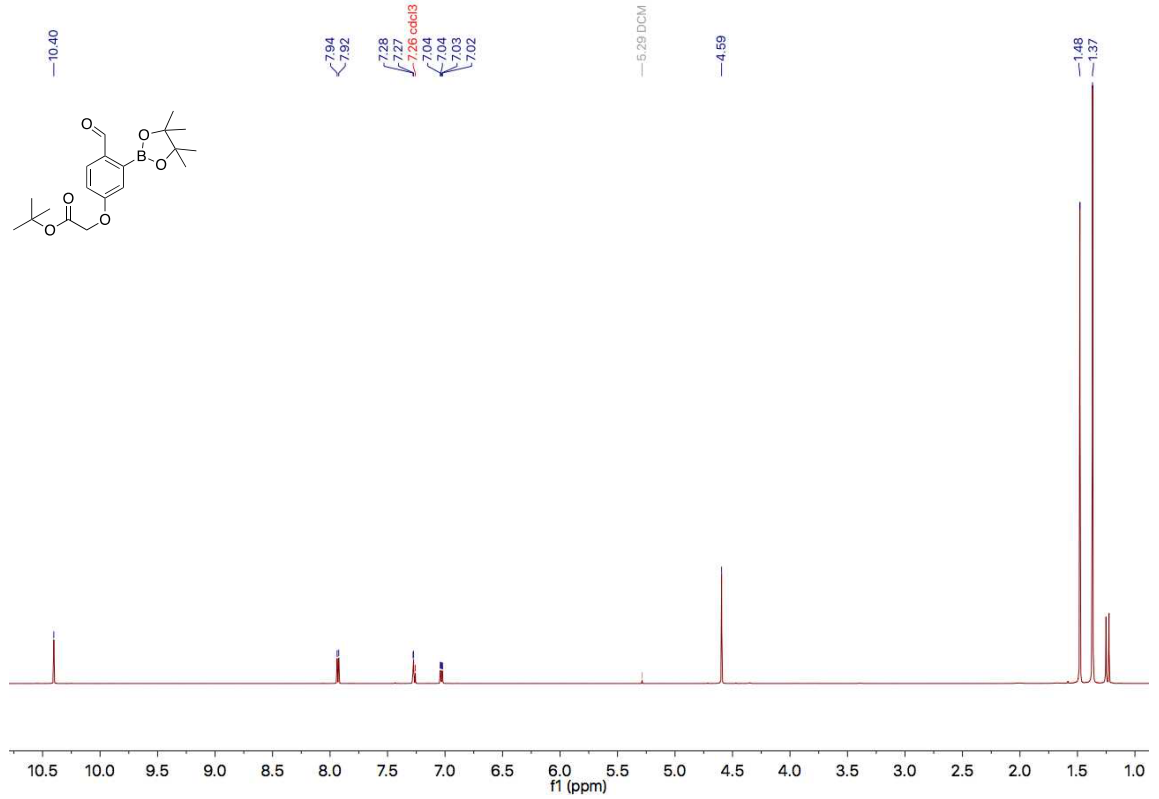
10.40
7.94
7.92
7.28
7.27
7.26 cdcl3
7.04
7.04
7.03
7.02
5.29 DCM
4.59
1.48
1.37
10.5 10.0 9.5 9.0 8.5 8.0 7.5 7.0 6.5 6.0 5.5 5.0 4.5 4.0 3.5 3.0 2.5 2.0 1.5 1.0
f1 (ppm)

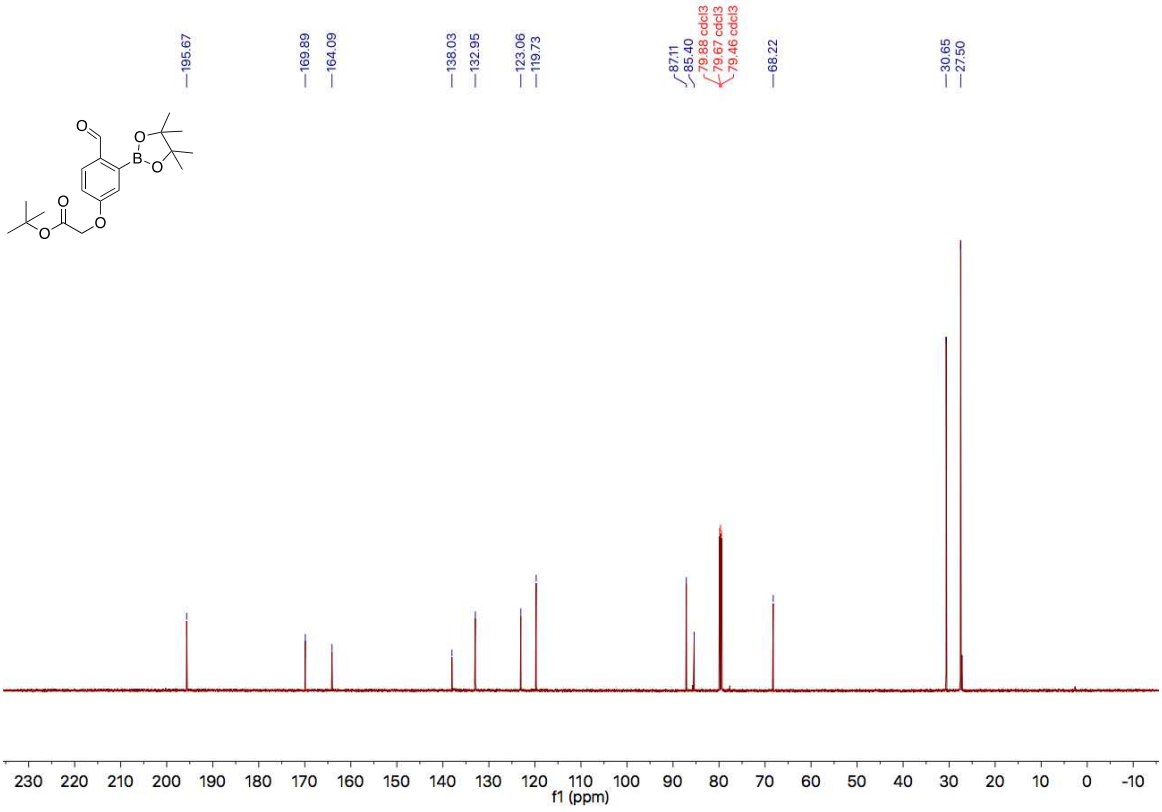
195.67
169.89
164.09
138.03
132.95
123.06
119.73
87.11
85.40
79.88 cdcl3
79.67 cdcl3
79.46 cdcl3
68.22
30.65
27.50
230 220 210 200 190 180 170 160 150 140 130 120 110 100 90 80 70 60 50 40 30 20 10 0 -10
f1 (ppm)

*Synthesis of **4***

3 (200 mg, 0.55 mmol) was dissolved in 2 mL of dichloromethane and stirred at 0 °C, to which 3 mL of trifluoroacetic acid (TFA) was added. The mixture was stirred at room temperature for 1 h before the dichloromethane and TFA were evaporated. The residue was treated with 5 mL of TFA for another hour at room temperature. Removing TFA completely via evaporation and washing with toluene and dichloromethane yielded an off-white powder as the desired product (150 mg, 89%).

^{1}H NMR (600 MHz, DMSO-d_6) δ 13.12 (s, 1H), 10.13 (s, 1H), 7.87 (d, J = 8.5 Hz, 1H), 7.16 – 7.10 (m, 2H), 4.82 (s, 2H), 1.32 (s, 12H).

^{13}C NMR (151 MHz, DMSO-d_6) δ 195.33, 172.74, 164.62, 137.18, 134.51, 123.14, 119.16, 87.21, 67.67, 27.77.

MS-ESI^{+}: m/z calculated for $C_{13}H_{16}BO_5$ $[M\text{-}Pin\text{-}H_2O+H]^{+}$ 207.0465, observed 207.0422.

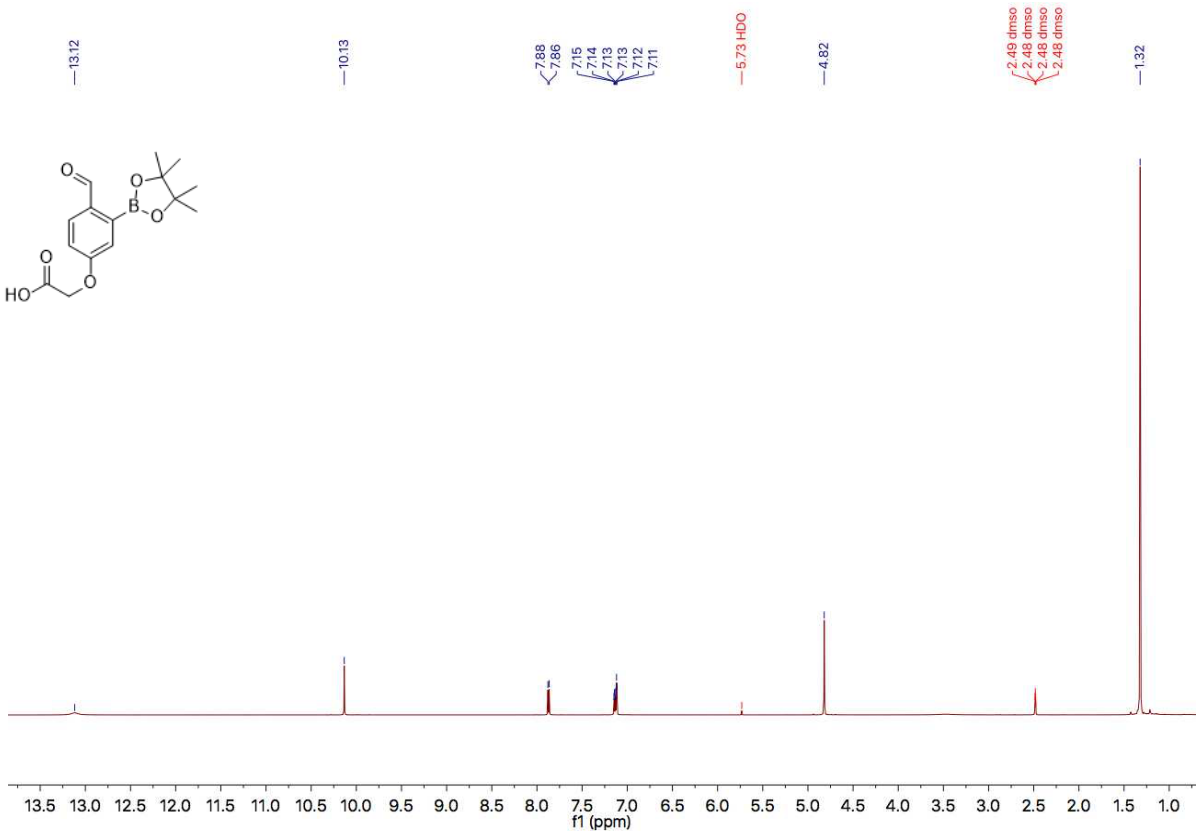

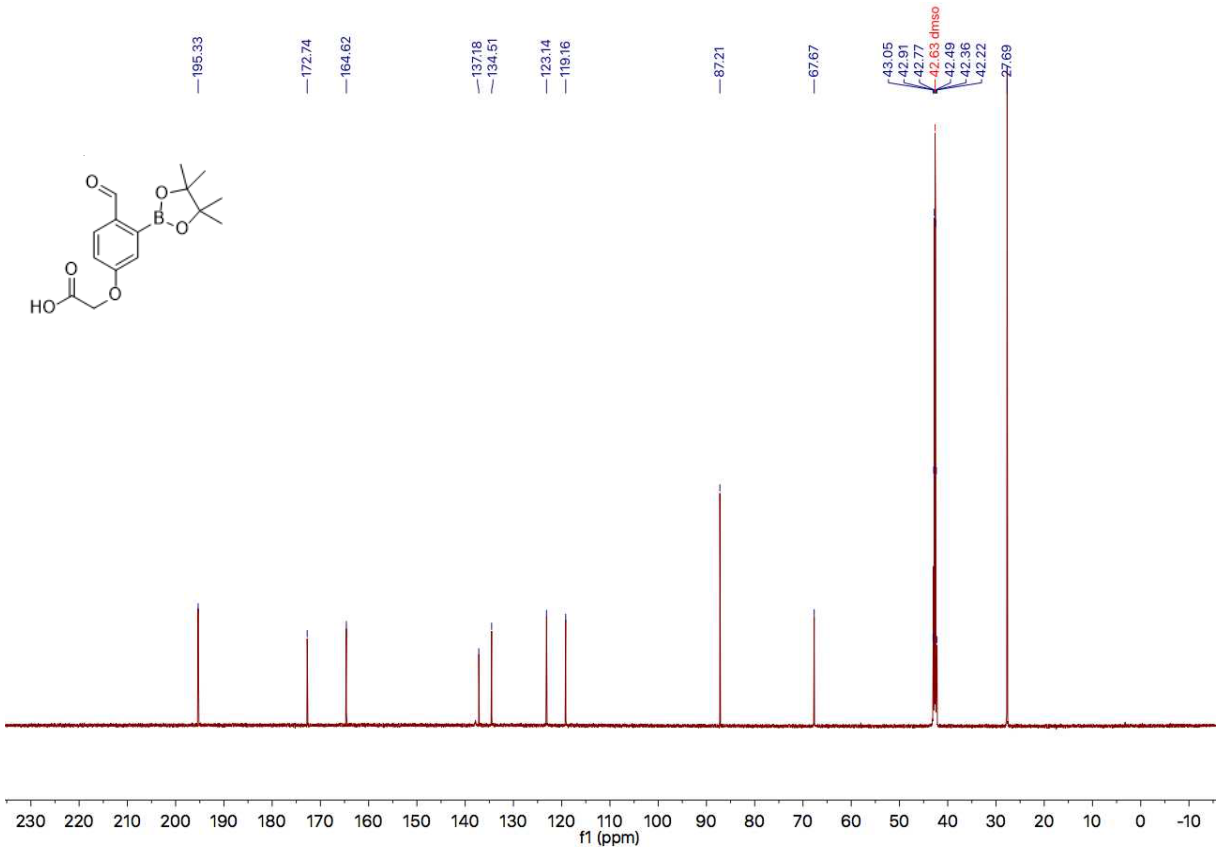

3.9 References

(1) Sletten, E. M.; Bertozzi, C. R. *Angew. Chem. Int. Ed.* **2009**, *48* (38), 6974–6998.

(2) Bertozzi, C. R. *Acc. Chem. Res.* **2011**, *44* (9), 651–653.

(3) Cougnon, F. B. L.; Sanders, J. K. M. *Acc. Chem. Res.* **2012**, *45* (12), 2211–2221.

(4) Bandyopadhyay, A.; Gao, J. *Curr. Opin. Chem. Biol.* **2016**, *34*, 110–116.

(5) Akçay, G.; Belmonte, M. A.; Aquila, B.; Chuaqui, C.; Hird, A. W.; Lamb, M. L.; Rawlins, P. B.; Su, N.; Tentarelli, S.; Grimster, N. P.; Su, Q. *Nat. Chem. Biol.* **2016**, *advance online publication*.

(6) James, T. D.; Sandanayake, K. R. A. S.; Shinkai, S. *Angew. Chem. Int. Ed. Engl.* **1996**, *35* (17), 1910–1922.

(7) Dowlut, M.; Hall, D. G. *J. Am. Chem. Soc.* **2006**, *128* (13), 4226–4227.

(8) Adams, J.; Kauffman, M. *Cancer Invest.* **2004**, *22* (2), 304–311.

(9) Bradshaw, J. M.; McFarland, J. M.; Paavilainen, V. O.; Bisconte, A.; Tam, D.; Phan, V. T.; Romanov, S.; Finkle, D.; Shu, J.; Patel, V.; Ton, T.; Li, X.; Loughhead, D. G.; Nunn, P. A.; Karr, D. E.; Gerritsen, M. E.; Funk, J. O.; Owens, T. D.; Verner, E.; Brameld, K. A.; Hill, R. J.; Goldstein, D. M.; Taunton, J. *Nat. Chem. Biol.* **2015**, *11* (7), 525–531.

(10) Serafimova, I. M.; Pufall, M. A.; Krishnan, S.; Duda, K.; Cohen, M. S.; Maglathlin, R. L.; McFarland, J. M.; Miller, R. M.; Frödin, M.; Taunton, J. *Nat. Chem. Biol.* **2012**, *8* (5), 471–476.
(11) Jiang, X.; Yu, Y.; Chen, J.; Zhao, M.; Chen, H.; Song, X.; Matzuk, A. J.; Carroll, S. L.; Tan, X.; Sizovs, A.; Cheng, N.; Wang, M. C.; Wang, J. *ACS Chem. Biol.* **2015**, *10* (3), 864–874.
(12) Umezawa, K.; Yoshida, M.; Kamiya, M.; Yamasoba, T.; Urano, Y. *Nat. Chem.* **2017**, *9* (3), 279–286.
(13) Cal, P. M. S. D.; Vicente, J. B.; Pires, E.; Coelho, A. V.; Veiros, L. F.; Cordeiro, C.; Gois, P. M. P. *J. Am. Chem. Soc.* **2012**, *134* (24), 10299–10305.
(14) Bandyopadhyay, A.; McCarthy, K. A.; Kelly, M. A.; Gao, J. *Nat. Commun.* **2015**, *6*, 6561.
(15) Bandyopadhyay, A.; Gao, J. *J. Am. Chem. Soc.* **2016**, *138* (7), 2098–2101.
(16) Li, K.; Gao, J. *Synlett* **2017**.
(17) Bandyopadhyay, A.; Cambray, S.; Gao, J. *Chem. Sci.* **2016**.
(18) Faustino, H.; Silva, M. J. S. A.; Veiros, L. F.; Bernardes, G. J. L.; Gois, P. M. P. *Chem. Sci.* **2016**, *7* (8), 5052–5058.
(19) Lang, K.; Chin, J. W. *ACS Chem. Biol.* **2014**, *9* (1), 16–20.
(20) Veber, D.; Milkowski, J.; Varga, S.; Denkewalter, R.; Hirschmann, R. *J. Am. Chem. Soc.* **1972**, *94* (15), 5456–5461.
(21) Durek, T.; Torbeev, V. Y.; Kent, S. B. H. *Proc. Natl. Acad. Sci.* **2007**, *104* (12), 4846–4851.
(22) Hunter, M. J.; Komives, E. A. *Anal. Biochem.* **1995**, *228* (1), 173–177.
(23) Maity, S. K.; Jbara, M.; Laps, S.; Brik, A. *Angew. Chem. Int. Ed.* **2016**, *55* (28), 8108–8112.
(24) Ruiz-Gayo, M.; Albericio, F.; Pedroso, E.; Giralt, E. *J. Chem. Soc. Chem. Commun.* **1986**, No. 20, 1501–1502.
(25) Sorkin, A.; von Zastrow, M. *Nat. Rev. Mol. Cell Biol.* **2002**, *3* (8), 600–614.

CHAPTER 4: CONCLUSIONS AND FUTURE DIRECTIONS

4.1 Targeting *S. aureus* Membrane Amines

The aim of this research was to study the effects of *S. aureus* surface charge on antimicrobial susceptibility via peptide and small molecule manipulation. Previous studies utilized bacterial gene knockouts to alter the expression of cationic membrane modifications, such as Lys-PG. To the best of our knowledge, manipulating membrane charge to directly study the electrostatic influence of CAMP effectiveness has not been well characterized.

Co-treatment with Gramicidin A3R or Protegrin-1 and an iminoboronate-forming cyclic peptide caused increased *S. aureus* susceptibility to those CAMPs. The cyclic peptide, KAM-CT, is known to bind potently to *S. aureus* through iminoboronate formation between the 2-APBA moiety in the peptide and free amines on the bacterial surface. Occupying free amines in an iminoboronate eliminates their cationic charge at physiological pH, thereby decreasing the membrane surface charge. CAMPs are more electrostatically attracted to anionic membranes, leading to greater binding and more potent antimicrobial activity.

Acetylating free surface amines achieved a similar effect by forming amides to quench the cationic amines. Treatment of *S. aureus* with sulfo-NHS-acetate followed by Gramicidin A3R and Protegrin-1 caused 2.5 or 10 times increase in *S. aureus* susceptibility to those CAMPs, respectively.

Nucleophilic cleavage of the lysine moiety of the Lys-PG headgroup to regenerate anionic PG was also explored. Initially, liposomes were treated with an esterase enzyme to selectively cleave the Lys-PG headgroup ester bond. However, no detectable lipids were extracted from the solution, so the experiment was inconclusive.

Next, non-specific small molecule nucleophiles were explored. Hydroxylamine was found to effectively cleave Lys-PG, by only at a 1 M concentration. As a more potent and specific cleavage moiety is desirable, the activity of the hydroxylamine-peptide conjugate AOA-Hlys was explored. The peptide, an antimicrobial fragment of human lysozyme called Hlys, would direct the hydroxylamine to the bacterial surface, where it should be in high enough concentration to effectively cleave Lys-PG, producing an anionic membrane. This was expected to increase CAMP activity based on a greater electrostatic interaction. Although AOA-Hlys did cause about 2-fold more Lys-PG cleavage in liposome models compared to hydroxylamine alone, it was less effective at killing *S. aureus* than the non-modified Hlys peptide. Binding of AOA-Hlys and Hlys to liposomes measured by Trp fluorescence was comparable. This indicates the importance of amphipathic balance in CAMPs – disrupting the amphipathicity by adding a hydrophilic moiety, such as hydroxylamine, might disrupt the propensity for membrane insertion, decreasing CAMP activity.

Interestingly, Hlys showed Lys-PG cleavage activity on its own in liposomes, which was not previously reported in literature. Quantification via ion intensity comparison using mass spectrometry (MS) is not typical, so NP-HPLC was used as a secondary analytical technique. After fluorescein labeling Lys-PG, the labeled lipid was quantified via fluorescein absorbance and compared to the remaining fluorescein as an internal standard. There appeared to be no significant difference in the Lys-PG amount extracted from untreated liposomes compared to liposomes treated with Hlys (100 μM). However, MS analysis showed twice as much Lys-PG cleavage in the presence of Hlys (100 μM) compared to untreated liposomes. Therefore, the Lys-PG cleavage activity of Hlys could not be confirmed.

Lipid fluorescein labeling and NP-HPLC analysis was used to label and quantify Lys-PG extracted from wild type *S. aureus* and *S. aureus* treated with 10 mM sulfo-NHS-acetate. This method allows for quantification of Lys-PG extracted from bacteria.

4.2 FPBA-Based Reversible Covalent Chemistries

Expanding the repertoire of reversible covalent chemistries, especially those applied to peptide cyclization, is desirable due to the high potency and selectivity of such interactions. Cyclic peptides are considered privileged scaffolds, displaying enhanced biostability and binding affinity than linear peptides. Cyclic peptides, such as KAM-CT, could be used as novel antibiotics or non-lethal membrane modifiers.

Initially, TzB-cyclized peptides were pursued based on our previously characterized potent interaction of free Cys and 2-FPBA. However, synthesis of peptides containing an N-terminal Cys residue and C-terminal residue functionalized with 2-FPBA proved difficult. The cleanest attempt gave multiple TIC peaks upon LC-MS analysis, all corresponding to the expected peptide mass or the peptide mass minus one or two water molecules. Seeing the peptide mass minus one or two water molecules would be expected due to a loss of water upon peptide cyclization and the known phenomena of boronic acids losing water during MS analysis. However, why the peptide gave multiple peaks with the same mass is yet to be understood.

Next, we explored the reactivity of moieties similar to the 1,2 aminothiol functionality in Cys. The Dap residue bears a 1,2-diamino moiety and it was found to form a similar complex with 2-FPBA, called IzB. IzB conjugation is potent (K_d = 100 μM) and quickly reversible under

physiological conditions. With little interference from reactive biologically relevant small molecules, except Cys, IzB formation was successfully utilized as a reversible covalent peptide cyclization strategy.

Cys interference of IzB conjugation was utilized to create “smart” peptides, which can linearize in response to both acidic pH and Cys concentration. Such peptides were found to be both stable and able to report on the Cys concentration in a FBS solution.

4.3 Future Directions

Further establishing the fluorescein labeling and HPLC analysis protocol by repeating literature findings would be advantageous. Ultimately, Lys-PG extracted from bacteria could be analyzed after treatment with various agents, such as antimicrobial peptides or Lys-PG cleavage inducing molecules.